Device Engineering of Organic Field Effect Transistors for Sensing Applications

A thesis submitted by

Anamika Dey

to

Indian Institute of Technology Guwahati

for the award of the degree of

Doctor of Philosophy

Centre for Nanotechnology
Indian Institute of Technology Guwahati
Guwahati – 781039, Assam
India

November 2017

Centre for Nanotechnology
IIT Guwahati
PhD Thesis

Device Engineering of Organic Field Effect Transistors for Sensing Applications

Anamika Dey

Supervisor

Prof. Parameswar Krishnan Iyer
November 2017

भारतीय प्रौद्योगिकी संस्थान गुवाहाटी
Indian Institute of Technology Guwahati
Guwahati- 781039, Assam, India

Statement

The work contained in this thesis titled '**Device Engineering of Organic Field Effect Transistors for Sensing Applications**' has been carried out by me under the supervision of Dr. Parameswar Krishnan Iyer, Professor, Department of Chemistry, Indian Institute of Technology Guwahati. This work has not been submitted elsewhere for the award of any degree.

Anamika Dey

Roll No. 136153003
Centre for Nanotechnology
IIT Guwahati
Guwahati-781039
Assam, India

November, 2017

भारतीय प्रौद्योगिकी संस्थान गुवाहाटी
Indian Institute of Technology Guwahati
Guwahati- 781039, Assam, India

Certificate

It is certified that the work contained in the thesis titled '**Device Engineering of Organic Field Effect Transistors for Sensing Applications**' by Anamika Dey, a student of Centre for Nanotechnology, Indian Institute of Technology Guwahati, for the award of the degree of Doctor of Philosophy has been carried out under my supervision. This work has not been submitted elsewhere for any degree.

Parameswar Krishnan Iyer

Professor,
Department of Chemistry and
Centre for Nanotechnology
IIT Guwahati
Guwahati – 781039
Assam, India

November, 2017

This Thesis is dedicated to my Family
for their endless love, support and encouragement.

Acknowledgements

Completion of this doctoral thesis was not possible unless I had the support and encouragement of several people around me. Today, when I am standing at the end of this journey, I would like to thank all those people who made this thesis possible and an unforgettable experience for me.

First of all, I would like to thank my supervisor, Prof. Parameswar Krishnan Iyer for his valuable guidance, scholarly inputs and consistent encouragement which I received throughout the research work. This milestone would have been a dream for ever if I hadn't had the fortune of meeting Prof. Iyer at a point in my life -full of struggles and difficulties. Without him, and his ability to raise my spirits whenever I was the most discouraged, I could have never made it this far. I am really thankful to him for giving me the wonderful opportunity to complete my Ph.D. thesis under his supervision.

I am also grateful to my doctoral committee members, Prof. Harshal B. Nemade, Prof. Perumal Alagarsamy and Dr. Partho Sarathi Gooh Pattader for periodically assessing my work and providing helpful suggestions and comments for its betterment. I want to sincerely thank and appreciate Prof. Siddhartha Sankar Ghosh for his tireless support and advices without which I would never have reached this feat.

I convey my special thanks to Ashish Singh for his support, valuable advices and assistance in my thesis work. This thesis would not have completed without his continuous help and motivation. I take this opportunity to express my sincere gratitude to some of my close friends- Ekta, Dip, Anand, Deepanjalee and Larionette who apart from their active help in my thesis work, always encouraged me in my academic and non-academic endeavours. I am indebted to my seniors Prasantada, Atul Bhaiya, Suresh Bhaiya, Radha Bhaiya, Bheem Bhaiya and Rumididi for their valuable suggestions and guidance. I am fortunate to have group members like Rahul, Ramesh Bhaiya, Ritesh, Niranjan, Sayan, Subrata, Anamika Kalita, Indrani, and Nystha, who provided me a healthy and enjoyable environment for the research.

I consider myself lucky enough to be able to meet and interact with some of the finest interdisciplinary researchers during my PhD tenure – when I participated in the

250th American Chemical Society National Meeting & Exposition in Boston, USA. I humbly appreciate the patience and interest of Prof. Tom Jackson of Pennsylvania State University, who earnestly listened to my research and gave his opinion on its future.

I gratefully acknowledge the funding sources that made my PhD work possible. I was initially funded by Department of Science and Technology (DST), India and later received financial assistances from Council of Scientific and Industrial Research (CSIR), India. For various characterization facilities, I remain thankful to the Central Instruments Facility (CIF) and DST funded Organic Electronics Lab, IIT Guwahati.

At the end, this thesis wouldn't have seen the light of this day without the care and encouragement of my teachers and elder brother Dr. Krishna Kanti Dey. I would like to offer my sincere gratitude to him- the person who actually teaches me the value of education. Finally, I would like to thank my parents for their understanding, and patience in my every endeavour.

Anamika

Abstract

The discovery of transistor in the 20th century by three great scientists, John Bardeen, William Shockley, and Walter Brattain is considered to be one of the most important inventions ever in inorganic-electronics world since it is the main building block of any modern electronic devices. However, since the inorganic transistors have some technological limitations, organic transistors are expected to be the best alternative for next generation of electronics. Among different types of organic transistors, organic field effect transistor (OFET) is one of the promising one because of its low-cost, easy fabrication, mechanical flexibility, biocompatibility and also flexibility towards large area applications. Additionally, the electro-optical properties of the organic semiconductors used for OFET fabrication can easily be designed or tuned due to the versatility of organic synthesis. Due to these reasons, OFET has been one of the most popular research topics in recent decades and expected to have wide applications in future from flexible displays to high-performance disposable sensors. However, to achieve the real applications, especially for the fabrication of OFET based sensing devices, more attention has to pay in the reduction of operating voltage of the devices. Generally, most of the reported OFETs are found to be operated under large operational voltage due to the high band gap of organic semiconductors and low k-value of gate insulator, which restricted their use towards low cost portable electronic applications. Hence, an OFET, which will be applicable for real application, like, chemo- and bio-sensor, electro-optical switch, smart card, e-skin etc., should be cost-effective and have low operational voltage, high stability with long lifetime.

Considering the demand of recent day's technology, several methods have been introduced in this thesis for reducing the operational voltage of OFET. The thesis mainly focuses to modify the gate dielectric layer to reduce the operational voltage of both p-type and n-type OFETs and used them for various sensing applications. By modulating gate dielectric layer with the combinations of one high-k inorganic and two low-k organic dielectric materials, the operational voltage of OFET was effectively reduced from 50 V to 7 V, which was later used for photo-sensing application. Again, by using the combination of two inorganic and one organic dielectric material, the operational voltage of OFET further successfully reduced from 7 V to 2 V and the same device structure was used for bio-sensing application. This thesis mainly described

very simple, unique and robust methodologies for lowering the operational voltage of OFETs up to 2 V, which can be further used as very effective and stable platforms in the next generation of portable electronics.

Contents

1

Introduction

Organic Electronics is a new division of electronics which have created tremendous revolution in the field of traditional electronics for the last two decades after the discovery of conducting polymers by Prof. Alan J. Heeger, Prof. Alan G. MacDiarmid and Prof. Hideki Shirakawa. The organic polymers, have a very important role in our daily life, due to their low cost and facile manufacturing protocol compared to many of the other commonly used materials. In the time of Bakelite, polymers were generally used as insulating materials in the fabrication of electronic products. However, this concept was absolutely transmuted in 1976, when these three scientists discovered that the conductivity of the organic polymer, polyacetylene, can be enhanced by several orders of magnitude by exposing it to iodine vapour.[1] Due to this outstanding discovery, in the year 2000, they were jointly awarded Nobel Prize in Chemistry. Since then, progresses have been made by developing various novel organic materials and optimizing their physical and chemical properties so that they can be extensively used as active layer in various electronic components like inorganic semiconductors. Organic semiconductors are materials based on molecules containing carbon compounds. They only become conductors of electric current when excess charge carriers are present inside them, which are either produced by the internal photo effect or are injected by applied voltages. Their semiconducting properties are attributed to the conjugated π-electron systems in their skeletal structures which is a consequence of sp^2 hybridization of the carbon atoms. The p_x and p_y orbitals form together with the s orbital and the σ bonds which are localized

between the carbon bonding atoms. The p_z orbitals of adjacent atoms, however, overlap perpendicular to the plane of the sp^2 orbitals and form an additional bond. Due to the weak contribution of the π electrons to bonding of the molecule, the conjugated π-electron system exhibits electronic excitation energies in the range of only a few electron volts (eV) and is therefore responsible for the optoelectronic properties of organic semiconductors. In contrast to inorganic semiconductors, where the band gap extends between valence and conduction band, the gap in organic semiconductors is determined by the difference between the highest occupied molecular orbital (HOMO) and the lowest unoccupied molecular orbital (LUMO). This band gap can be varied to a certain extent by synthesizing derivative molecules which differ in size, atomic arrangement and functional groups in order to tune their electronic properties.

Generally, organic semiconducting molecules can be classified into two main groups: polymers and oligomers. Polymers are long flexible molecules which are characterized by the formation of unbounded repetitive molecular units with molecular weight larger than 10,000. Oligomers or small weight organic molecules consist of a finite number of monomer units thus leading to a well-defined mass in contrast to polymers. Both, polymers and oligomers show similar electronic and optical properties with typical energy band gaps nearly a few eV. The major difference is found in the thin film deposition techniques and in the resulting structural properties. Polymers can be easily processed from solution which decreases the production costs dramatically. Oligomers, however, are very often insoluble and technique using ultra high vacuum is required which is associated with high costs. Nevertheless, oligomers or small molecule have the crucial advantage over polymers that they allow the preparation of very well ordered films of high purity and crystalline order, which are the two main fundamental prerequisites to enhance charge carrier mobility. Depending upon the chemical, electrical and optical properties of organic semiconductors they are widely used as an active material in fabrication of various electronic devices including organic light emitting diodes (OLEDs), organic solar cells (OSCs) and organic thin film transistors (OTFTs).[2-6]

It has been found that among various types of OTFTs, organic filed effect Transistors (OFETs) have been intensively investigated since they are basic elements of electronics, which have many applications like flexible active matrix displays, radio-frequency identification (RFID) tags, efficient sensors and optoelectronic devices. An OFET-based sensor normally has high sensitivity because the device is the combination of a sensor and an amplifier, in which a small change of the effective gate voltage induced by analyte may lead to a pronounced variation of channel current.[7-12] Hence the sensors

based on OFET have many advantages, including high sensitivity, feasibility for miniaturization, high throughput sensing, etc.[13] It has been recognized that OFET-based sensors have a broad range of applications, such as light sensing, artificial skin, environmental monitoring, food safety detection, drug delivery and medical diagnostics.[14-19] More importantly, OFETs can be used in flexible and disposable sensors. Due to these reasons, OFETs have been found to be one of the most popular research topics in recent decades and expected to have wide applications in future from flexible displays to high-performance disposable sensors. Generally, OFETs are operated within large operating voltage range due to the high band gap of the organic semiconductors and low k-value of gate insulator, which is one of the major limitations in finding their application in futuristic electronics.[20-22] Hence, an ideal OFET should have low operational voltage, high electrical stability and high lifetime for real application. However, to achieve these targets practically, more attention has to be devoted in reducing the operating voltage and electrical stability of the fabricated OFET device. Therefore, considering the demand of present day technology, decreasing the operating voltage and increasing the stability of an OFET-based sensing device has become one of the most interesting research topics due to their promising application in future as a replacement to their inorganic counter parts.

1.1 Organic Thin Film Transistors (OTFTs)

OTFTs are three-terminal electrical devices which controls the flow of electrical current between two electrodes i.e., source and drain, through the modulation of voltage or current by the third gate electrode. The electrical behaviour of OTFT is analogous to the behaviour of conventional transistor. The term OTFT can be generically used to refer to most types of organic transistors. However, depending on the mechanism used to achieve the current modulation, OTFTs can be mainly classified into two types of transistors, i.e., organic electro-chemical transistors (OECT) and organic field effect transistors (OFET).

1.1.1 Organic Electro-Chemical Transistors (OECTs)

The OECT is one of special type of OTFT in which the channel current can be modulated by electrochemical doping or de-doping from the electrolyte when gate voltages are applied. In many instances, these devices can resemble the conventional three-terminal electro-chemical cells in which the source, drain and gate electrodes play

the roles of working, counter and reference electrodes. Depending on the device architecture and operational mechanism, OECT is further divided into various sub-categories, which are- (a) electrolyte-gated organic field effect transistors (EGOFETs), (b) ion-sensitive OFETs (ISOFETs) and (c) organic charge-modulated FETs (OCMFETs) respectively. The schematic of all these sub-categories of OECT device architecture are shown in Figure 1.1 below-

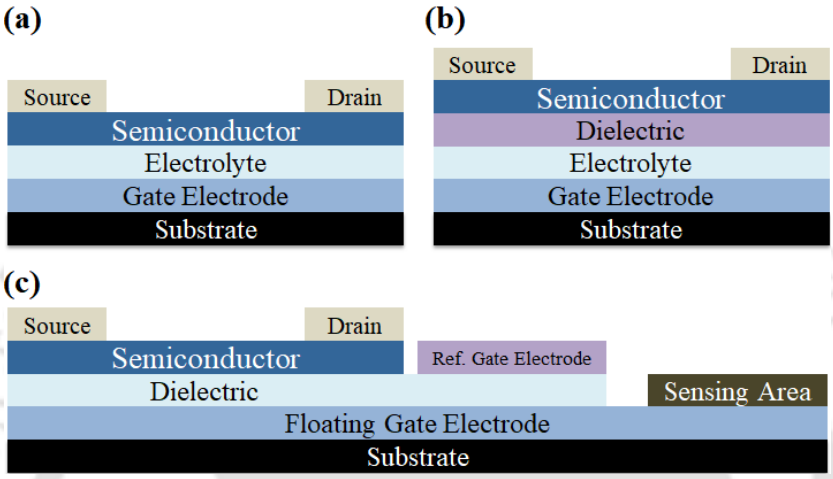

Figure 1.1 Simplified diagrams of various types of Organic Electro-Chemical Transistors (OECTs): (a) electrolyte-gated organic field effect transistor (EGOFET), (b) ion-sensitive OFET (ISOFET) and (e) organic charge-modulated FET (OCMFET).

1.1.2 Organic Field Effect Transistors (OFETs)

On the other hand, an OFET is another branch of OTFT which is composed of an organic semiconductor film, a gate dielectric (insulator), and three electrodes (source, drain, and gate). When a source-drain voltage is applied, there is a channel current flowing through the organic semiconductor layer due to the charge carrier transport. The channel current can be modulated by the gate electrode through field effect doping when a gate voltage is applied across the gate insulator. Similar like OECT, depending on various device architectures, OFET is further divided into four sub-categories which are- (a) bottom gate with top contact (BGTC), (b) bottom gate with bottom contact (BGBC), (c) top gate with top contact (TGTC) and (d) top gate with bottom contact (TGBC) respectively. The schematic of all these sub-categories of OFET device architectures are shown in Figure 1.2 below-

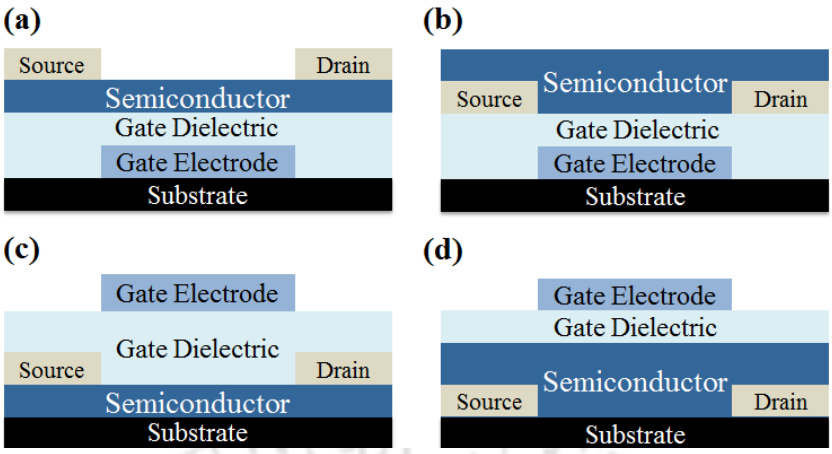

Figure 1.2 Simplified diagrams of various types of Organic Field Effect Transistors (OFETs) (a) bottom gate with top contact (BGTC), (b) bottom gate with bottom contact (BGBC), (c) top gate with top contact (TGTC) and (d) top gate with bottom contact (TGBC).

(a) *Bottom Gate with Top Contact (BGTC):* Usually, the BGTC OFET structure exhibits much better performance than the BGBC structure with source and drain contacts below the semiconductor layer. The advantage of this structure is low contact resistance, due to the large effective area for injecting charge into the semiconductor channel and corresponds to the gate/drain and gate/source overlap areas. In this structure the induced channel occurs on the opposite side of the deposited channel material compared to where the source and drain contacts are located. Thus, the main disadvantage of this configuration is that the charges have to transport from the source to the channel through an undoped highly resistive semiconductor layer. Thus, the experimentally obtained mobility and threshold voltage of OFETs can exhibit thickness dependence. On the other hand, since photolithographic patterning of the source and drain contacts is not possible due to solvents damage of organic layer they should be deposited on top of the organic semiconductor typically through a shadow mask, limiting lithographic resolution. Schematic diagram of this configuration is shown in Figure 1.2a.

(b) *Bottom Gate with Bottom Contact (BGBC):* The BGBC OFET structure is commonly used for fabricating organic FETs since the organic semiconductor is deposited at last. For this reason, photolithographic patterning of gate and source/drain electrodes is possible, and the gate insulator can be deposited from a wide range of methods (e.g. plasma-enhanced chemical vapor deposition, RF magnetron sputtering). One major disadvantage of this structure is the large contact resistance due to the very small effective area for charge injection into the

channel. Moreover, this configuration has the disadvantage that the organic semiconductor is deposited on two different materials simultaneously (i.e., the gate dielectric and the source/drain contacts), so that the morphology of the organic thin film can be disrupted by the non-uniformity of the substrate. The differences in surface energy and surface roughness between the electrodes and the dielectric cause the organic film to adapt different microstructures in the two regions, resulting in regions of disorder at the source/drain contacts. As a result, BGBC structures typically suffer from larger source and drain contact barriers and contact resistance. This configuration is shown in Figure 1.2b.

(c) *Top Gate with Top Contact (TGTC)*: The TGTC is rarely used due to the very small effective area for charge injection into the channel that determines very large contact resistance. In this configuration, since the organic layer should be deposited before other processing steps, the gate insulator could not be compatible with physical deposition methods such as sputtering, due to the damage to the organic material caused by energetic ions during deposition. Moreover, photolithographic patterning of the source and drain contacts is not possible. On the other hand, gate insulator material can act also as an encapsulation layer protecting device from oxygen and air exposure. This configuration is shown in Figure 1.2c.

(d) *Top Gate with Bottom Contact (TGBC)*: Also in the case of TGBC structure, the gate insulator and gate electrode can act as an encapsulation layer protecting the organic material from moisture or oxygen degradation. Nevertheless, there are number of process integration challenges associated with this configuration. First, the gate dielectric and gate electrode have to be deposited and structured on top of the organic semiconductor layer, and this process must preserve the organic material. Secondly, vertical interconnections and via between the conductive layers have to be built through the organic semiconductor needing the development of compatible etching process for the organic layer. In addition, the subsequent deposition of the dielectric material can either damage or unintentionally dope the underlying organic semiconductor. On the other hand, a fundamental advantage of this structure is represented by the low contact resistance, due to the large effective area for injecting charge into the semiconductor channel, which corresponds to the gate/drain and gate/source overlap areas. Since photolithographic patterning of gate and source/drain

electrodes is possible, the TGBC structure allows high-resolution and integration of OFETs. This configuration is illustrated in Figure 1.2d.

1.2 Working Principle of OFETs

The operating principle of OFETs based on p-type and n-type organic semiconductors can be demonstrated by the simplified energy level diagram as shown in Figure 1.3. The Figure 1.3 demonstrates the alignment of HOMO, LUMO levels of the molecule with Fermi level of the metal contact with the variation of gate voltage (V_{GS}) in n/p –type semiconductors.

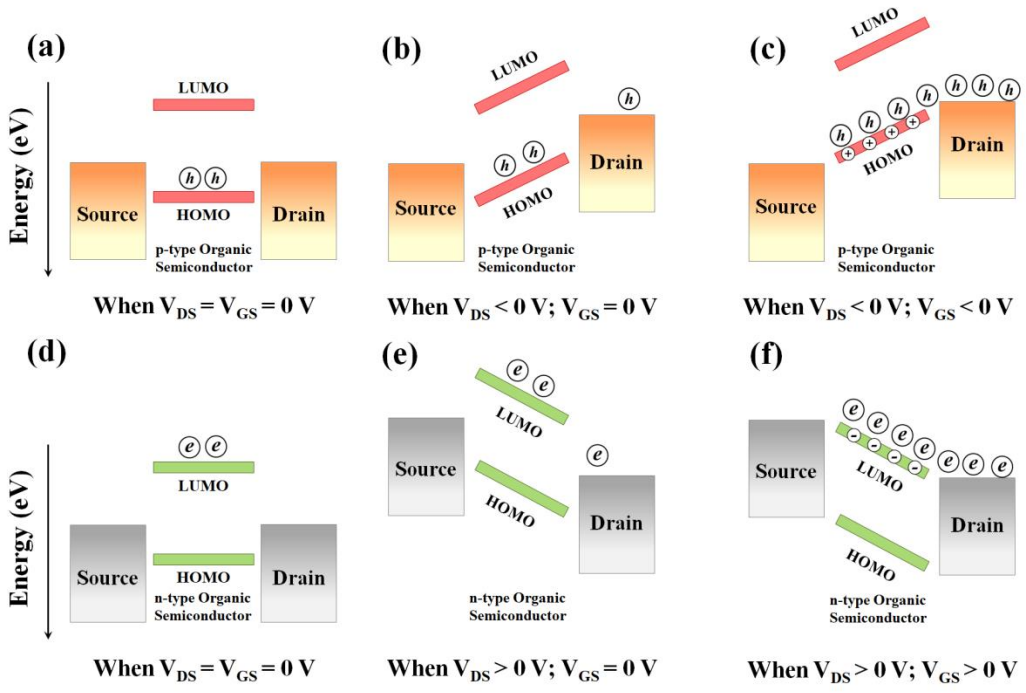

Figure 1.3 Illustration of the working principle of (a-c) p-type and (d-f) n-type OFETs with respect to the applied V_{GS}

Figure. 1.3a represents the equilibrium condition of p-type OFETs when V_{DS}= V_{GS}= 0V. At this condition, the device is in "OFF" state because no current flows from source to drain contacts. When V_{DS}< 0V and V_{GS}= 0V (Figure. 1.3b), positively charged holes, initially present in the p-type semiconductor, start moving towards the negatively biased drain contact. Since there are no mobile charges present at this condition (since V_{GS}= 0V) the current between the source to drain is negligible. When the gate voltage is applied, i.e. V_{DS}< 0V and V_{GS}< 0V, (Figure. 1.3c) mobile charges are induced in the semiconductor thin film through the dielectric layer and the transistor becomes in its "ON" state. These

mobile charges create a large electric field at semiconductor-dielectric interface which shifted the HOMO and LUMO levels of the semiconductor upwards to match the HOMO to the Fermi level of the drain contact. Since V_{DS} is already less than 0V at this condition, more number of positively charged holes will flow through the channel, thereby increasing the drain current. Similar phenomena also happen in case of n-type OFET (Figure. 1.3d to Figure. 1.3f). When V_{DS}> 0V and V_{GS}= 0V (Figure. 1.3e), negatively charged electrons, initially present in the n-type semiconductor, start moving towards the positively biased drain contact. When the gate voltage is applied, i.e. V_{DS}> 0V and V_{GS}> 0V, (Figure. 1.3f) mobile charges are induced in the semiconductor layer through the dielectric and the transistor becomes in its "ON" state.

1.3 Parameters of OFETs

In the schematic diagram, an OFET and its characteristics curves are shown in Figure 1.4 and Figure 1.5 respectively.

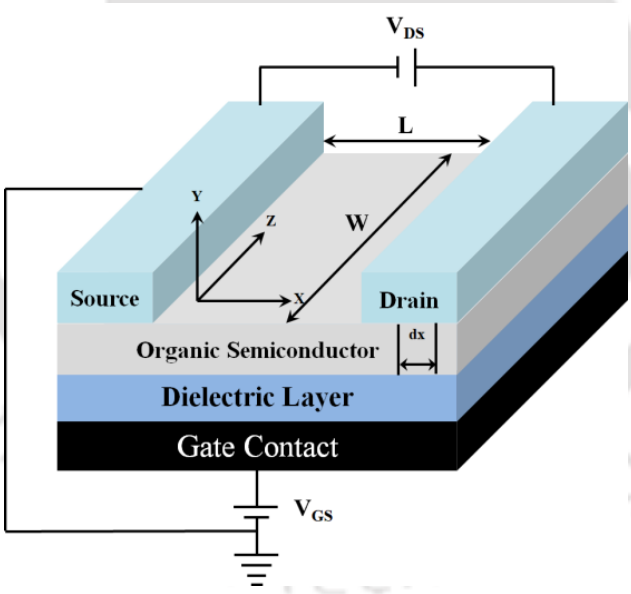

Figure 1.4 The schematic diagram an OFET.

In the output characteristics shown for n-type material (see Figure 1.5a), V_{DS} is swept while a constant V_{GS} is applied. If a positive V_{GS} is applied to an *n*-type OFET, I_{DS} will increase linearly as V_{DS} increases from 0V to a positive voltage. When V_{DS} is as large as V_{GS}, the field at the drain electrode is reduced to 0 and the channel is "pinches off". As a result, I_{DS} saturates. The maximum I_{DS} is therefore defined by V_{GS}. To measure transfer characteristics, V_{GS} is swept while a constant V_{DS} is applied (as shown in Figure 1.5b).

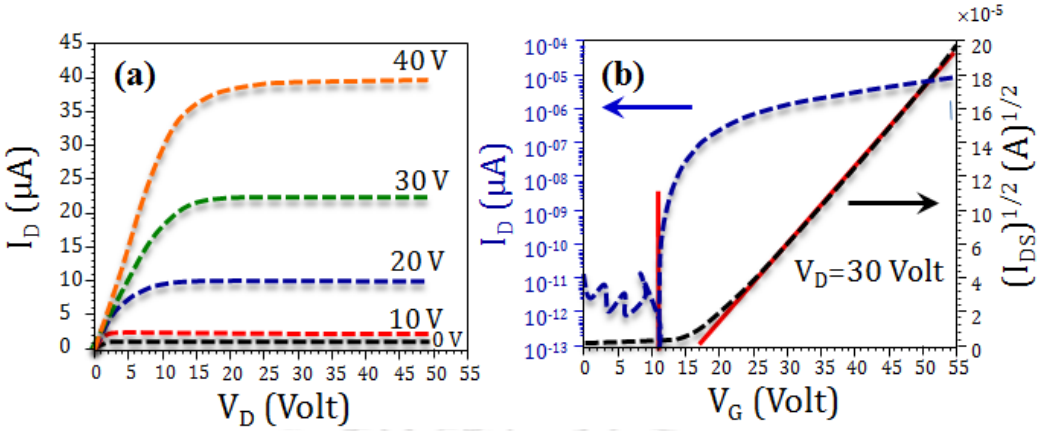

Figure 1.5 (a) Drain and (b) transfer characteristics of an ideal OFETs.

The drain characteristics can be measured in the linear region for lower V_{DS} and in the saturation regime for higher V_{DS}. The device parameters can be extracted from the equations derived for the drain current in the linear and saturation region.

$$I_{DS} = \frac{\mu W C_i}{L}\left[(V_{GS} - V_{Th})V_{DS} - \frac{{V_{DS}}^2}{2}\right] \quad (1.1)$$

This is the general form of the equation for I_{DS}, but we can apply it to the two regimes of OFETs, namely, linear and saturation. In the linear regime $V_{GS} - V_{Th} >> V_{DS}$, the accumulation region is uniform along the channel, and hence in linear region at low V_{DS},

$$I_{DS} = \frac{\mu_{in} W C_i}{L}\left[(V_{GS} - V_{Th})V_{DS}\right] \quad (1.2)$$

In the saturation regime where pinch-off of the accumulation region occurs and $V_{DS} = V_{GS} - V_{Th}$, we have,

$$I_{DS} = \frac{\mu_{sat}\, W C_i}{2L}(V_{GS} - V_{Th})^2 \quad (1.3)$$

These two equations are valid under the assumptions, that (a) the field along the channel is much lower than across it (gradual channel approximation) and (b) that the mobility is constant.[23] Here, μ (i.e. μ_{lin} *and* μ_{sat}) is the field-effect mobility in two regions for the majority charge carriers, C_i is the geometric capacitance of the dielectric and V_{Th} is the threshold voltage and k is the dielectric constant of the insulator.

From these equations, we can therefore calculate the field-effect mobility within the OFET as follows,

$$\mu_{lin} = \frac{L}{WC_iV_{DS}}\left(\frac{\partial I_{DS_{lin}}}{\partial V_{GS}}\right) \quad (1.4)$$

$$\mu_{sat} = \frac{L}{WC_i}\left(\frac{\partial I_{DS_{sat}}}{\partial V_{GS}}\right) = \frac{2L}{WC_i}\left(\frac{\partial \sqrt{I_{DS_{sat}}}}{\partial V_{GS}}\right)^2 \quad (1.5)$$

Where $$C_i = \frac{k\varepsilon_0 A}{d} \quad (1.6)$$

Fitting a straight line to the square root of the measured I_{DS} yields the band mobility μ and the threshold voltage V_{Th}. The number charge carriers (ΔN) generated in the interface can be calculated with the change in the threshold voltage (ΔV_{Th}) between two measurements using the following relation-

$$\Delta N = \frac{C_i \Delta V_{Th}}{q} \quad (1.10)$$

This ideal behaviour can be observed in organic field-effect transistors with a low trap density as shown in Figure 1.5b.

1.4 Charge Transport Mechanism in OFETs

Charge transport in OFETs is currently not fully understood. Thin film organic semiconductors are even more difficult to understand since transport, which is taking place in the vicinity of the dielectric interface, can be affected by interface defects and trap states in the dielectric. The different grain shapes, molecular packing structures, and orientations have also complicated charge transport analysis due to their complexity and variation by material and deposition technique. Despite these complexities, several transport models are proposed to interpret OFET characteristics. Charge transport in single crystal organic materials has been widely studied using time of flight measurements. Below several possible transport mechanisms are briefly discussed to account for the variety in electronic properties observed in active organic semiconductors.

1.4.1. Hopping Model

In metals and conventional semiconductors, charge transport occurs in delocalized states and is limited by the thermally induced lattice scattering (phonon) of carriers. However, such a model is no longer valid in low conductivity materials such as amorphous or organic semiconductors, where the mean free path of the carriers becomes lower than atomic distance. In these materials, hopping is the dominant charge transport mechanism between localized states. A main difference between the delocalized and localized transport is that, in the former, the transport is limited by phonon scattering whereas in the latter, it is phonon assisted. The phonon-assisted charge transport

overcomes or tunnels the potential barrier separating two adjacent molecular or ionic sites. Hopping denotes some localization of charge generally associated with the lack of long range order. Mobility is shown to be proportional to the product of two terms and given by the following relation;[24]

$$\mu = \mu_0 . \exp\left[\left(-\frac{T_0}{T}\right)^{\frac{1}{\alpha}}\right] \qquad (1.11)$$

Where, α is an integer ranging from 1 to 4. The second term also indicates hopping is a thermally activated process, and mobility should increase with temperature. Long or variable-range hopping consists of non-coherent charge transfer between non-adjacent molecular sites. Variable range hopping can occur at temperatures too low for phonon assisted hopping. In this case, when T is small, hops between nearest neighbours become increasingly unlikely. The boundary between the localized and delocalized processes is usually said to occur between mobilities of 0.1 and 1 $cm^2.V^{-1}.s^{-1}$. The mobility in highly ordered molecular crystals is close to that limit, so there is still some controversy as to whether the conductivity in these materials should be described by localized or delocalized transport. [25]

1.4.2. Band Theory Model

A useful way to visualize the difference between conductors, insulators and semiconductors is to plot the available energies for electrons in the materials. Instead of having discrete energies as in the case of free atoms, the available energy states form bands. Crucial to the conduction process is whether or not there are electrons in the conduction band. In insulators the electrons in the valence band are separated by a large gap from the conduction band. In conductors like metals the valence band overlaps the conduction band, and in semiconductors there is a small enough gap between the valence and conduction bands that thermal or other excitations can bridge the gap. With such a small gap, the presence of a small percentage of a doping material can increase conductivity dramatically. Analogous to transport of charge carriers in the extended states of the conduction and valence bands of single crystal inorganic semiconductors, the mechanism of band transport must be modified to include several important distinctions for organic semiconductors. Molecular solids can be characterized by strong covalent bonds within molecules and weak bonds between molecules which consist mostly of dipole-dipole attractions and van der Waals forces. This result in considerably less overlap of wave functions giving bandwidths in organic semiconductors that is significantly narrower, on the order of 0.1 kT (that is ~10% of the thermal energy). [26] This

gives a shorter mean free path (50 - 100 Å) and larger effective mass. In addition, the band model used in inorganic semiconductors is a one-electron approximation, whereas in organic semiconductors polarization is a many-electron phenomenon. For these reasons, the band theory alone cannot fully satisfy the transport mechanism of organic semiconductors.

1.4.3. Small Polaron or Energy Transfer Model

In some organic semiconductors, such as conjugated organic materials, energy transfer rather than charge transfer may be more favorable. This is accomplished by transferring the energy of a free charge carrier in the form of a polaron. A polaron results from the deformation of a conjugated chain under the action of a charge. In a conjugated molecule, a charge is self-trapped by the deformation it induces in the chain. The self-trapping of the charge may induce localized sites in the gap between valance and conduction band of the molecule. The creation of such interstates in conjugated organic semiconductors has been studied and identified by UV-visible spectroscopy, especially in conjugated polymers and oligomers. [27] The small polaron or energy transfer model has been one of the useful tools to describe the charge transport mechanism in organic semiconductors.[28]

From the Holstein model, small polaron, the mobility of organic semiconductor can be described as,

$$\mu = \sqrt{\frac{\pi}{2}} \cdot \frac{ea^2}{h} \cdot \frac{J^2}{\sqrt{E_b}} \cdot (kT)^{-\frac{3}{2}} \cdot exp\left(\frac{-E_b}{2kT}\right) \qquad (1.12)$$

Where E_b is polaron binding energy, which is defined as energy gain of an infinitely slow carrier due to the polarization and deformation of lattice. J is electron transfer energy and a is lattice constant. This popular model is also still only based on a one-electron model (electron-electron interactions are neglected) and tight-binding approximation.

1.4.4. Multiple Trap and Release Models

The multiple trapping and release (MTR) model is currently one of the most widely used tool to describe charge transport in amorphous silicon.[29] In this model, a narrow delocalized band is associated with a high concentration of localized states that act as charge traps. During their transit through the delocalized states, the charge carriers interact with the localized states through trapping and thermal release. This model typically has several assumptions. First, the carriers arriving at the localized states are

instantaneously trapped with a probability of close to 1. Second, the release of trapped carriers is controlled by a thermally activated process. As a result, the effective mobility can be related to the delocalized band mobility (μ_0), trap density (E_t), and thermal energy(α).

$$\mu = \mu_0 . \alpha . \exp\left[\frac{-E_t}{kT}\right] \quad (1.13)$$

In the case of a single trapping state, E_t corresponds to the distance between the trap state and delocalized band edge, and α is the ratio of the effective density of states between the trap level and the delocalized band edge. [29]

1.4.5. Grain Boundary Models

The grain boundary model has been one of the most useful tools to explain charge transport in polycrystalline materials. Grain boundaries can have a significant influence on the mobility as well as on the subthreshold behavior of TFTs, which is known from polysilicon devices. Evaporated pentacene OTFTs have often shown large crystals which form grain boundaries in the channel region. Recently, grain size dependent mobility was also observed in soluble small molecule organic semiconductors and thieno [3,2-b] thiophene.[30,31]

Trapping at the grain boundary can generally be described by two different methods. In the distributed trap approximation the gap states associated with grain boundaries are treated as uniformly distributed over the entire volume. In this model, it can be assumed that the grain boundary has a negligible thickness compared to the grain size L and contains a concentration n_t of traps at an energy E_t localized at the grain boundary. The barrier height E_B determined by charges at the grain boundary can be important for the charge transport. Therefore, the mobility of the polycrystalline material significantly depends on the position of the Fermi energy and therefore on the gate voltage. The effective mobility μ_{eff} in polycrystalline materials is given by [32],

$$\mu_{eff}^{-1} = \mu_0^{-1} + \mu_{GB}^{-1} \quad (1.14)$$

Where, μ_0 is the bulk mobility inside the grain, and μ_{GB} is the grain boundary mobility, which is generally given by thermal ionic emission over the barrier. In general, in the grain boundary model we should consider one more factor, the ratio of free to trapped carriers which depends on the gate voltage (φ), to determine real field effect mobility of the device. Therefore, the field effect mobility μ_{FET} can be described as the product of two gate voltage dependent factors. [32]

$$\mu_{FET}(V_g) = \varphi(V_g).\mu_{eff}(V_g) \quad (1.15)$$

The barrier height increases with carrier concentration p until the critical concentration $p = \frac{n_t}{L}$ is reached. Therefore, in some cases most of traps within the grain and at the interface can be filled. However, the barrier height is still increasing with increasing gate voltage. As a result, a maximum mobility can be observed at some initial gate voltage and decreases with increasing gate voltage until carrier concentration p reaches the critical concentration.

1.5 Stability of OFETs

The stability of the FET devices can be classified into two categories - (1) operational stability (2) environmental stability. OFETs are layered structures consisting of a semiconductor, a dielectric, a gate electrode, and source/drain electrodes, so each layer as well as the interfaces between the layers plays an important role in the stability. The electrical performance and operational stability of the OFETs are correlated closely with the dielectric surface properties and microstructural order of the organic semiconducting layer moreover on the density of interface traps. The semiconductor, dielectric, and semiconductor/dielectric interface are the most vulnerable sites for charge trapping. The understanding of nature and origin of these traps is critical. The operational stability is related to the stability under bias stress. Hysteresis is the main cause for the bias stress and device degradation. In the subsequent sections, hysteresis and bias-stress of the devices are discussed.

1.5.1. Hysteresis

Organic field effect transistors often exhibit a current hysteresis which is the difference between the forward and the reverse sweeps. The hysteresis effects are very well observed in OFETs and causes instability in the device operation. Therefore, it is important to study and understand the origin of the hysteresis effects in the OFETs. Hysteresis indicates the bistability in the OFET drain current (I_{DS}). It is essentially the difference in the I_{DS} curves observed during forward and backward sweeping of V_{GS} of transfer characteristic curves. It could be useful in non-volatile memory devices, but it has to be avoided in standard integrated circuits particularly for display applications.

1.5.2. Bias-stress effect

Bias-stress is the application of a (usually) constant V_{DS} and V_{GS} for an extended period of time. Moreover, we often have a persistent shift of the transfer characteristic when a gate bias is applied for a prolonged time. These phenomena are known as electrical instability or bias-stress effects. Electrical instability is most likely caused by the trapping of charge in long-lived trap states in the device layers. The term "long-lived" refers to a trapping and release time, which is long compared to the time needed to measure a transfer characteristic. Depending on the variation of I_{DS} with time, bias-stress effects are classified into two types. They are (1) bias-stress effect and (2) anomalous bias-stress effect. The bias-stress effect is due to the charge trapping at the interface and anomalous bias stress is due to the slow polarization of the gate dielectric or charge injection from the gate electrode. Under bias-stress the direction of the threshold voltage shift is such that a fully turned on OFET slowly turns itself off and vice versa under bias-stress.[33] Investigating the bias-stress in an OFET can also cause a change in effective field-effect mobility, which is attributed to an irreversible structural change in the semiconductor due to the electro-strictive effect.[34-40]

1.6 Sensors

A sensor is an analytical device, which has a response to a physical entity (such as a chlorine molecule, a photon or an electron) and converts the response into a signal that can be analysed. A sensor is composed by three main components: the *detection unit*, the *transducer* and the *processing unit* as shown schematically in Figure 1.6.[41]

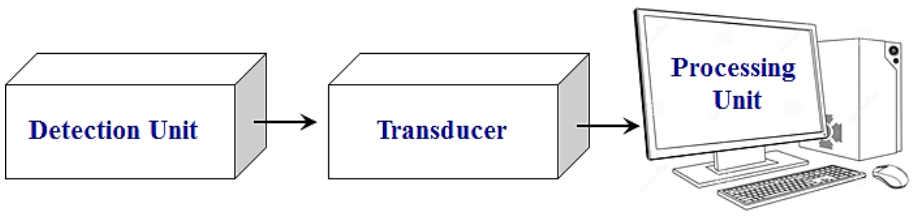

Figure 1.6 Schematic diagram of a sensor showing the three main components.

The detection unit is part of the sensor which interacts and detects the physical entity one desires to measure, which is defined here as *analyte*. The interaction can be either physical, such as photo-excitation in silicon or chemical, such as doping of an

organic semiconductor. The transducer is the component that translates the changes in the detection unit into measurable signals, usually electric signals. The processing unit is the surrounding hardware and software necessary to convert the signal from the transducer into an analysable output. The two most important features for any sensor are selectivity and sensitivity. Selectivity is the property of a sensor to selectively detect the desired analyte without interference from other species present in the system. Sensitivity determines the strength of the sensor response when it detects the analyte. OFETs are seem ideal for use in sensing applications in which there may be a desire for cheap, single-use or disposable devices that can deliver accurate results. Since the FET itself will act as a transducer, the detection unit will be integrated with the transducer itself, greatly simplifying the sensor structure. For example, an array of sensing devices can be printed in one device to realize a true lab-on-chip proposition for determining the concentration of certain target analyses in a sample. There are different types of OFET based sensor already reported in the literature, e.g. light sensor, gas sensor, explosive sensor, chemical sensor etc. In addition, organic materials are more likely to be compatible with highly selective biological recognition elements for bio-sensor application.

1.7 Thesis Synopsis

Considering the demand of recent days technology, the aim of this thesis is to introduce various methods for reducing the operational voltage of both p-channel and n-channel OFET and used them for different type of sensing applications. The main research results are detailed in seven chapters of this thesis, the contents of which can be outlined below-

Chapter 2 describes the fabrication and characterisation of a low cost, high performance, n-type organic field effect transistor on glass substrate using poly(vinyl alcohol) (PVA) as the gate dielectric material. Prior to the device fabrication, initially a conjugated molecule, namely N, N′-dioctadecyl-1, 4, 5, 8-naphthalenetetracarboxylic diimide (NDI-OD2) was synthesised as the active layer material and characterised systematically by different standard characterisation techniques. The OFET consisting of NDI-OD2 exhibits excellent output characteristics such as high electron mobility and I_{on}/I_{off} ratio with an operational voltage of 50 V. The concept describe in this chapter of developing a low cost, biodegradable and high performance OFET with biocompatible PVA dielectric with excellent electron mobility is expected to have diverse applications in disposable electronic tags, biomedical devices, and food industry packing.

After successful standersizatuon of NDI-OD2 based n-type OFET, in **Chapter 3**, we tried to reduced the operational voltage of the device below 10 V. This chapter basically discuss about the the fabrication and characterisation of low operated, electrically stable n-type organic field effect transistor using inorganic-organic bi-layer dielectric system. In this study two different derivatives NDI, namely NDI-OD2 and newly synthesised N, N′-dicyclohexyl-1, 4, 5, 8-naphthalenetetracarboxylic diimide (NDI-CY2) were used for device fabrication. Two different bi-layer dielectric configurations namely aluminium oxide/ poly (vinyl alcohol) (Al_2O_3/PVA) and aluminium oxide/poly (methyl methacrylate) (Al_2O_3/PMMA) were used in order to reduce the operating voltage of the device. It was observed that the operational voltage of both the devices consisting of NDI-OD2 and NDI-CY2 with Al_2O_3/PMMA bilayer dielectric system was reduces from 50 V to 7 V. Addition to this the devices with top contact aluminium electrodes exhibited excellent stable, n-channel behaviour for both the molecule under vacuum condition.

In **Chapter 4** we used bi-layer dielectric configuration which is mentioned in previous chapter for the fabrication of photo sensitive-organic field effect transistors (PS-OFETs). This chapter discuss in detail the basic operation, fabrication and characterisation of zinc phthalocyanine (ZnPc) based PS-OFETs which was fabricated on glass substrate using the same Al_2O_3/PMMA bi-layer dielectric configuration. The device with low operational voltage showed remarkable photo-responsivity under various incident optical power which are not previously observed. The bias stress effect of the device was investigated under both light and dark condition in vacuum. The device with high electrical stability and low threshold voltage under constant electrical bias stress is expected to have potential applications in optoelectronic devices and energy efficient sensors.

In **Chapter 5** we discuss about the key impact and the significance of multilayer polymer based dielectric system on the remarkable photo response properties of ZnPc based PS-OFETs, at various incidents optical powers. The combination of inorganic Al_2O_3 and organic non-polar PMMA are used as the bilayer dielectric configuration, whereas, in case of tri-layer dielectric system, bilayer polymer dielectrics, consisting of PMMA as a low-k dielectric polymer, on top of high-k polar PVA dielectrichave been fabricated along with Al_2O_3 as the third layer. It has been observed that with Al_2O_3/PVA/PMMA tri-layer dielectric configuration the device showed best p-channel behavior with enhanced and remarkable photo responsivity compared to Al_2O_3/PMMA due to the polarization of dipoles inside the polar-PVA dielectric which increases the charge transport through

channel. To the best of our knowledge, the photoresponsivity (R) reported here with Al_2O_3/PVA/PMMA tri-layer dielectric configuration, is the highest reported value for thin film based PS-OFETs with remarkably low operating voltage of -7 V.

The **Chapter 6** describe the importance of controlled thickness of Titanium dioxide (TiO_2) nanoparticle (NPs) thin film in hybrid tri-layer dielectric system, for reducing the operational voltage of OFET from 7 V to 2 V. This chapter successfully describe the synthetic procedure of TiO_2 sol-gel NPs and their used for the fabrication of ultra-low operation OFET. The synthesized sol-gel was thoroughly examined by different characterisation techniques prior to the device fabrication. It has been observed that at 4000 r.p.m. (~100 nm of TiO_2) the devices with N, N′-dioctyl-3, 4, 9, 10-perylenedicarboximide (PDI-C8) as the active material was showed best n-channel behaviour with operating voltage of only 2V, which is due to the better capacitor coupling among the tri-layer dielectric materials which further help to accumulate maximum numbers charge at the channel at very low gate bias. It has been also demonstrated that this optimum low-cost hybrid tri-layer dielectric system showing similar suitable gate dielectric property for flexible and transparent organic devices to operate under same ultra-low voltage which is expected to have diverse applications in future for portable organic electronics application

In **Chapter 7**, we use the tri-layer dielectric configuration which is mentioned in the previous chapter for bio-sensing application. This chapter successfully demostrated the fabrication and rapid detection method of ultra-low operating voltage, highly sensitive, n-type OFET based low-cost, disposable biosensor for the detection of gram positive and gram negative bacteria. PDI-C8 was used as the active layer material for fabrication of the device. For the detection of bacteria it has been found that due to the interaction between the surface charges of bacteria cell wall and the charge carriers in the channel, in presence of gram positive bacteria the mobility and threshold voltage of the device increases significantly whereas the opposite behaviour was observed in present of gram negative bacteria. This invention is conceptually very important because to the best of our knowledge this is the first report of such rapid method of bacterial detection with the help such low cost, disposable OFET device.

The **Chapter 8** consists of epilogue of the thesis. This chapter concludes the thesis with a summary of our main research results. A brief discussion on the exciting future prospects of organic field effect transistor based sensor at the subnanoscale is included at the end.

1.8 References

[1] Shirakawa, H.; Louis, E. J.; MacDiarmid, A. G.; Chiang, C. K.; Heeger, A. J. Synthesis of Electrically Conducting Organic Polymers : Halogen Derivatives of Polyacetylene, $(CH)_x$. *J. Chem. Soc., Chem. Commun.* **1977**, *0*, 578-580.

[2] Tang, C. W.; Vanslyke, S. A. Organic Electroluminescent Diodes. *Appl. Phys. Lett.* **1987**, *51*, 913-915.

[3] Friend, R. H.; Gymer, R. W.; Holmes, A. B.; Burroughes, J. H.; Marks, R. N.; Taliani, C.; Bradley, D. D. C.; Dos Santos, D. A.; Bredas, J. L.; Logdlund, M.; Salaneck, W. R. Electroluminescence in Conjugated Polymers. *Nature* **1999**, *397*, 121-128.

[4] Li, G.; Shrotriya, V.; Huang, J. S.; Yao, Y.; Moriarty, T.; Emery, K.; Yang, Y. High-Efficiency Solution Processable Polymer Photovoltaic Cells by Self-Organization of Polymer Blends. *Nat. Mater.* **2005**, *4*, 864-868.

[5] Kim, J. Y.; Lee, K.; Coates, N. E.; Moses, D.; Nguyen, T. Q.; Dante, M.; Heeger, A. J. Efficient Tandem Polymer Solar Cells Fabricated by All-Solution Processing. *Science* **2007**, *317*, 222-225.

[6] Facchetti, A.; Yoon, M. -H.; Marks, T. J. Gate Dielectrics for Organic Field-Effect Transistors: New Opportunities for Organic Electronics. *Adv. Mater.* **2005**, *17*, 1705-1725.

[7] Sirringhaus, H.; Tessler, N.; Friend, R. H. Integrated Optoelectronic Devices Based on Conjugated Polymers. *Science* **1998**, *280*, 1741-1744.

[8] Dodabalapur, A.; Bao, Z.; Makhija, A.; Laquindanum, J. G.; Raju, V. R.; Feng, Y.; Katz, H. E.; Rogers, J. Organic Smart Pixels. *Appl. Phys. Lett.* **1998**, *73*, 142-144.

[9] Baude, P. F.; Ender, D. A.; Haase, M. A.; Kelley, T. W.; Muyres, D. V.; Theiss, S. D. Pentacene-Based Radio-Frequency Identification Circuitry. *Appl. Phys. Lett.* **2003**, *82*, 3964-3966.

[10] Steudel, S.; Myny, K.; Arkhipov, V.; Deibel, C.; Vusser, S. De.; Genoe, J.; Heremans, P. 50 MHz Rectifier Based on an Organic Diode. *Nat. Mater.* **2005**, *4*, 597-600.

[11] Janata, J.; Josowicz, M. Conducting Polymers in Electronic Chemical Sensors. *Nat. Mater.* **2003**, *2*, 19-24.

[12] Sun, Z. H.; Li, J. H.; Liu, C. M.; Yang, S. H.; Yan, F. Enhancement of Hole Mobility of Poly(3-hexylthiophene) Induced by Titania Nanorods in Composite Films. *Adv. Mater.* **2011**, *23*, 3648-3652.

[13] Yan, F.; Tang, H. Application of Thin-Film Transistors in Label-Free DNA Biosensors. *Expert Rev. Mol. Diagn.* **2010**, *10*, 547-549.

[14] Mok, S. M.; Yan, F.; Chan, H. L. W. Organic Phototransistor Based on Poly (3-Hexylthiophene)/TiO2 Nanoparticle Composite. *Appl. Phys. Lett.* **2008**, *93*, 023310 (1-3).

[15] Mannsfeld, S. C. B.; Tee, B. C-K.; Stoltenberg, R. M.; Chen, C. V. H-H.; Barman, S.; Muir, B. V. O.; Sokolov, A. N.; Reese, C.; Bao, Z. Highly Sensitive Flexible Pressure Sensors with Microstructured Rubber Dielectric Layers. *Nat. Mater.* **2010**, *9*, 859-864.

[16] Johnson, K. S.; Needoba, J. A.; Riser, S. C.; Showers, W. J. Chemical Sensor Networks for the Aquatic Environment. *Chem. Rev.* **2007**, *107*, 623-640.

[17] Bartic, C.; Borghs, G. Organic Thin-Film Transistors as Transducers for (Bio) Analytical Applications. *Anal. Bioanal. Chem.* **2006**, *384*, 354-365.

[18] Berggren, M.; Richter-Dahlfors, A. Organic Bioelectronics. *Adv. Mater.* **2007**, *19*, 3201-3213.

[19] Owens, R. M.; Malliaras, G. G. Organic Electronics at the Interface with Biology. *MRS Bull.* **2010**, *35*, 449-456.

[20] Dey, A.; Kalita, A.; Iyer, P. K. High-Performance n-Channel Organic Thin-Film Transistor based on Naphthalene Diimide. *ACS Appl. Mater. Interfaces* **2014**, *6*, 12295–12301.

[21] Shukla, D.; Nelson, S. F.; Freeman, D. C.; Rajeswaran, M.; Ahearn, W. G.; Meyer, D. M.; Carey, J. T. Thin-Film Morphology Control in Naphthalene-Diimide-based Semiconductors: High Mobility n-Type Semiconductor for Organic Thin-Film Transistors. *Chem. Mater.* **2008**, *20*, 7486–7491.

[22] Xu, X.; Yao, Y.; Shan, B.; Gu, X.; Liu, D.; Liu, J.; Xu, J.; Zhao, N.; Hu, W.; Miao, Q. Electron Mobility Exceeding 10 $cm^2 V^{-1} s^{-1}$ and Band-Like Charge Transport in Solution-Processed n-Channel Organic Thin-Film Transistors. *Adv. Mater.* **2016**, *28*, 5276–5283.

[23] Horowitz, G. *Organic Electronics: Materials, Manufacturing and Applications*; Wiley-VCH Verlag GmbH & Co. KGaA, Weinheim, FRG, Germany, 2006.

[24] Holstein, T. Studies of Polaron Motion: Part I. The Molecular-Crystal Model. *Ann. Phys.* **1959,** *8*, 325-342.

[25] Horowitz, G. Organic Field-Effect Transistors. *Adv. Mater.* **1998**, *10*, 365-377.

[26] Warta, W.; Stehle, R.; Karl, N. Ultrapure, High Mobility Organic Photoconductors. *Appl. Phys. A* **1985**, *36,* 163-170.

[27] Salaneck, W. R. Conjugated Polymer Surfaces and Interfaces. *Phil. Trans. R. Soc. Lond. A* **1997,** *355,* 789-799.

[28] Holstein, T. Studies of Polaron Motion: Part II. The Molecular-Crystal Model. *Ann. Phys.* **1959,** *8,* 343-389.

[29] Le Comber P. G.; Spear, W. E. Electronic Transport in Amorphous Silicon Films. *Phys. Rev. Lett.* **1970,** *25,* 509-511.

[30] Gundlach, D. J.; Royer, J. E.; Park, S. K.; Subramanian, S.; Jurchescu, O. D.; Hamadani, B. H.; Moad, A.J.; Kline, R.J.; Teague, L.C.; Kirillov, O.; Richter, C.A. Contact-Induced Crystallinity for High-Performance Soluble Acene-Based Transistors and Circuits. *Nat. Mater.* **2008**, *7*, 216-221.

[31] Kuo, C. C.; Payne, M. M.; Anthony, J. E.; Jackson, T. N. TES Thienyl Pentacene Solution-Processed OTFTs with 1 cm^2/V.s Mobility. *IEDM Technical. Digest.* **2004,** 373-376.

[32] Ahmed, S. S.; Kim, D. M.; Shichijo, H. Modeling of Accumulation-Mode MOSFET's in Polysilicon Thin Films. *IEEE Electron Device Lett.* **1985,** *6,* 313-315.

[33] Salleo, A.; R. A. Street. Light-Induced Bias Stress Reversal in Polyfluorene Thin-Film Transistors. *J. Appl. Phys.* **2003,** *94,* 471-479.

[34] Street, R. A. Bias-Induced Change in Effective Mobility Observed in Polymer Transistors. *Phys. Rev. B* **2008,** *77,* 165311 (1-8).

[35] Majewski, L. A.; Grell, M.; Ogier, S. D.; Veres, J. A Novel Gate Insulator for Flexible Electronics. *Org. Electron.* **2003,** *4*, 27-32.

[36] Veres, J.; Ogier, S. D.; Leeming, S. W.; Cupertino, D. C.; Khaffaf, S. M. Low-K Insulators as the Choice of Dielectrics in Organic Field-Effect Transistors. *Adv. Funct. Mater.* **2003,** *13*, 199-204.

[37] Stassen, A. F.; de Boer, R. W. I.; Iosad, N. N.; Morpurgo, A. F. Influence of the Gate Dielectric on the Mobility of Rubrene Single-Crystal Field-Effect Transistors. *Appl. Phys. Lett.* **2004,** *85*, 3899-3901.

[38] Zirkl, M.; Haase, A.; Fian, A.; Schon, H.; Sommer, C.; Jakopic, G.; Leising, G.; Stadlober, B.; Graz, I.; Gaar, N.; Schwodiauer, R.; Bauer-Gogonea, S.; Bauer, S. Low-Voltage Organic Thin-Film Transistors with High-K Nanocomposite Gate Dielectrics for Flexible Electronics and Optothermal Sensors. *Adv. Mater.* **2007,** *19*, 2241-2245.

[39] Haas, U.; Gold, H.; Haase, A.; Jakopic, G.; Stadlober, B. Submicron Pentacene-Based Organic Thin Film Transistors on Flexible Substrates. *Appl. Phys. Lett.* **2007,** *91*. 043511 (1-3).

[40] Irimia-Vladu, M.; Marjanovic, N.; Vlad, A.; Ramil, A. M.; Hernandez-Sosa, G.; Schwodiauer, R.; Bauer, S.; Sariciftci, N. S. Vacuum-Processed Polyaniline-C-60 Organic Field Effect Transistors. *Adv. Mater.* **2008,** *20*, 3887-3892.

[41] Grimes, C. A.; Dickey, E. C. Pishko, M. V. *Encyclopedia of Sensors*, American Scientific Publishers, 2006.

2

Low Cost, High Performance n-type Organic Field Effect Transistor

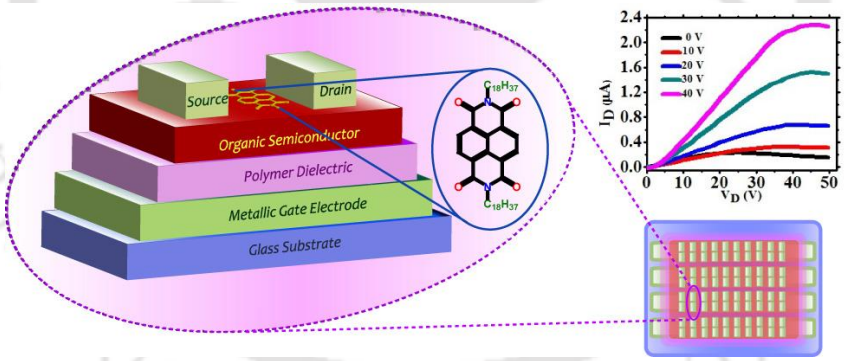

[1] **Dey, A.;** Kalita, A.; Iyer, P. K. High-Performance n-Channel Organic Thin-Film Transistor Based on Naphthalene Diimide. ***ACS Appl. Mater. Interfaces*** 2014**,** *6,* 12295-12301.

2

Low Cost, High Performance n-type Organic Field Effect Transistor

Organic Semiconductors have attracted increasing attention because of their important roles in electronics, such as display, power, sensor and memory chips.[1–9] Among them, OFETs represent one of the important building blocks for developing organic and printed electronics because their transistor performance is comparable to that of Si-FETs and they have advantages of light weight, flexibility, transparency, facile processing methods, and low manufacturing costs. However, the development of n-type OFETs still lags behind that of p-type OFETs because of their inferior performance, air instability, and few other issues.[10–15] The performance of p-type OFETs has recently improved substantially and become comparable to that of a Si-FETs: for example, the hole mobilities of pentacene,[16] and a rubrene single crystal,[17] have been reported to be as high as 3 and 15 $cm^2V^{-1}s^{-1}$ respectively. In contrast, progress in n-type OFET materials has been inadequate and delayed by several inherent problems.[18–21] It is recognized that the electron carriers in n-type OFET materials undergo detrimental trapping processes, i.e., they show strong instability[22] when they are exposed to H_2O and O_2 in air.[23] As a consequence, in most cases, the electron mobility (μ_e) of n-type OFET materials dramatically decreases when exposed to air. Among the rare building blocks useful for producing n-type OSCs, rylene diimides, especially perylene and naphthalene derivatives, have so far proved to be the most successful electron-

transporting units.[24–34] Small molecule perylene diimides (PDIs) are good candidates for n-type organic semiconductors because they assemble in π-stacks that enhance the intermolecular π-orbital overlap and facilitate charge transport. Many modifications have been introduced in PDIs that have led to the improved solubility in common solvents, in addition to the improvement in electron mobility and enlarged electron affinity for operation stability in air. Naphthalene diimide (NDI) based molecules have also been intensively investigated as n-type semiconductors for OFETs.[35,36] This class of material not only demonstrates a highly planar conjugated backbone, but also easily tuneable electronic properties through modification at the core and/or the imide position with electron-withdrawing groups or conjugated units.[37] On the basis of core expansion or core-substitution strategies, several NDI derivatives with symmetrical structures have been designed and synthesized for n-type OFETs with high electron mobility.[38] The electron-accepting NDI material is an analogue of PDI, provides a planar conjugated bicyclic structure, which leads to strong π–π interactions and offers improved charge-transporting properties between the chains. In addition, the introduction of alkyl chains at the 'N' position of the imide ring allows good control over physical properties such as solubility and processability, crystallization, and self-assembly capability. Moreover, the presence of strong electron-withdrawing groups within the naphthalene moiety also lowers the LUMO level, thereby increasing the air stability of the n-type semiconductor.[39-43] The performances of OFETs are not only dependent on the organic semiconductors and their molecular arrangement within the active channel of the device but also on the gate dielectric that controls the charge flow. Inorganic oxides such as SiO_2, Al_2O_3, TiO_2, etc. are frequently utilized for OFET fabrication as gate dielectric materials with higher gate dielectric constant. But most of these high dielectric constant materials suffer from expensive deposition methods. Therefore, organic dielectric materials which can be processed by solution casting methods such as PVA, PMMA etc. are frequently utilized in OFET device fabrication as well as for biomedical and biodegradable device application.[44]

In this chapter, we have described the synthesis and characteristics of a new n-type organic small molecule namely, NDI-OD2 and its application toward highly efficient OFET devices. We have exploited the biocompatibility and low-cost design of the devices using pristine PVA as organic dielectric material spin-casted on the glass substrate and used it without further treatment. PVA is very economical, has high dielectric constant and good surface alignment, and is well known to be

compatible with electronic devices; because of the US FDA approval, it has also been utilized extensively in biomedical devices. Despite these advantages, PVA has a fundamental drawback of degrading the devices because of its hygroscopic nature. Hence, this material has not been generally preferred as a dielectric for OFET or if utilized, it must be cross-linked with a linker such as ammonium dichromate or an additional buffer layer is needed to prevent the device degradation. We optimized a well-ordered smooth film of NDI-OD2 by thermal deposition method directly over the pristine PVA layer, such that the fabricated devices demonstrated excellent performances with very low leakage current and excellent mobility. However, it was observed that when NDI-OD2 was processed by solution method, it forms needle shaped crystalline microstructures, whereas when thermally deposited, it assumes the form of smooth 2D film following Stranski–Krastanov growth pattern. The NDI-OD2 showed typical n-type OFET performance with the maximum electron mobility found to be 1.0 $cm^2 V^{-1} s^{-1}$ under vacuum. Most notably we have been successful in performing experiments which demonstrate that the NDI-OD2 devices can work in the presence of spin-casted pristine PVA, with a conceptually important feature that these n-type OFETs can also be biodegraded when exposed to environment having high moisture content because of the presence of this PVA dielectric. We observed that these NDI-OD2 devices exhibit performance loss in a controlled manner followed by complete failure on continuous exposure for few days to high moisture environment. Thus, low-cost and environmentally friendly n-type OFETs with high electron mobility can be achieved utilizing a combination of conjugated small molecules and biodegradable dielectric material such PVA.

2.1 Experiments

2.1.1 Materials

1, 4, 5, 8-naphthaleneteracarboxylic dianhydride, octadecylamine, quinoline, zinc acetate, and aluminum wire (99.999% purity) were used as received from Sigma Aldrich. PVA (M_W= 1, 15,000 g/mol) was purchased from Loba Chemie (99% purity) and used as received. Microscope glass slides (thickness 1-1.2mm) purchased from Jain Scientific Glass Works, India, was used as the device substrate without any surface modification. NDI-OD2 molecule was synthesized following the procedure reported in literature by the

direct condensation of 1, 4, 5, 8-naphthalene dianhydride with octadecylamine reported previously.[45]

2.1.2 Characterization Details

The solution and thin film UV-visible absorption spectra of NDI-OD2 molecule were recorded on a Perkin Elmer Lambda 35 spectrophotometer. Emission Spectra were measured on a Varian-Cary Eclipse spectrophotometer. Field emission scanning electron microscopy (FESEM) images were recorded in a Sigma Carl Zeiss scanning electron microscope. Atomic force microscopy (AFM) images were taken by Agilent 5500-STM instrument. Transmission electron microscopic (TEM) studies were done using a Tecnai G2 F20 S-twin JEOL 2100 transmission electron microscope. Electrochemical measurements were done using CH instrument. Thermo gravimetric analysis (TGA) measurements were performed on Shimadzu thermo gravimetric analyser (model DTG-60) under a nitrogen flow at a heating rate of 10 °C min^{-1}. The powder and thin film X-ray diffraction (XRD) pattern was recorded by high power (18 kW) X-ray diffractometer (Rigaku TTRAX III) with Cu Kα radiation.

2.2 Results and Discussion

2.2.1 Theoretical Study

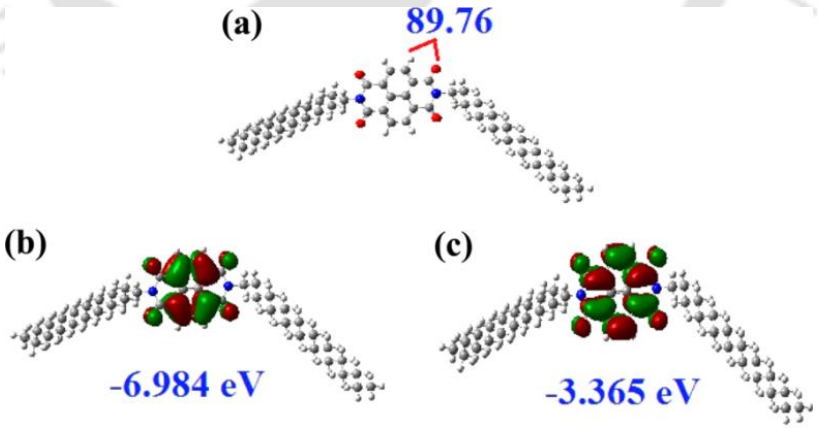

Figure 2.1 (a) Optimized structure, (b) HOMO and (c) LUMO energy levels of the NDI-OD2 molecule, obtained by DFT calculation.

To predict the minimum-energy confirmation of the monomer backbone and the LUMO/HOMO, we performed the DFT calculation (B3LYP/6-31G (d)) on the NDI-OD2

molecule. The dihedral angle between the main NDI core and the neighbouring C-18 alkyl unit is calculated to be ~89.76°. The theoretical HOMO-LUMO position of NDI-OD2 was found to be (−6.984 eV, −3.365 eV), which reveals that the energy gaps reflect the chemical activity of the molecule. LUMO as an electron acceptor represents the ability to obtain an electron, HOMO represents the ability to donate an electron. The geometrically optimized structures and their corresponding HOMO and LUMO structures are shown in Figure 2.1.

2.2.2 Band Gap Analysis

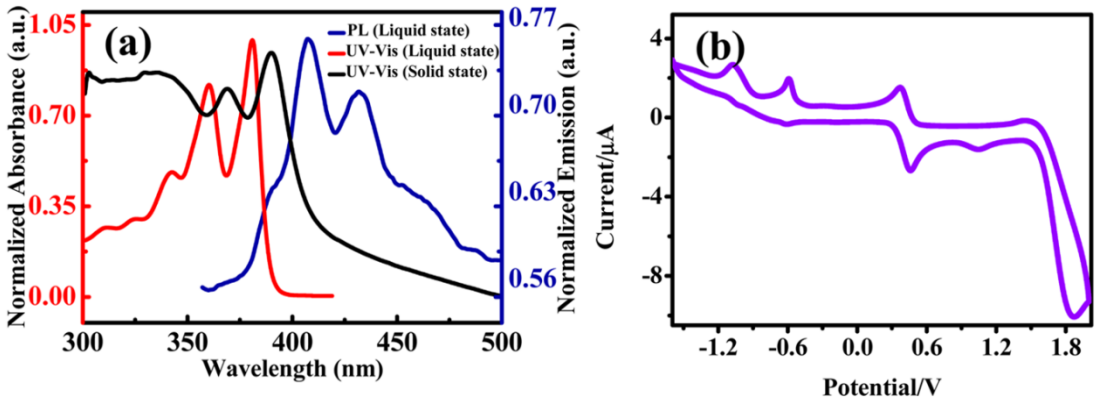

Figure 2.2 (a) Absorption and emission spectra of NDI-OD2 monomer. (b) Cyclic voltammogram of NDI-OD2 monomer at a scan rate of 50 mV/s.

The optical, electrochemical and theoretical band gap of the material was estimated by UV-Vis absorption and cyclic voltammetry analysis. UV-visible absorption and emission spectra of the molecule were measured in a dilute solution of chloroform (1×10^{-3} M). For solid state study, a thin film of the molecule was thermally deposited on glass substrate under 1×10^{-7} mbar pressure. The UV-visible spectrum of NDI-OD2 shows absorption peaks at 381, 360, and 341 nm due to characteristic π–π* transitions.[46] The spectral absorptions of a thin film of NDI-OD2 is red-shifted by about 10 nm as compared to the solution (Figure 2.2a). This shift in the film form is due to the additional intermolecular interactions leading to conformational adjustments of the molecules that impose changes in the conjugation length.[47] The absorption pattern similarity between the thin film and the solution spectra suggests a structurally well-organized molecular system.[48] In $CHCl_3$, the emission spectrum shows peaks at 406 and 431 nm, with a weak blue emission and displaying almost similar mirror image of the absorption spectrum (Figure 2.2a).[49]

The redox properties of the NDI-OD2 were evaluated using cyclic voltammetry. NDI-OD2 film was drop-casted from chloroform solution onto a 2 mm diameter Glassy carbon electrode. The cyclic voltammogram was recorded against Ag/Ag+ reference electrode in anhydrous acetonitrile with 0.1 M tetrabutylammonium perchlorate (TBAP) as the supporting electrolyte at a scan rate of 50 mV/s. The electrochemical potentials were estimated from the onset of the oxidation and reduction sweeps. The voltammogram was calibrated using Fc/Fc^{+} redox couple. The redox potential thus obtained was converted to the corresponding energy levels assuming the absolute HOMO energy level of ferrocene to be −4.8 eV. (Equation 2.1 and Equation 2.2).[50]

$$E_{HOMO} = -(E_{ox\ onset} + 4.8)\ eV \quad (2.1)$$

$$E_{LUMO} = -(E_{red\ onset} + 4.8)\ eV \quad (2.2)$$

The estimated HOMO and LUMO energy levels and the electrochemical as well as optical band gap of the NDI-OD2 is summarized in Table 2.1, whereas the representative scans of the NDI-OD2 thin films are shown in Figure 2.2b.

Table 2.1 Summary of Band Gap Calculation Data for NDI-OD2*

$E_{HOMO}^{(CV)}$ (eV)	$E_{LUMO}^{(CV)}$ (eV)	E_g^{CV} (eV)	E_g^{UV} (eV)	E_g^{Th} (eV)
-6.414	-3.394	3.02	3.18	3.61

2.2.3 Thermal Studies

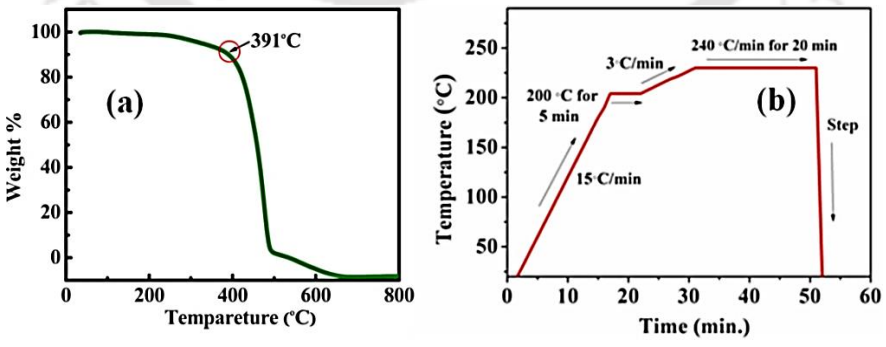

Figure 2.3 (a) TGA plot with heating rate of 10°C min^{-1} and (b) Thermal deposition curve of NDI-OD2.

For any organic device, especially for n-type OFETs, superior thermal properties are very important since they are directly related to practical issues such as device fabrication, operation and longevity. The thermal stability of NDI-OD2 was investigated

with thermo gravimetric analysis (TGA) at a heating rate of 10 °C min^{-1} under nitrogen atmosphere. The NDI-OD2 was thermally stable up to 391 °C. The degradation begins at ~393 °C and complete degradation is observed above 500 °C (Figure 2.3a). Because the maximum deposition temperature attained during the device fabrication (room temperature to ~230 °C sublimation) (Figure 2.3b) was much below the degradation temperature of the NDI-OD2, its performance remained unaffected as observed from the smooth film formation and the OFET device data.

2.2.4 Thin Film Microstructure

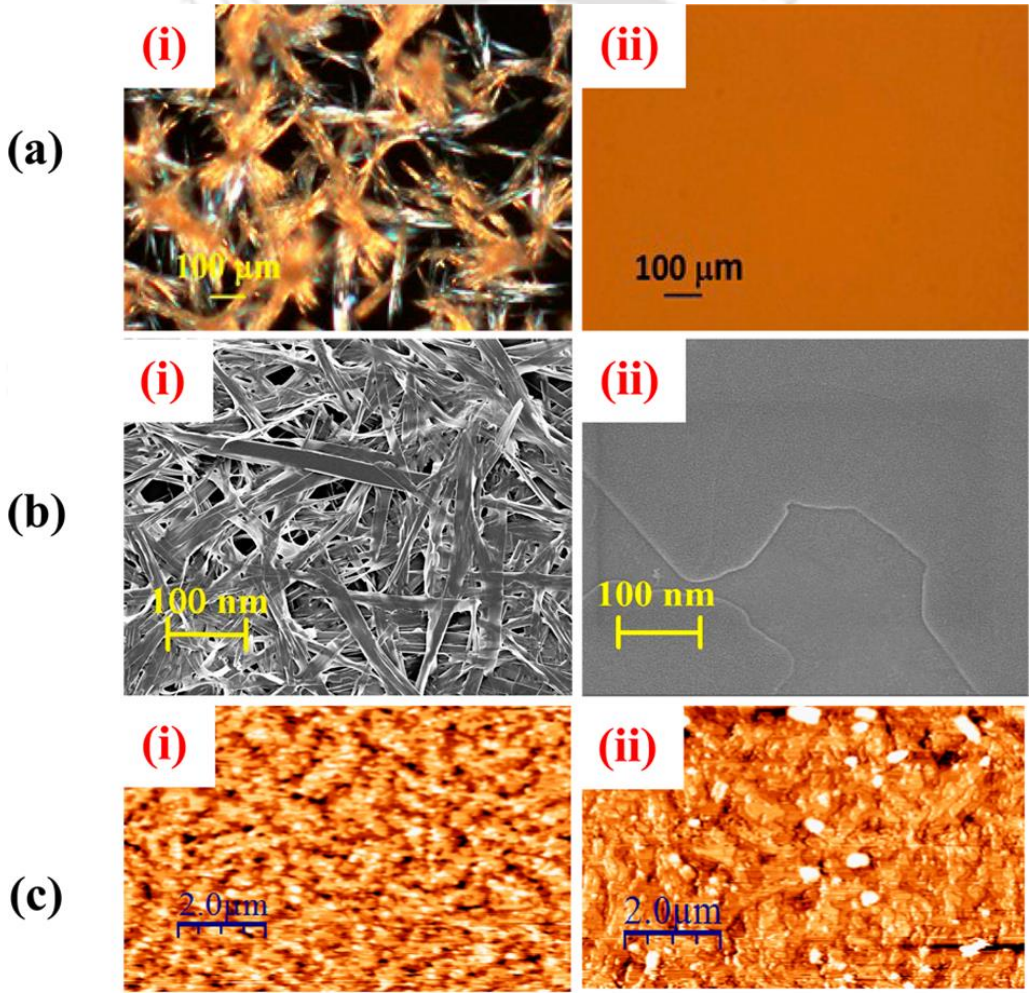

Figure 2.4 (a) Optical microscopy images, (b) FESEM images, and (c) AFM images of (i) spin-cast and (ii) thermally deposited films of NDI-OD2.

Different microscopic analysis and XRD studies were utilized to investigate the surface morphologies of the fabricated thin films. Figure 2.4 shows the optical

microscopic images, FESEM and AFM of spin-cast (~55 nm, 2000 rpm) and thermally deposited (~60 nm, 1 × 10^{-7} mbar pressure) NDI-OD2 film at room temperature. In polarized optical microscopy (Figure 2.4a, i and ii) and FESEM (Figure 2.4b, i and ii) the NDI-OD2 appeared as a sharp single needle-type microstructure when spin-cast by solution method, whereas, the thermally deposited films give highly smooth 2D film following Stranski-Krastanov growth pattern. The thermally grown thin film of NDI-OD2 shows a very densely packed smooth film in AFM analysis with RMS roughness of ~5.64 nm (Figure 2.4c, ii) which is requisite for efficient FET behaviour, whereas, the spin-cast film (Figure 2.4c, i) shows ~47.90 nm roughness.

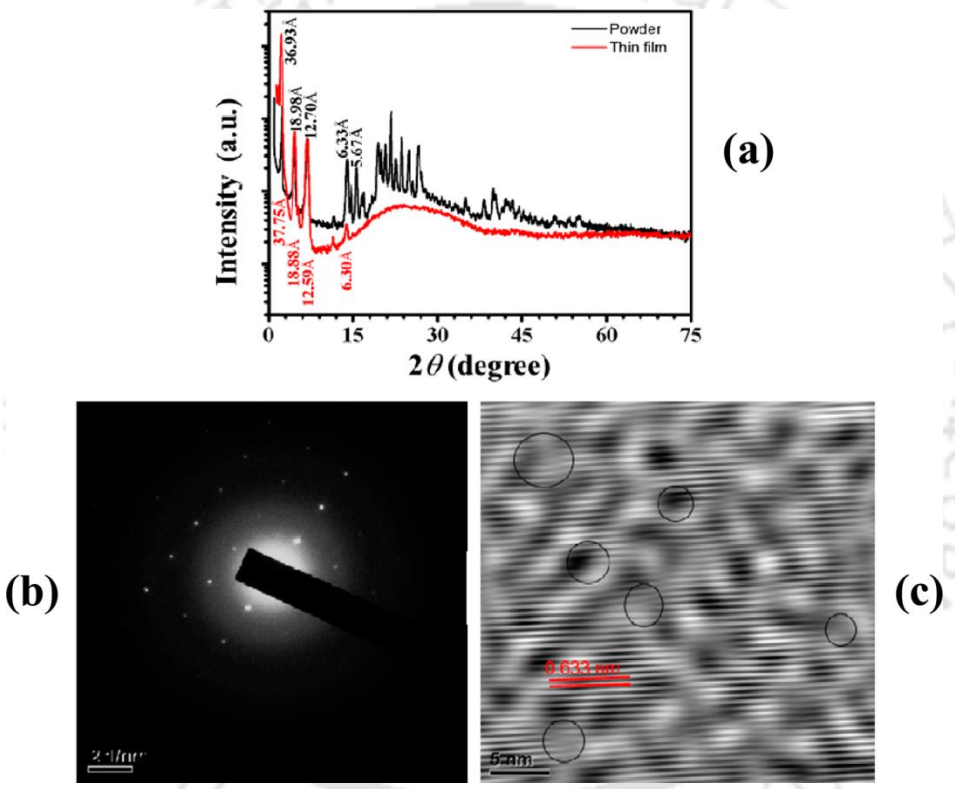

Figure 2.5 (a) XRD patterns, (b) SAED pattern, and (c) HRTEM of NDI-OD2.

The crystalline nature of NDI-OD2 was confirmed by using high power (18 kW) X-ray diffractometer. Figure 2.5a displays XRD patterns for both thin film and powder. It is evident that the sharp peaks observed in the small-angle regions support the formation of molecules that were highly ordered and crystalline in nature. The lamellar d-spacing for powder and thin film of around 2θ = 2.4° was found to be 36.93 and 37.75 Å, respectively. However, a careful observation of the XRD patterns reveals that (i) majority of the diffraction peaks observed in the powder were also obtained in thin films for 2θ ≤ 15° confirming that the thin films have the same molecular packing motif as seen in powders.

With increasing 2θ > 15°, both powder and thin film exhibit completely different properties, i.e., while the powder sample exhibits more number of diffraction lattice planes giving rise to different Bragg peaks, the thin film displays a broad peak in the 2θ range of 16 to 34°. This could be correlated to the growth nature of the evaporated film on the substrate. This is also in excellent agreement with the earlier reports on similar system.[51] (ii) the XRD peaks of the powder sample exhibits more asymmetry in nature and the broadness of the peaks is observed to be larger in the thin films as compared to the powders. The average size of the crystallites calculated using the Bragg peak at around 2θ = 14° corresponding to 25 and 23 nm for powder and thin film, respectively. To further investigate the crystalline nature, we obtained selected area electron diffraction (SAED) patterns and high-resolution transmission electron microscope (HRTEM) images as shown in Figure 2.5b and Figure 2.5c respectively. Closer observation of the HRTEM image reveals the presence of finite dislocations as highlighted by circles causing possible strain and resulting in asymmetric XRD peaks (Figure 2.5a). In addition, the interplanar spacing determined from HRTEM image is about 6.33 Å, which is in good agreement with the value calculated from the XRD peak at around 2θ = 14°. The crystalline nature of NDI-OD2 is also confirmed from SAED results as shown in Figure 2.5b.

2.2.5 OFET Device Fabrication and Characterization

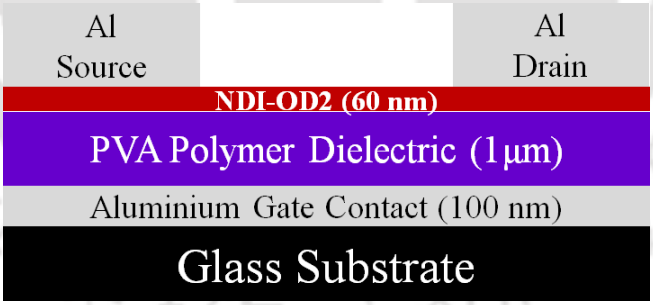

Figure 2.6 Device structure of the fabricated NDI-OD2 based n-type OFET.

OFETs based on NDI-OD2 were fabricated with a bottom gate top contact configuration (Figure 2.6). A simple glass slide was used as a substrate and aluminium (Al) (100 nm) gate electrode was thermally deposited above it. A spin-coated film of poly(vinyl alcohol) (PVA) thickness ~1 μm (1000 rpm) was used as a dielectric material having capacitance ~8.854 nF cm^{-2}. A 60 nm thick (±10 nm) NDI-OD2 semiconductor film was thermally deposited on the Al coated glass slide (substrate temperature = room temperature), at a pressure of 1 × 10^{-7} mbar. Al source and drain contacts (100 nm) were

deposited on the organic layer through a shadow mask with channel length (L) and width (W) of 50 μm and 1 mm, respectively. All the electrical properties were measured under vacuum using a Keithley 4200-SCS semiconductor parameter analyser. The mobility of the saturated region was extracted from the following Equation 2.3-

$$I_{DS} = C_i \mu_e . \left(\frac{W}{2L}\right) . (V_{GS} - V_{Th})^2 \qquad (2.3)$$

Where, I_{DS} is the drain current, C_i is the capacitance per unit area of the gate dielectric layer, μ_e is the field effect electron mobility, W and L are the channel width and length, V_{GS} and V_{Th} are the gate voltage and threshold voltage, respectively. The output and transfer characteristic curves for NDI-OD2 based OFET are shown in Figure 2.7.

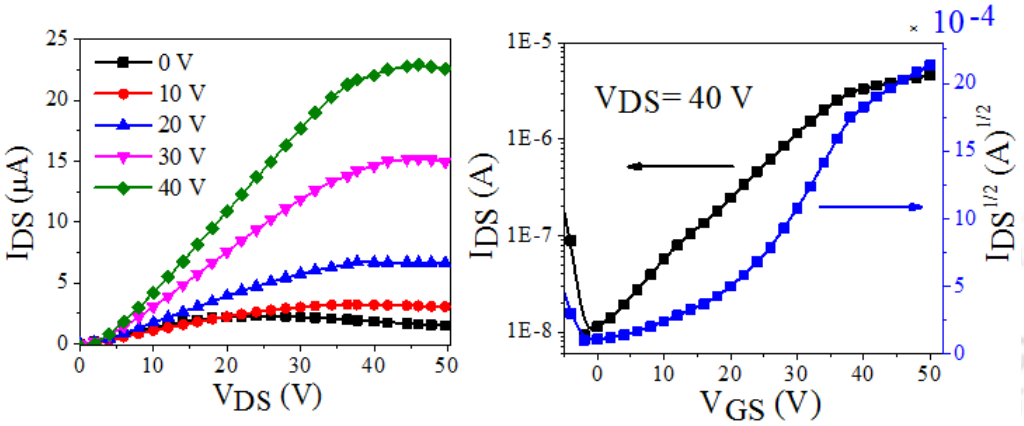

Figure 2.7 (a) Output and (b) transfer characteristics curves of OFET device based on NDI-OD2 monomer; I_{DS} was obtained at drain-source voltage V_{DS} = 40 V.

The NDI-OD2 molecules in OFET devices, sublimed at room temperature over pristine PVA dielectric, exhibited excellent electron mobility as high as 1.0 $cm^2\ V^{-1}\ s^{-1}$ (average value for 75 devices was ~0.68 $cm^2\ V^{-1}\ s^{-1}$) under vacuum with threshold voltage of 16.24 V and current on-to-off ratio 1×10^2. Because the XRD pattern of the evaporated film of NDI-OD2 reveals very good crystalline nature and AFM analysis confirms that these thermally grown thin film shows a very densely packed smooth morphology, such densely packed semiconducting layers tend to exhibit larger off-current levels, resulting in smaller on-to-off current ratios and is in agreement with a recent report.[52] The mobility values which we report here are one of the highest in a bottom-gated n-type OFET device fabricated on glass substrate using biocompatible PVA dielectric. In addition, the use of PVA dielectric further allowed us to degrade the device in a highly controlled manner on simple exposure to moisture, thereby, further reducing the recycling cost of the product after end use. On exposure of these NDI-OD2 molecule-based devices to an environment having >80% moisture, the drastic degradation of the device commences with observation

of loss in mobility followed by complete device failure within 10 days and confirms with conventional knowledge that pristine PVA dielectrics degrade the OFET devices when exposed to moisture containing environment. The thermally evaporated films of NDI-OD2 molecules on PVA were found to have very good layer structure. PVA is known for its high surface energy compared to other organic dielectric materials due to its hydrophilic nature.[53] Closer inspection revealed that NDI-OD2 forms a very smooth, amorphous-like film on PVA surface with surface roughness of less than ~5.64 nm. Hence, higher mobility values are observed with NDI-OD2 active layer and PVA dielectric here. In addition to the role of dielectric, it is known that the length of the alkyl chains can also effectively improve the OFET device performance. According to Pei et al., organic materials that possess longer alkyl chains (branched or linear) exhibited higher carrier mobilities.[54] The NDI-OD2 molecule based material reported here possesses two symmetrical octadecyl chains and demonstrates excellent electron mobility in the presence of low-cost device using commercially available materials such as aluminium and PVA on glass substrate, which allows to scale up the device fabrication and production on larger substrates and quantities.

2.3 Conclusion

The synthesis, fabrication, and characterization of alkyl chain-substituted naphthalene diimide molecule was described, which in combination with a biocompatible PVA dielectric was utilized to fabricate n-type OFETs with high electron mobility on glass substrate. The NDI-OD2 material is obtained in a single step from commercially available materials allowing development of these materials up to a large scale. We have also avoided the use of Si-substrates and gold electrodes and instead used glass and aluminium, in addition to the economical PVA as the dielectric material to keep the overall cost of this device very low as well as degradable after use. A combination of several thin film characterizations (Optical microscopy, FESEM, AFM, XRD and TEM) techniques reveals that the thermally deposited NDI-OD2 has significant influence on film morphology and molecular packing which enhanced the charge.

2.4 References

[1] Yan, H.; Chen, Z.; Zheng, Y.; Newman, C.; Quinn, J. R.; Dotz, F.; Kastler, M.; Facchetti, A. A High-Mobility Electron-Transporting Polymer for Printed Transistors. *Nature* **2009,** *457,* 679–686.

[2] Usta, H.; Facchetti, A.; Marks, T. J. n-Channel Semiconductor Materials Design for Organic Complementary Circuits. *Acc. Chem. Res.* **2011,** *44,* 501–510.

[3] Guo, X.; Kim, F. S.; Seger, M. J.; Jenekhe, S. A.; Watson, M. D. Naphthalene Diimide-Based Polymer Semiconductors: Synthesis, Structure–Property Correlations, and n-Channel and Ambipolar Field-Effect Transistors. *Chem. Mater.* **2012,** *24,* 1434–1442.

[4] Guo, Y.; Yu, G.; Liu, Y. Functional Organic Field-Effect Transistors. *Adv. Mater.* **2010,** *22,* 4427–4447.

[5] Chen, H.; Guo, Y.; Mao, Z.; Yu, G.; Huang, J.; Zhao, Y.; Liu, Y. Naphthalene Diimide-Based Copolymers Incorporating Vinyl-Linkages for High-Performance Ambipolar Field-Effect Transistors and Complementary-Like Inverters under Air. *Chem. Mater.* **2013,** *25,* 3589–3596.

[6] Dodabalapur, A. Organic and Polymer Transistors for Electronics. *Mater. Today* **2006,** *9,* 24–30.

[7] Anthony, J. E.; Facchetti, A.; Heeney, M.; Marder, S. R.; Zhan, X. n-Type Organic Semiconductors in Organic Electronics. *Adv. Mater.* **2010,** *22,* 3876–3892.

[8] Facchetti, A. Semiconductors for Organic Transistors. *Mater. Today* **2007,** *10,* 28–37.

[9] Usta, H.; Risko, C.; Wang, Z.; Huang, H.; Deliomeroglu, M. K.; Zhukhovitskiy, A.; Facchetti, A.; Marks, T. J. Design, Synthesis, and Characterization of Ladder-Type Molecules and Polymers. Air-Stable, Solution-Processable n-Channel and Ambipolar Semiconductors for Thin-Film Transistors via Experiment and Theory. *J. Am. Chem. Soc.* **2009,** *131,* 5586–5608.

[10] Bao, Z.; Locklin, J. *Organic Field-Effect Transistor;* CRC Press Taylor and Francis Group: Boca Raton, FL, 2007.

[11] Wang, C.; Dong, H.; Hu, W.; Liu, Y.; Zhu, D. Semiconducting π-Conjugated Systems in Field-Effect Transistors: A Material Odyssey of Organic Electronics. *Chem. Rev.* **2012,** *112,* 2208–2267.

[12] Zaumseil, J.; Sirringhaus, H. Electron and Ambipolar Transport in Organic Field-Effect Transistors. *Chem. Rev.* **2007,** *107,* 1296–1323.

[13] Newman, C. R.; Frisbie, C. D.; Filho, D. A. S.; Brédas, J. L.; Ewbank, P. C.; Mann, K. R. Introduction to Organic Thin Film Transistors and Design of n-Channel Organic Semiconductors. *Chem. Mater.* **2004,** *16,* 4436–4451.

[14] Shirota, Y.; Kageyama, H. Charge Carrier Transporting Molecular Materials and Their Applications in Devices. *Chem. Rev.* **2007,** *107,* 953–1010.

[15] Katz, H. E.; Lovinger, A. J.; Johnson, J.; Kloc, C.; Siegrist, T.; Li, W.; Lin, Y.; Dodabalapur, A. A Soluble and Air-stable Organic semiconductor with High Electron Mobility. *Nature* **2000,** *404,* 478–481.

[16] Klauk, H.; Halik, M.; Zschieschang, U.; Schmid, G.; Radlik, W.; Weber, W. High-Mobility Polymer Gate Dielectric Pentacene Thin Film Transistors. *J. Appl. Phys.* **2002,** *92,* 5259–5263.

[17] Sundar, V. C.; Zaumseil, J.; Podzorov, V.; Menard, E.; Willett, R. L.; Someya, T.; Gershenson, M. E.; Rogers, J. A. Elastomeric Transistor Stamps: Reversible Probing of Charge Transport in Organic Crystals. *Science* **2004,** *303,* 1644–1646.

[18] Bao, Z. Materials and Fabrication Needs for Low-Cost Organic Transistor Circuits. *Adv. Mater.* **2000,** *12,* 227–230.

[19] Jones, B. A.; Facchetti, A.; Wasielewski, M. R.; Marks, T. J. Effects of Arylene Diimide Thin Film Growth Conditions on n-Channel OFET Performance. *Adv. Funct. Mater.* **2008,** *18,* 1329–1339.

[20] Haddon, R. C. C70 Thin Film Transistors. *J. Am. Chem. Soc.* **1996,** *118,* 3041–3042.

[21] Horowitz, G.; Kouki, F.; Spearman, P.; Fichou, D.; Nogues, C.; Pan, X.; Garnier, F. Evidence for n-Type Conduction in a Perylene Tetracarboxylic Diimide Derivative. *Adv. Mater.* **1996,** *8,* 242–245.

[22] Horowitz, G. Organic Field-Effect Transistors. *Adv. Mater.* **1998,** *10,* 365–377.

[23] Jones, B. A.; Facchetti, F.; Wasielewski, M. R.; Marks, T. J. Tuning Orbital Energetics in Arylene Diimide Semiconductors: Materials Design for Ambient Stability of n-Type Charge Transport. *J. Am. Chem. Soc.* **2007,** *129,* 15259–15278.

[24] Wen, Y.; Liu, Y. Recent Progress in n-Channel Organic Thin-Film Transistors. *Adv. Mater.* **2010,** *22,* 1331–1345.

[25] Zhang, F.; Di, C.-a.; Berdunov, N.; Hu, Y.; Gao, X.; Meng, Q.; Sirringhaus, H.; Zhu, D. Ultrathin Film Organic Transistors: Precise Control of Semiconductor Thickness via Spin-Coating. *Adv. Mater.* **2013,** *25,* 1401–1407.

[26] Zhan, X.; Facchetti, A.; Barlow, S.; Marks, T. J.; Ratner, M. A.; Wasielewski, M. R.; Marder, S. R. Rylene and Related Diimides for Organic Electronics. *Adv. Mater.* **2011,** *2,* 268–284.

[27] Zhang, F.; Hu, Y.; Schuettfort, T.; Di, C.-a.; Gao, X.; McNeill, C. R.; Thomsen, L.; Mannsfeld, S. C. B.; Yuan, W.; Sirringhaus, H.; Zhu, D. Critical Role of Alkyl Chain Branching of Organic Semiconductors in Enabling Solution-Processed N-Channel Organic Thin-Film Transistors with Mobility of up to 3.50 $cm^2\ V^{-1}\ s^{-1}$. *J. Am. Chem. Soc.* **2013,** *135,* 2338–2349.

[28] Würthner, F.; Stolte, M. Naphthalene and Perylene Diimides for Organic Transistors. *Chem. Commun.* **2011,** *47,* 5109–5115.

[29] Suraru, S. L.; Zschieschang, U.; Klauk, H.; Würthner, F. A Core-Extended Naphthalene Diimide as a p-Channel Semiconductor. *Chem. Commun.* **2011,** *47,* 1504–11506.

[30] Oh, J. H.; Suraru, S.-L.; Lee, W.-Y.; Könemann, M.; Höffken, H. W.; Röger, C.; Schmidt, R.; Chung, Y.; Chen, W.-C.; Würthner, F.; Bao, Z. High-Performance Air-Stable n-Type Organic Transistors Based on Core-Chlorinated Naphthalene Tetracarboxylic Diimides. *Adv. Funct. Mater.* **2010,** *20,* 2148–2156.

[31] Jung, B. J.; Tremblay, N. J.; Yeh, M. L.; Katz, H. E. Molecular Design and Synthetic Approaches to Electron-Transporting Organic Transistor Semiconductors. *Chem. Mater.* **2011,** *23,* 568–582.

[32] Li, C.; Xiao, C.; Li, Y.; Wang, Z. Synthesis and Properties of Heterocyclic Acene Diimides. *Org. Lett.* **2013,** *15,* 682–685.

[33] Ye, Q.; Chang, J.; Huang, W. K.; Shi, X.; Wu, J.; Chi, C. Cyanated Diazatetracene Diimides with Ultrahigh Electron Affinity for n-Channel Field Effect Transistors. *Org. Lett.* **2013,** *15,* 1194–1197.

[34] Chen, X.; Guo, Y.; Tan, L.; Yang, G.; Li, Y.; Zhang, G.; Liu, Z.; Xu, W.; Zhang, D. Dithiazole-Fused Naphthalene Diimides Toward New n-Type Semiconductors. *J. Mater. Chem. C* **2013,** *1,* 1087–1092.

[35] Chang, J.; Ye, Q.; Huang, W. K.; Zhang, J.; Chen, K. J.; Wu, J.; Chi, C. Stepwise Cyanation of Naphthalene Diimide for n-Channel Field-Effect Transistors. *Org. Lett.* **2012,** *14,* 2964–2967.

[36] Laquindanum, J. G.; Katz, H. E.; Dodabalapur, A.; Lovinger, A. J. n-Channel Organic Transistor Materials Based on Naphthalene Frameworks. *J. Am. Chem. Soc.* **1996,** *118,* 11331–11332.

[37] Chang, J.; Shao, J.; Zhang, J.; Wu, J.; Chi, C. A Phthalimide-Fused Naphthalene Diimide with High Electron Affinity for a High Performance n-Channel Field Effect Transistor. *RSC Adv*. **2013,** *3,* 6775–6778.

[38] Shao, J.; Chang, J.; Chi, C. Solution-Processable n-Type Semiconductors Based on Unsymmetrical Naphthalene Imides: Synthesis, Characterization, and Applications in Field- Effect Transistors. *Chem. Asian J*. **2014,** *9,* 253–260.

[39] Lv, A.; Puniredd, S. R.; Zhang, J.; Li, Z.; Zhu, H.; Jiang, W.; Dong, H.; He, Y.; Jiang, L.; Li, Y.; Pisula, W.; Meng, Q.; Hu, W.; Wang, Z. High Mobility, Air Stable, Organic Single Crystal Transistors of an n-Type Diperylene Bisimide. *Adv. Mater.* **2012,** *24,* 2626–2630.

[40] Crone, B.; Dodabalapur, A.; Lin, Y.-Y.; Filas, R. W.; Bao, Z.; LaDuca, A.; Sarpeshkar, R.; Katz, H. E.; Li, W. Large-Scale Complementary Integrated Circuits Based on Organic Transistors. *Nature* **2000,** *403,* 521–523.

[41] Yan, H.; Chen, Z.; Zheng, Y.; Newman, C.; Quinn, J. R.; Dötz, F.; Kastler, M.; Facchetti, A. A High-Mobility Electron-Transporting Polymer for Printed Transistors. *Nature* **2009,** *457,* 679–686.

[42] Junga, Y.; Baeg, K. J.; Kim, D.; Someya, T.; Park, S. Y. A Thermally Resistant and Air-Stable n-Type Organic Semiconductor: Naphthalene Diimide of 3,5-Bis-Trifluoromethyl Aniline. *Synth. Met.* **2009,** *159,* 2117–2121.

[43] Horowitz, G. Organic Thin Film Transistors: From Theory to Real Devices. *J. Mater. Res.* **2004,** *19,* 1946–1962.

[44] Bettinger, C. J.; Bao, Z. Organic Thin-Film Transistors Fabricated on Resorbable Biomaterial Substrates. *Adv. Mater.* **2010,** *22,* 651–655.

[45] Shukla, D.; Nelson, S. F.; Freeman, D. C.; Rajeswaran, M.; Ahearn, W. G.; Meyer, D. M.; Carey, J. T. Thin-Film Morphology Control in Naphthalene-Diimide-Based Semiconductors: High Mobility n-Type Semiconductor for Organic Thin-Film Transistors. *Chem. Mater.* **2008,** *20,* 7486–7491.

[46] Avinash, M. B.; Govindaraju, T. A Bio-Inspired Design Strategy: Organization of Tryptophan-Appended Naphthalenediimide into Well-Defined Architectures Induced by Molecular Interactions. *Nanoscale* **2011,** *3,* 2536–2543.

[47] Pron, A.; Gawrys, P.; Zagorska, M.; Djuradoa, D.; Demadrillea, R. Electroactive Materials for Organic Electronics: Preparation Strategies, Structural Aspects and Characterization Techniques. *Chem. Soc. Rev.* **2010,** *39,* 2577–2632.

[48] Li, J.; Qin, F.; Li, C. M.; Bao, Q.; Chan-Park, M. B.; Zhang, W.; Qin, J.; Ong, B. S. High-Performance Thin-Film Transistors from Solution-Processed

Dithienothiophene Polymer Semiconductor Nanoparticles. *Chem. Mater.* **2008,** *20,* 2057–2059.

[49] Bell, T. D. M.; Bhosale, S. V.; Forsyth, C. M.; Hayne, D.; Ghiggino, K. P.; Hutchison, J. A.; Jani, C. H.; Langford, S. J.; Lee, M. A.-P.; Woodward, C. P. Melt-Induced Fluorescent Signature in a Simple Naphthalenediimide. *Chem. Commun.* **2010,** *46,* 4881–4883.

[50] Popere, B. C.; Pelle, A. M. D.; Thayumanavan, S. BODIPYBased Donor Acceptor π-Conjugated Alternating Copolymers. *Macromolecules* **2011,** *44,* 4767–4776.

[51] Fritz, S. E.; Martin, S. M.; Frisbie, C. D.; Ward, M. D.; Toney, M. F. Structural Characterization of a Pentacene Monolayer on an Amorphous SiO2 Substrate with Grazing Incidence X-ray Diffraction. *J. Am. Chem. Soc.* **2004,** *126,* 4084–4085.

[52] Fukuda, K.; Takeda, Y.; Mizukami, M.; Kumaki, D.; Tokito, S. Fully Solution-Processed Flexible Organic Thin Film Transistor Arrays with High Mobility and Exceptional Uniformity. *Sci. Rep.* **2014,** *4,* 3947–3954.

[53] Singh, Th. B.; Erten, S.; Gunes, S.; Zafer, C.; Turkmen, G.; Kuban, B.; Teoman, Y.; Sariciftci, N. S.; Icli, S. Soluble Derivatives of Perylene and Naphthalene Diimide for n-Channel Organic Field-Effect Transistors. *Org. Electron.* **2006,** *7,* 480–489.

[54] Lei, T.; Wang, J. Y.; Pei, J. Roles of Flexible Chains in Organic Semiconducting Materials. *Chem. Mater.* **2014,** *26,* 594–603.

3

Effect of Bilayer Dielectric for Low Operated n-type Organic Field Effect Transistor

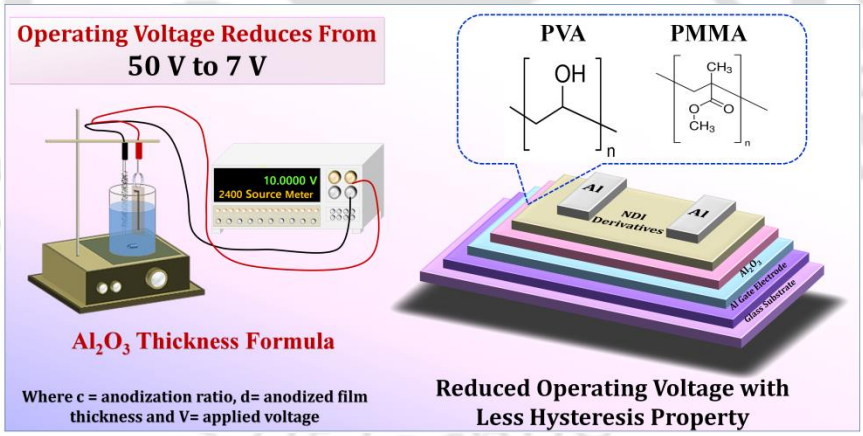

[1] **Dey, A.;** Singh, A.; Kalita, A.; Das, D.; Iyer, P. K. High Performance, Low Operating Voltage n-Type Organic Field Effect Transistor Based on Inorganic-Organic Bilayer Dielectric System. **Journal of Physics: Conference Series,** 2016, 704, 012017 (1-8).

भारतीय प्रौद्योगिकी संस्थान गुवाहाटी
Indian Institute of Technology Guwahati

3

Effect of Bilayer Dielectric for Low Operated n-type Organic Field Effect Transistor

OFETs are the basic elements of organic electronic and optoelectronic applications. Due to their low-cost, large-area fabrication possibility, in near future OFET technologies are expected to build a new alternative market compared to conventional inorganic technology. Generally, OFETs are operated within large operating voltage range, which is one of the major limitations in finding their application in futuristic electronics.[1-5] Hence, an ideal OFET should have low operational voltage, high electrical stability and lifetime for real-life application, such as radio frequency identification (RFID) tag, sensor, electro-optical switch etc. It has already been reported that in order to achieve excellent device performance with low operating voltage, high-k inorganic dielectrics have been traditionally used.[6-10] The popular choice has always been Al_2O_3 because of its high insulating property and low-cost deposition technique.[11-15] However, the single Al_2O_3 film shows huge leakage current because of the inferior film forming quality. In contrast, PVA and PMMA, the polymer dielectric materials, have emerged as the viable choice since they can be processed through solution processing methods, thereby reducing the overall cost of device fabrication. However, PVA-based OFETs often suffer from relatively low stability and large drain current (I_{DS}) hysteresis, which could be possibly associated due to the presence of -OH groups on the PVA surface.[16-18] On the other hand, due to the remarkable film forming ability and non-interacting nature of PMMA, it can be used to achieve high quality films in the organic-organic interface.

However, these dielectric materials possess very low capacitance value, requiring very high threshold and operating voltages for device operation.[19-21] Considering the advantages of polymer dielectric for better interfacial effect and high k-inorganic dielectric for low voltage operation, the concept of inorganic-organic bilayer dielectric was proposed.

In this chapter we have discussed the effect of inorganic-organic bilayer dielectric system for low operated n-type OFETs. For this analysis, two different derivatives of NDI's were synthesized, namely N, N′-dioctadecyl-1, 4, 5, 8-naphthalenetetracarboxylic diimide (NDI-OD2) and N, N′-dicyclohexyl-1, 4, 5, 8-naphthalenetetracarboxylic diimide (NDI-CY2) and characterized by different characterization techniques before the device fabrication. The bilayer systems contain two different device configurations namely Al_2O_3/PVA and Al_2O_3/PMMA, where Al_2O_3 is a high-k inorganic dielectric whereas PVA and PMMA are two polymer dielectric materials. As mentioned previously, PVA is a high-k polar polymer dielectric material whereas the PMMA is a non-polar dielectric. Both this bilayer dielectric system is expected to have significant influence on the dielectric-semiconductor interface. The high capacitance, pinhole-free Al_2O_3 gate insulator was deposited by electrochemical oxidation or anodization method to form a ~13 nm Al_2O_3 layer over the aluminium film gate electrode. It has been observed that with top contact aluminium electrodes both the molecules exhibit excellent n-channel behaviour under vacuum condition with remarkably low operating voltage (~7V). This low operating voltage, high performance OFET device with bilayer dielectric system is expected to have diverse applications in the next generation of OFET technologies.

3.1 Experiments

3.1.1 Materials

1, 4, 5, 8-naphthaleneteracarboxylic dianhydride, octadecylamine, cyclohexylamine, quinoline, zinc acetate, PMMA (M_W=550000 g/mol) and aluminium wire (99.999% purity) were used as received from Sigma Aldrich. PVA (M_W= 1, 15,000 g/mol) was purchased from Loba Chemie (99% purity) and used as received. Microscope glass slides (thickness 1-1.2mm) purchased from Jain Scientific Glass Works, India, was used as the device substrate without any surface modification. The active layer molecule, namely, NDI-OD2 molecule was synthesized following the procedure reported in Chapter 2 by the direct condensation of 1, 4, 5, 8-naphthalene dianhydride with octadecylamine

whereas NDI-CY2 molecule was synthesized following the procedure reported in the literature by simple condensation method.[22]

3.1.2 Characterization Details

The thickness of the thin films of NDI-OD2 and NDI-CY2, thermally evaporated by Excel Instrument, were measured by Veeco Dektak 150 Surface Profilometer. All AFM images were recorded by Agilent 5500-STM instrument under non-contact mode. Gaussian 03 software was used to perform the DFT simulation of the materials. CH instrument was used to perform the electrochemical analysis of NDI-OD2. Finally, all the electrical properties were recorded by Keithley 2400 and 4200 semiconductor characterization system (SCS).

3.2 Results and Discussion

3.2.1 Band Gap Analysis

The optical, electrochemical and theoretical band gap of the active layer materials were estimated by UV-Vis absorption cyclic voltammetry and theoretical Gaussian simulation considering B3LYP/6-31G (d) basis set using the methods mentioned in the literature.[23-27] The estimated HOMO and LUMO energy levels and the band gap of the materials were summarized in Table 3.1. It has been observed that both the materials have almost similar type of HOMO, LUMO position and band gap value.

Table 3.1 Summary of band gap of NDI-OD2 and NDI-CY2 active layer materials.

Molecules	$E_{HOMO}^{(CV)}$ (eV)	$E_{LUMO}^{(CV)}$ (eV)	E_g^{CV} (eV)	E_g^{UV} (eV)	E_g^{Th} (eV)
NDI-OD2	-6.41	-3.39	3.02	3.18	3.61
NDI-CY2	-6.79	-3.38	3.39	3.16	3.59

3.2.2 Thin Film Microstructure

The thin film growth natures of both the active layer molecules were standardized systematically prior to the device fabrication. The morphology of NDI-OD2 was already discussed in detail in the chapter 2. Before the device fabrication, the NDI-CY2 molecule

was characterized by different characterization techniques which are presented in Figure 3.1.

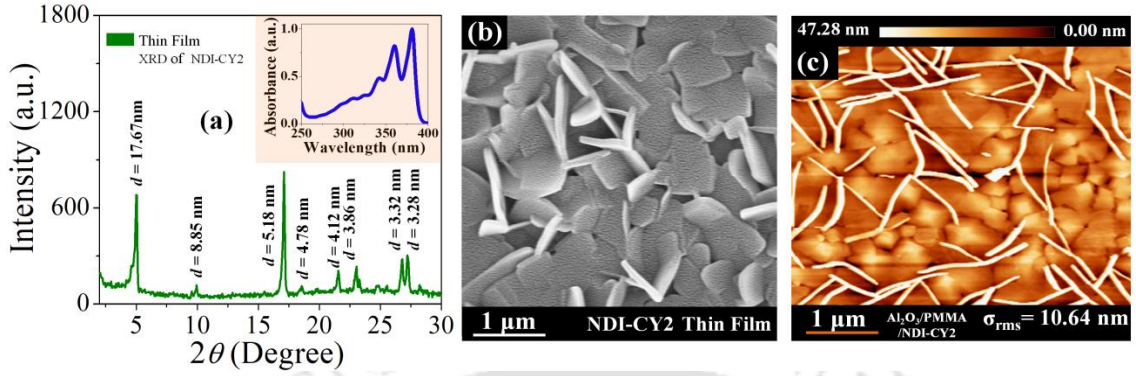

Figure 3.1 (a) Thin film XRD spectra, Inset: thin film UV-Vis absorption spectra of NDI-CY2 molecule. (b) FESEM image and (c) AFM image of thin film NDI-CY2 molecule.

From Figure 3.1a, the crystalline nature of NDI-CY2 was confirmed. It is evident that the sharp peaks observed in 2θ≤ 30°C supports the formation of molecules that were highly ordered and crystalline in nature. The observed lamellar d-spacing for 2θ = 5°, 10° and 17° were found to be 17.67 Å, 8.85 Å. and 5.18 Å.respectively. Further the thin film UV-Vis absorption spectra of the molecule (in the inset of Figure 3.1a) shows mainly three characteristics peak at 381, 360, and 341 nm wavelengths range. These three peaks subsequently signify the characteristic π–π* transitions of NDI-CY2 molecule.[25,26] Figure 3.1b and Figure 3.1c represents the FESEM and AFM image of the thin film NDI-CY2 molecule respectively. From these images it was observed that at 60°C substrate temperature the molecules form densely packed thin film with larger grains (in µm range in size) which is highly suitable for OFET fabrication.

3.2.3 Device Fabrication Method

The OFETs based on NDI-OD2 and NDI-CY2 were fabricated with bottom gate top contact architecture with inorganic-organic bilayer dielectric configuration (Figure 3.2). In this method, the Al_2O_3, inorganic dielectric layer was deposited by anodic oxidation method. Anodization is a very good, effective and solution based technique to grow metal oxide films with nanometer control. The high capacitance, pinhole-free Al_2O_3 gate insulators can be fabricated by electrochemical oxidation (or anodization) of the gate metal on desired substrates, such as, glass and flexible transparent sheets etc. In addition, this process can yield a high-quality metal-oxide insulator at room temperature with very low cost and less time.

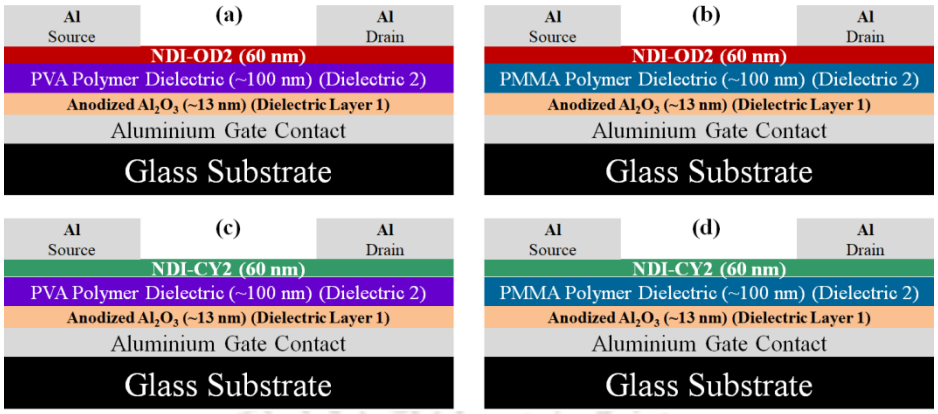

Figure 3.2 Schematic of the fabricated OFETs device structure of NDI-OD2 and NDI-CY2 with (a), (c) Al_2O_3/PVA and (b), (d) Al_2O_3/PMMA bilayer dielectric system.

Herein, we used cleaned glass slides (size: 15 mm × 25 mm) to serve as a device substrates onto which >200 nm thick aluminium gate with dimensions 1 mm × 20 mm, was deposited by thermal evaporation method through a shadow mask. The film was then anodized with a constant current density of 0.06 mA cm^{-2} and a voltage of 10 V in a 0.001 M citric acid monohydrate electrolyte solution at 25°C (room temperature) using a square-shaped platinum mesh as counter electrode to form a ~13 nm thick Al_2O_3 layer over the aluminium film gate electrode. The thickness of the Al_2O_3 was calculated using the following Equation 3.1-

$$d = cV \qquad (3.1)$$

where, c is the anodization ratio, d is anodized film thickness and V is the applied voltage.

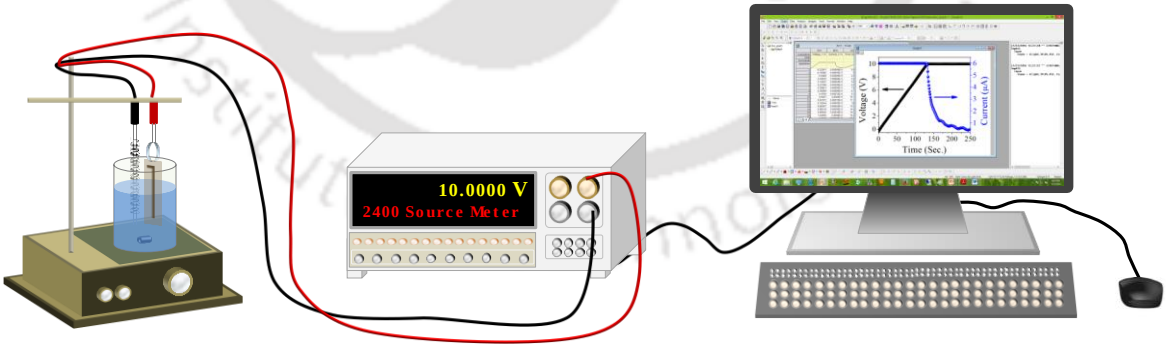

Figure 3.3 Anodic oxidation setup for aluminium.

Figures 3.3 and Figure 3.4 demonstrate the anodization setup which was used for growing Al_2O_3 film, the typical anodization graph and the AFM images of aluminium film before and after anodic oxidation. After iodization, to reduce the surface roughness, ~100 nm PVA and PMMA thin film was separately spin coated on the two device configurations, to

form Al_2O_3/PVA and Al_2O_3/PMMA bilayer dielectric and dried for 1 h at 100 °C under nitrogen atmosphere.

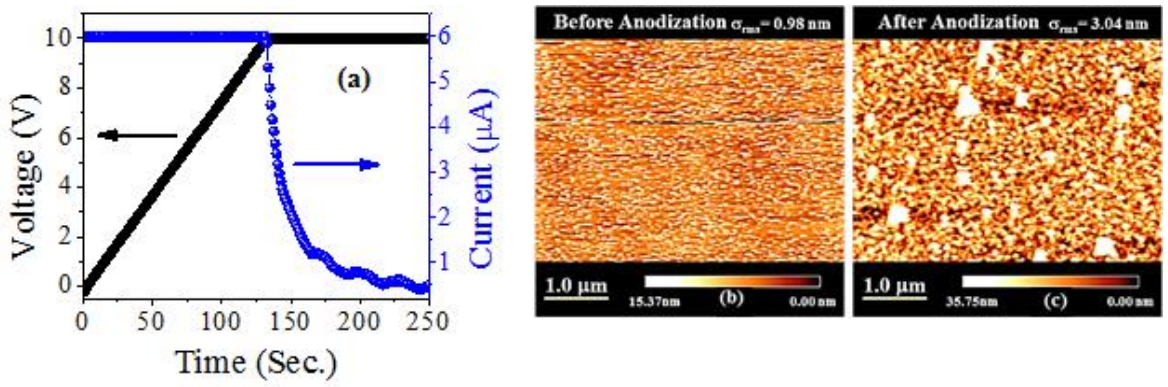

Figure 3.4 (a) Anodic oxidation curve for aluminium, AFM image of aluminium thin film (b) before and (c) after the anodization.

Both the organic dielectric polymer solutions were prepared by dissolving 30 mg/mL of PVA in de-ionized water and 30 mg/mL of PMMA in anisole. The capacitance of the Al_2O_3/PVA and Al_2O_3/PMMA bilayer dielectric systems were observed as ~6 $nF.cm^{-2}$ and ~27 $nF.cm^{-2}$ respectively. The AFM images of PVA and PMMA dielectrics on anodized Al_2O_3 inorganic dielectric layer are shown in Figures 3.5.

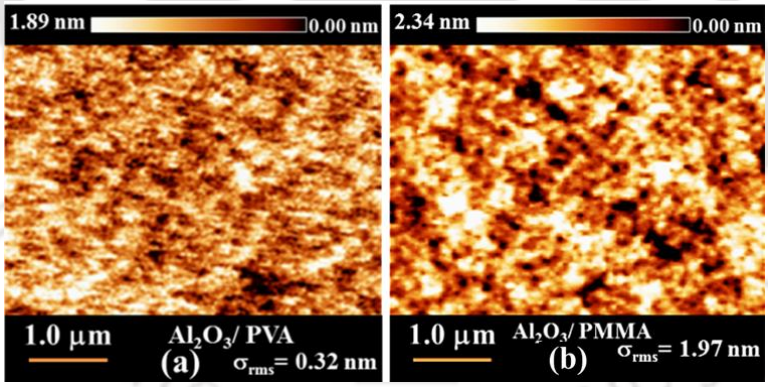

Figure 3.5 AFM image of (a) PVA and (b) PMMA polymer dielectric thin film on Al_2O_3 inorganic dielectric layer.

Followed by the spin coating of organic dielectric layer, ~60 nm (± 10 nm) of the active materials were deposited by thermal deposition method under a base pressure of 10^{-6} mbar. After that, Al source and drain contacts (100 nm) were deposited on the organic layers through a shadow mask with channel length (L) and width (W) of 50 μm and 1 mm, respectively.

3.2.4 Device Characterizations

The OFET mobility value of NDI-OD2 and NDI-CY2 were estimated from the saturated region by using the following Equation 3.2-

$$I_{DS} = C_i \mu_e . \left(\frac{W}{2L}\right) . (V_{GS} - V_{Th})^2 \quad (3.2)$$

where I_{DS} is the drain current, C_i is the capacitance per unit area of the gate dielectric layer, μ_e is the field effect electron mobility, W and L are the channel width and length, V_{GS} and V_{Th} are the gate voltage and threshold voltage, respectively. Figures 3.6 and Figure 3.7 demonstrate the OFET characteristics curve of NDI-OD2 and NDI-CY2 molecule on bilayer Al_2O_3/PVA and Al_2O_3/PMMA dielectric system respectively. The calculated OFET parameters of the molecule are listed in Table 3.2.

Table 3.2. Summary of OFETs device performance with Al_2O_3/PVA and Al_2O_3/PVA bilayer dielectric system.

Bilayer Dielectric System	Active Layer molecule	Average Electron Mobility, μ (cm^2/Vs)	Threshold Voltage, V_{Th} (V)	I_{ON}/I_{OFF}	Hysteresis	Stability
Al_2O_3/PVA	NDI-OD2	0.53	3.8	10^3	Very High	Unstable
	NDI-CY2	0.20	0.5	10^5	Very Less	Less Stable
Al_2O_3/PMMA	NDI-OD2	0.32	0.5	10^4	No	Unstable
	NDI-CY2	0.02	0.5	10^4	No	Stable

It has been observed that with Al_2O_3/PVA bilayer dielectric, both the molecules show hysteresis property whereas with Al_2O_3/PMMA bilayer dielectric they show much stable characteristics. The NDI-OD2 and NDI-CY2 molecules based OFET devices, over bilayer Al_2O_3/PMMA gate dielectric, exhibited excellent average electron mobility as 0.32 cm^2/Vs and 0.02 cm^2/Vs respectively under vacuum with a threshold voltage of 0.5 V. The ON/OFF current ratio of the devices were observed to be of the order of 10^4 up to an operating voltage of only 7 V. On the other hand the device with Al_2O_3/PVA showed high electron mobility but less stability likely due to the presence of -OH group in the PVA dielectric which creates charge traps at the dielectric-semiconductor interface. These traps also reduce the overall stability and degrade the devices very fast (~1 day).

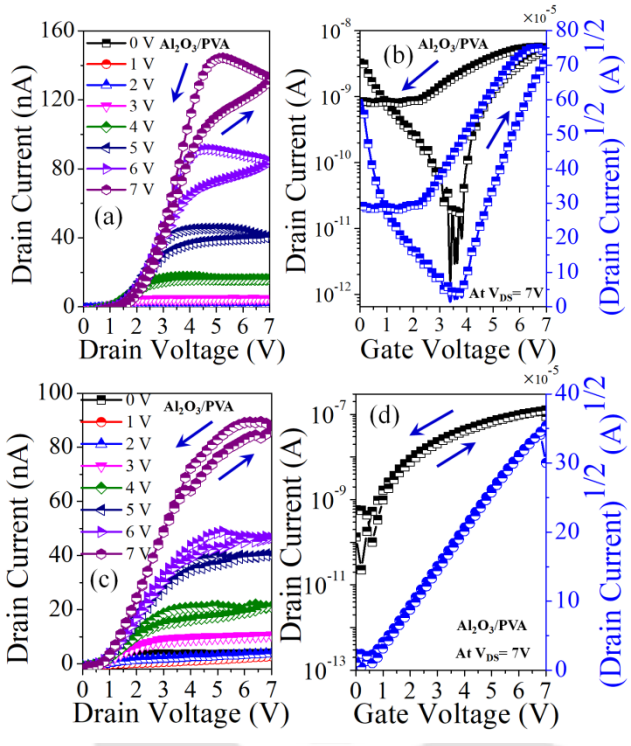

Figure 3.6 Drain and Transfer characteristics curves of [(a) and (b)] NDI-OD2 and [(c) and (d)] NDI-CY2 molecule with Al_2O_3/PVA bilayer dielectric system.

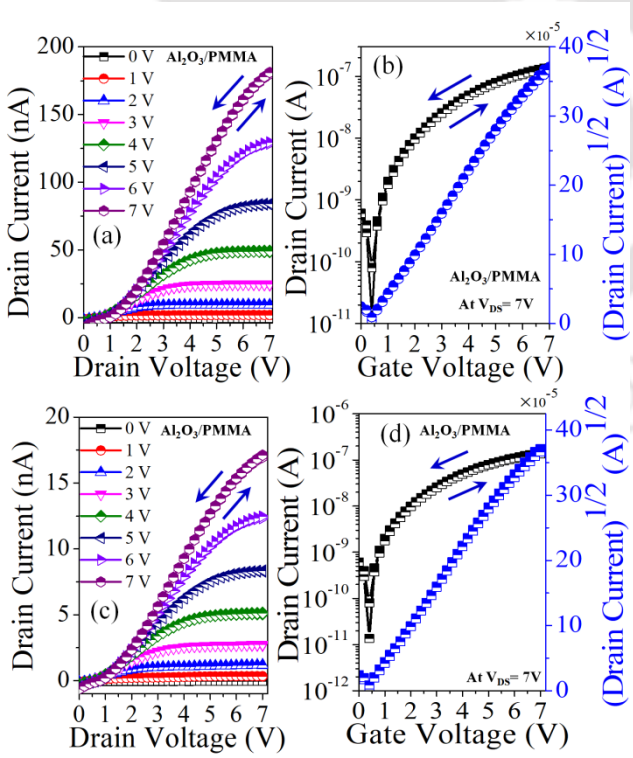

Figure 3.7. Drain and Transfer characteristics curves of [(a) and (b)] NDI-OD2 and [(c) and (d)] NDI-CY2 molecule with Al_2O_3/PMMA bilayer dielectric system.

Thus the Al_2O_3/PMMA bilayer dielectric system demonstrates drastic improvement in the device performance due to better capacitive coupling between the gate and the channel through the dielectric layer to enhance field-effect carrier mobility and the threshold voltage compared to the PVA dielectric system.

3.3 Conclusion

In conclusion, the influence of cost effective inorganic-organic bilayer dielectric system for the low operated n-channel organic field effect transistor is demonstrated. For this analysis, two different derivatives of naphthalene diimide (NDI) were synthesized, namely NDI-OD2 and NDI-CY2 and characterized by different characterization techniques. The bilayer systems contain two different device configurations namely Al_2O_3/PVA Al_2O_3/PMMA, where Al_2O_3 is a high-k inorganic dielectric whereas PVA and PMMA are two polymer dielectric materials. The high capacitance, pinhole-free Al_2O_3 gate insulators was deposited by electrochemical oxidation or anodization method to form a ~13 nm Al_2O_3 layer over the aluminum film gate electrode. It has been observed that with top contact aluminium electrodes both the molecules exhibited excellent n-channel behavior under vacuum condition with remarkable low operating voltage (~7V). This low operating voltage, high performance OFET device with bilayer dielectric system is expected to have diverse applications in the next generation of OFET technologies.

3.4 References

[1] Ong, B.S.; Wu, Y.; Liu, P; Gardner, S. High-Performance Semiconducting Polythiophenes for Organic Thin-Film Transistors. *J. Am. Chem. Soc.* **2004**, *126*, 3378-3379.

[2] Li, Y.; Wu, Y.; Liu, P.; Birau, M.; Pan, H.; Ong, BS. Poly (2, 5-bis (2-thienyl)-3, 6-dialkylthieno [3, 2-b] thiophene) s-High-Mobility Semiconductors for Thin-Film Transistors. *Adv. Mater.* **2006**, *18*, 3029–3032.

[3] Noh, Y. -Y.; Kim, D-.Y.; Yoshida, Y.; Yase, K.; Jung, B. -J.; Lim, E.; Shim, H. -K. High-Photosensitivity *p*-Channel Organic Phototransistors based on a Biphenyl end-capped Fused Bithiophene Oligomer. *Appl. Phys. Lett.* **2005**, **86** 043501.

[4] Kang, H.-S.; Choi, C.-S.; Choi, W.-Y.; Kim D.-H.; Seo, K.-S. Characterization Of Phototransistor Internal Gain in Metamorphic High-Electron-Mobility Transistors. *Appl. Phys. Lett.* **2004**, *84*, 3780–3782.

[5] Noh, Y.-Y.; Kim, D.-Y.; Yase, K. Highly Sensitive Thin-Film Organic Phototransistors: Effect of Wavelength of Light Source on Device Performance. *J. Appl. Phys.* **2005**, *98*, 074505.

[6] Baeg, K. J.; Noh, Y. Y.; Ghim, J.; Kang, S. J.; Lee, H.; Kim, D.Y. Organic Non-Volatile Memory based on Pentacene Field-Effect Transistors using a Polymeric Gate Electret. *Adv. Mater.* **2006**, *18*, 3179–3183.

[7] Noh, Y.-Y.; Zhao, N.; Caironi, M.; Sirringhaus, H. Downscaling of Self-Aligned, All-Printed Polymer Thin-Film Transistors. *Nat. Nanotechnol.* **2007**, *2*, 784-789.

[8] Tang, Q. X.; Li, L. Q.; Song, Y. B.; Liu, Y. L.; Li, H. X.; Xu, W.; Liu, Y. Q.; Hu W. P.; Zhu, D. B. Photoswitches and Phototransistors from Organic Single-Crystalline Sub-micro/nanometer Ribbons. *Adv. Mater.* **2007**, *19*, 2624–2628.

[9] Saragi, T. P. I.; Londenberg J.; Salbeck, J. Photovoltaic and Photoconductivity Effect in Thin-Film Phototransistors Based on a Heterocyclic Spiro-Type Molecule. *J. Appl. Phys.* **2007**, *102*, 046104.

[10] Meixner, R. M.; Gobel, H.; Yildirim, F. A.; Bauhofer W.; Krautschneider, W. Wavelength-Selective Organic Field-Effect Phototransistors Based on Dye-Doped Poly-3-hexylthiophene. *Appl. Phys. Lett.* **2006**, 89, 092110.

[11] Iba, S.; Sekitani, T.; Kato, Y.; Someya, T.; Kawaguchi, H.; Takamiya, M.; Sakurai, T.; Takagi, S. Control of Threshold Voltage of Organic Field-Effect Transistors with Double-Gate Structures. *Appl. Phys. Lett.* **2005**, 87, 023509.

[12] Koo, J. B.; Ku, C. H.; Lim, S. C.; Kim, S. H.; Lee, J. H.; Hysteresis and Threshold Voltage Shift of Pentacene Thin-Film Transistors and Inverters with Al_2O_3 Gate Dielectric. *Appl. Phys. Lett.* **2007**, 90, 133503.

[13] Yang, C.; Shin, K.; Yang, S. Y.; Jeon, H.; Choi, D.; Chung, D. S.; Park, C. E.; Low-Voltage Organic Transistors on a Polymer Substrate with an Aluminum Foil Gate Fabricated by a Laminating and Electropolishing Process. *Appl. Phys. Lett.* **2006**, 89, 153508.

[14] Ha, W. H.; Choo, M. H.; Im, A. S.; Electrical Properties of Al_2O_3 Film Deposited at Low Temperatures. *J. Non-Cryst. Solids* **2002**, *303*, 78-82.

[15] Majewski, L. A.; Schroeder, R.; Grell, M.; Flexible High Capacitance Gate Insulators for Organic Field Effect Transistors. *J. Phys. D: Appl. Phys.* **2004**, *37*, 21.

[16] Kim, J. M.; Lee, J. W.; Kim, J. K.; Ju, B. K.; Kim, J. S.; Lee, Y. H.; Oh, M. H.; An Organic Thin-Film Transistor of High Mobility by Dielectric Surface Modification with Organic Molecule. *Appl. Phys. Lett.* **2004**, *85*, 6368-6370.

[17] Liu, C.; Zhu, Q.; Jin, W.; Gu, W.; Wang, J.; The Ultraviolet-Ozone Effects on Organic Thin-Film Transistors with Double Polymeric Dielectric Layers. *Synth. Met.* **2011,** *161*, 1635-1639.

[18] Peng, X.; Horowitz, G.; Fichou, D.; Garnier, F.; All-Organic Thin-Film Transistors Made of Alpha-Sexithienyl Semiconducting and Various Polymeric Insulating Layers. *Appl. Phys. Lett.* **1990,** *57,* 2013-2015.

[19] Deman, A. L.; Tardy, J.; PMMA-Ta_2O_5 Bilayer Gate Dielectric for Low Operating Voltage Organic FETs. *Org. Electron.* **2005**, *6*, 78-84;

[20] Huang, T. S.; Su, Y. K.; Wang, P. C.; Study of Organic Thin Film Transistor with Polymethylmethacrylate as a Dielectric Layer. *Appl. Phys. Lett.* **2007**, *91*, 092116.

[21] Cheng, J.-A.; Chuang, C. -S.; Chang, M. -N.; Tsai, Y. –C; and Shieh, H. -P. D.; Controllable Carrier Density of Pentacene Field-Effect Transistors using Polyacrylates as Gate Dielectrics. *Org. Electron.* **2008**, *9*, 1069-1075.

[22] Shukla, D.; Nelson, S. F.; Freeman, D. C.; Rajeswaran, M.; Ahearn, W. G.; Meyer, D. M.; Carey, J. T. Thin-Film Morphology Control in Naphthalene-Diimide-Based Semiconductors: High Mobility n-Type Semiconductor for Organic Thin-Film Transistors. *Chem. Mater.* **2008,** *20,* 7486-7491.

[23] Dey, A.; Kalita, A.; Iyer, P. K.; High-Performance n-Channel Organic Thin-Film Transistor Based on Naphthalene Diimide. *Appl. Mater. Interfaces* **2014,** *6,* 12295-12301.

[24] Jones, B. A.; Facchetti, A.; Wasielewski, M. R.; Marks, T. J.; Tuning Orbital Energetics in Arylene Diimide Semiconductors. Materials Design for Ambient Stability of n-Type Charge Transport. *J. Am. Chem. Soc.* **2007,** *129,* 15259-15278.

[25] Avinash, M. B.; Govindaraju, T. A Bio-Inspired Design Strategy: Organization of Tryptophan-Appended Naphthalenediimide into Well-Defined Architectures Induced by Molecular Interactions. *Nanoscale* **2011,** *3,* 2536-2543.

[26] Pron, A.; Gawrys, P.; Zagorska, M.; Djuradoa, D.; Demadrillea, R. Electroactive Materials for Organic Electronics: Preparation Strategies, Structural Aspects and Characterization Techniques. *Chem. Soc. Rev.* **2010,** *39,* 2577-2632.

[27] Li, J.; Qin, F.; Li, C. M.; Bao, Q.; Chan-Park, M. B.; Zhang, W.; Qin, J.; Ong, B. S. High-Performance Thin-Film Transistors from Solution-Processed Dithienothiophene Polymer Semiconductor Nanoparticles. *Chem. Mater.* **2008,** *20,* 2057-2059.

4

Influence of Bilayer Dielectric for Photosensitive Organic Field Effect Transistor

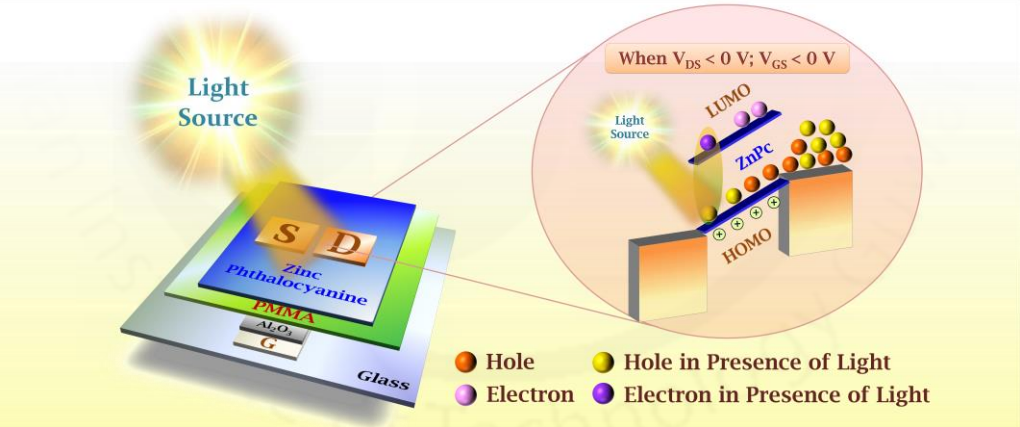

[1] **Dey, A.;** Singh, A.; Das, D.; Iyer, P. K. Photosensitive Organic Field Effect Transistor: Influence of ZnPc Morphology and Bilayer Dielectrics to Achieve Low Operating Voltage and Low Bias Stress Effect. ***Phys. Chem. Chem. Phys.*** 2016, *18,* 32602-32609.

4

Influence of Bilayer Dielectric for Photosensitive Organic Field Effect Transistor

Optical sensors have a very significant role for the development of various electronic equipment such as bar-code scanners, security vision system, HD-cameras, etc.[1,2] Most of the widely used optical sensors, such as photodiodes, charge-coupled devices etc. consist of inorganic semiconductors, which, although show fine performances, their higher fabrication cost, higher power consumption and poor flexibility reduces the demand for these materials in the new generation of wearable and flexible electronics. For an ideal optical sensor it is necessary that the device should be cost-effective and versatile to be fabricated on desired substrate. In this regard, organic π-conjugated small molecules and polymers based optical sensors have recently been developed due to their potential to be fabricated on flexible substrates, textiles, low-cost and large-area.[3-5] Especially, metal-substituted phthalocyanine (MPcs) based optical sensors show remarkable performance due to their superior film forming ability. In addition, the physical and optoelectronic properties of these organic semiconductors can be tuned by chemical synthesis and controlling their thin film growth structure to optimize the device performance. From the device point of view, because of the simplicity in fabrication process and device architecture, MPcs based organic photodiodes are one of the prime electronic components used in light sensing application.[6-8] However, since these devices require additional driving circuits for showing this behaviour, Photo-Sensitive organic field effect transistors (PS-OFETs) have been introduced to

simultaneously show better light sensitivity as well as amplify the input signal in single device configuration with low noise compared to its analogues organic devices like photodiodes.[9-18] A major drawback of PS-OFET is its large operating voltage due to the use of Si/SiO_2 and ITO substrate, which resists their application potential in futuristic electronics.[19-24] Hence, an ideal PS-OFET should have low operational voltage, high optical and electrical stability as well as be highly photo responsive for real-life practical application. Though there has been some progress in the development of MPcs based PS-OFETs, very few reports discuss the combined issues of high performance PS-OFETs that are economical and work at low operating voltage, under very less incident light illumination with good bias stress stability.[25-29]

In this chapter we report the fabrication and characterization of ZnPc based PS-OFETs, on Al_2O_3/PMMA based bilayer dielectric system to achieve remarkable light sensitivity at low operating voltage (0 to -7V) with the illumination of different incident optical power. Since the molecular packing of the active layer have a strong influence on the mobility of OFETs and also the high mobility of the active layer help to get easy transportation of the photo generated charge carrier through the channel, so it is very important to clearly understand the growth mechanism of the active layer on the dielectric layer to achieve enhanced photo responsivity prior to device fabrication. In this study, before fabricating the PS-OFET device, a systematic analysis of the growth nature of ZnPc molecule deposited at different substrate temperatures (Ts) were performed *viz.* at room temperature (RT), 60°C, 90°C and 120°C respectively on Al_2O_3/PMMA bilayer gate dielectric surface to optimize the Ts for the best device performance. The responsivity of the ZnPc based PS-OFET deposited at Ts= 90°C was observed to be 2679.4 $A.W^{-1}$ at V_{DS}= -7 V; V_{GS}= -8 V under the illumination of lowest optical power, P_{in}= 0.002 Wm^{-2}. However the photo ON/OFF current ratio of the same device was observed to be 933.6 with the same biasing condition under the irradiation of highest optical power, P_{in}= 0.2957 Wm^{-2}. The bias stress analysis of the device revealed that the stress effect is extremely small in presence of light (decay of I_{DS} ~ 20% after 30 min) compared to dark, with characteristic carrier relaxation time τ'~10^4 sec. This low-cost, low bias stress, electrically stable device is expected to have potential applications in optoelectronic devices.

4.1 Experiments

4.1.1 Materials

Zinc phthalocyanine (99.999% purity), PMMA (M_W=120 kg/mol), aluminium wire (99.999% purity) and copper wire (99.9% purity) were used as received from Sigma Aldrich. Anisole, purchased from Loba Chemie (99% purity) was used as received for preparing PMMA dielectric solution without any modification. Microscope glass slides (thickness ~1.2 mm) purchased from Jain Scientific Glass Works, India, was used as the device substrate without any surface modification.

4.1.2 Characterization Details

The thickness of the thermally deposited ZnPc thin film was measured by Veeco Dektak 150 Surface Profilometer. AFM images and XRD pattern of the thin film were recorded by Agilent 5500-STM instrument under non-contact mode and Rigaku TTRAX III with Cu Kα radiation respectively. Keithley 2400 source meter was used for anodic oxidation of aluminium thin film. Light irradiation was performed by Oriel DC regulated illuminator connected with Lake Shore fibre optic probes having core diameter ~18μm. The optical power of the illuminated light was measure by Tenmars TM-207 power meter. All the three terminals opto-electrical properties were characterized by Keithley 4200 semiconductor characterization system with Lake Shore vacuum probe station (Figure 4.1).

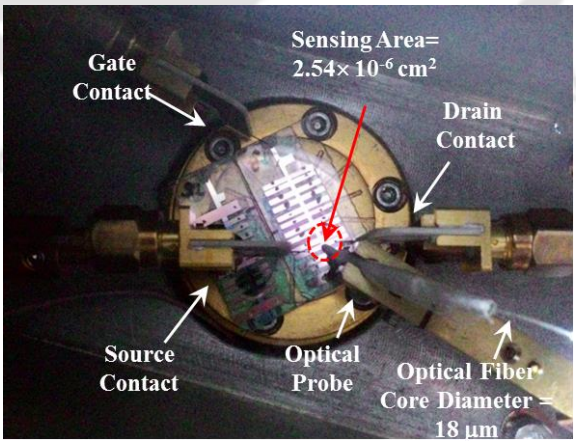

Figure 4.1 Experimental setup for ZnPc based PS-OFET.

4.1.3. Device Fabrication

The ZnPc based PS-OFET was fabricated in a bottom gate top contact Al_2O_3/PMMA bilayer gate dielectric configuration (Figure 4.2). To fabricate pinhole-free films, Al_2O_3 gate insulators, >200 nm thick Al-gate was thermally deposited through a shadow mask on piranha-cleaned glass substrate (1 mm × 20 mm). The film was then electrochemically oxidized by a similar method as explain previously in chapter 2. The thickness of the Al_2O_3 was calculated to be ~13 nm by using the Equation (4.1) given below-

$$d = cV \qquad (4.1)$$

where, c is the anodization ratio, d is anodized film thickness and V is the applied voltage.

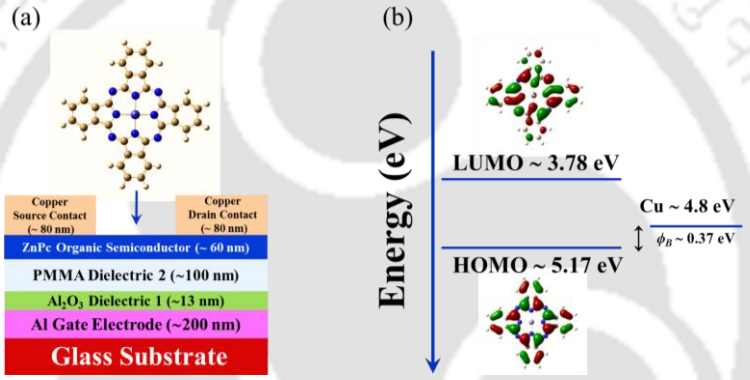

Figure. 4.2 (a) Cross-sectional schematic diagram of a top contact PS-OFET. (b) Illustration of simplified energy band diagram of ZnPc PS-OFET under zero bias condition, with barrier height Φ_B~0.37 eV.

Since the grown Al_2O_3 thin film inherently has very high surface roughness (σ_{rms} ~11.22 nm), a ~100 nm PMMA (30 mg.mL^{-1} in anisole) thin film was spun on top of the Al_2O_3 layer and dried for 1 h at 100°C under inert atmosphere to obtain a smooth surface (σ_{rms} ~2.34 nm).

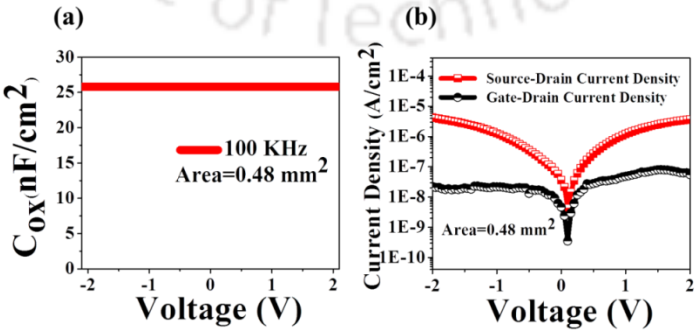

Figure. 4.3 (a) Capacitance of Al_2O_3 /PMMA gate insulators as a function of voltage at 100 kHz and (b) Leakage current density, J (A.cm^{-2}) vs. bias voltage (V), characteristics of MIM structures bilayer gate dielectric system.

The capacitance density (C_{ox}~25.8 nF.cm^{-2}) and the leakage current density (J) of this Al_2O_3 /PMMA bilayer gate insulator were calculated separately from metal-insulator-metal (MIM) structure of parallel plate capacitor using copper as the top electrodes (Figure. 4.3). It was observed that under an applied field the leakage current density J between the gate to drain contacts through the dielectric layers was very low (~10^{-8} A.cm^{-2}) compared to the source to drain contacts (~10^{-5} A.cm^{-2}) which confirms that the dielectric layers demonstrate excellent capacitive behavior and are suitable for OFETs fabrication. After the deposition of bilayer gate dielectric, a 60 nm (± 10 nm) ZnPc active material was deposited by thermal deposition method under a base pressure of 10^{-6} mbar at Ts= 90°C. Further, Cu source-drain electrodes were thermally deposited, at RT up to ~80 nm thickness to calculate three terminal properties of the PS-OFETs.

4.2 Results and Discussion

4.2.1 Morphology and Optical Analysis

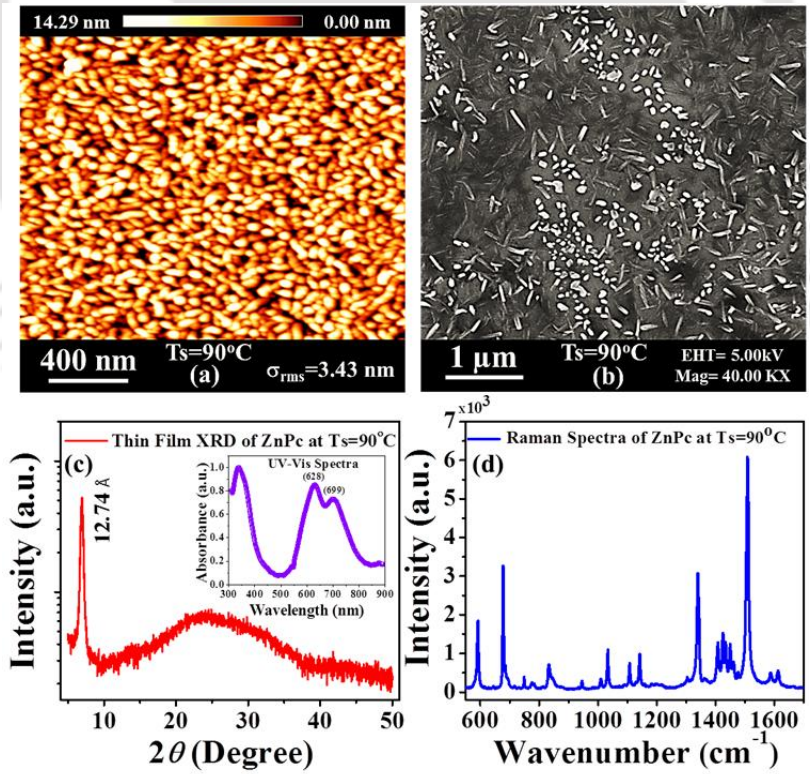

Figure 4.4 (a) AFM topography images (2µm×2µm), (b) FESEM image (Mag. 40.00 KX), (c) XRD spectra and (d) Raman spectra of ~60 nm ZnPc thin films deposited on top of PMMA coated glass substrate at Ts= 90°C. Inset of (c): UV-vis absorbance spectra of ZnPc molecule at Ts= 90°C.

The growth structure and thin film morphology of thermally deposited ZnPc molecule at Ts = 90°C on PMMA coated glass substrates along with its respective root mean square roughness (σ_{rms}) is shown in Figure 4.4. At 90°C, the AFM and FESEM images of ZnPc thin film (Figure 4.4a and 4.4b) showed continuous and uniform fibre like crystallinity, with very less σ_{rms} ~3.43 nm compared to the films deposited at other temperatures (Figure 4.5 and Figure 4.6).

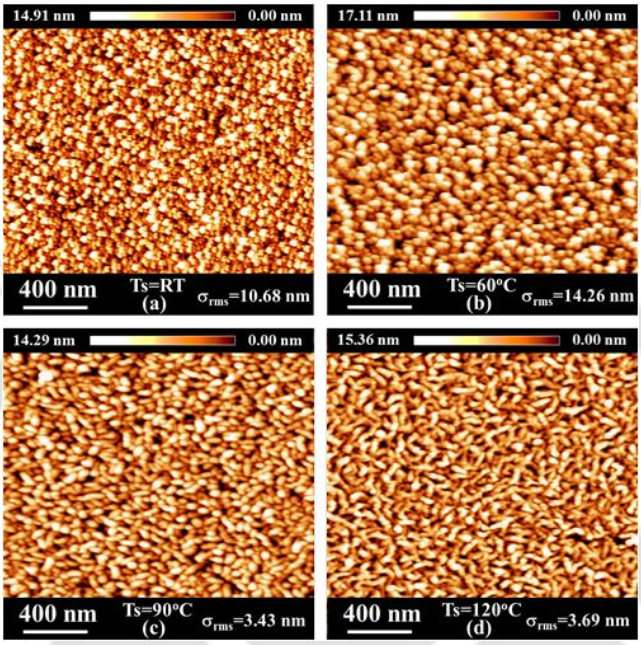

Figure 4.5 AFM topography images (2μm×2μm) of 60nm ZnPc thin films deposited on top of PMMA coated glass substrate at Ts= (a) RT, (b) 60°C, (c) 90°C and (d) 120°C respectively.

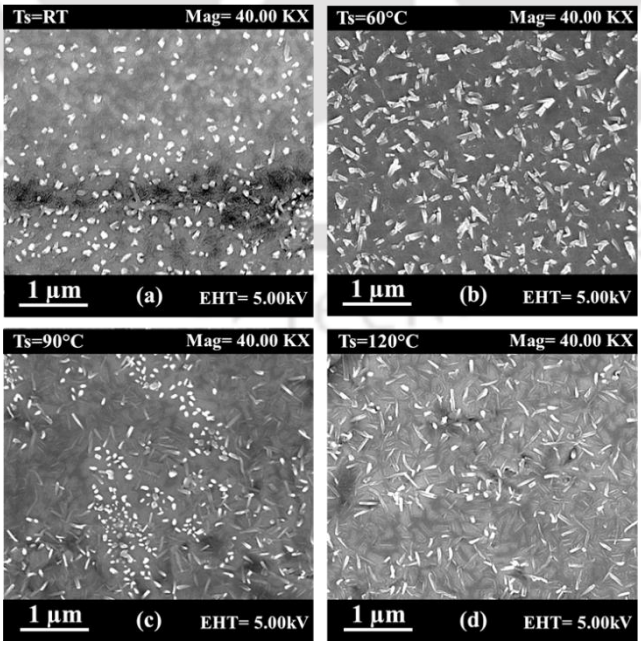

Figure 4.6 FESEM images (Magnification: 40.00 KX) of 60nm ZnPc thin films deposited on top of PMMA coated glass substrate at Ts= (a) RT, (b) 60°C, (c) 90°C and (d) 120°C respectively.

This observation was also supported by the XRD and Raman analysis (see Figures 4.4c and 4.4d). It was observed that the XRD spectra of ZnPc molecule at 90°C showed the highest particle size, D= 22.7 nm and d-spacing value of 12.7 Å at 2θ = 6.9°. The calculated d-spacing of all the thin films deposited at different Ts along with their respective peak positions are shown and summarized in Figure 4.7 and Table 4.1 respectively.

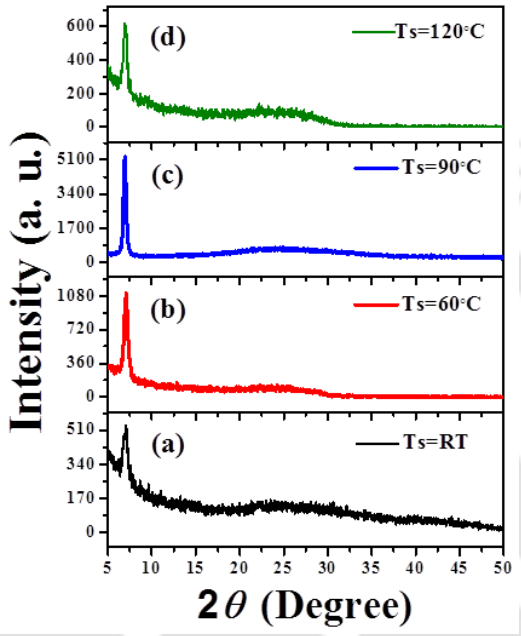

Figure 4.7 X-ray diffractograms of ZnPc thin films deposited on PMMA coated glass substrate at Ts= (a) RT, (b) 60°C, (c) 90°C and (d) 120°C respectively.

Table 4.1. X-ray diffraction analysis of ZnPc films prepared on PMMA coated glass substrate at different Ts.

Ts (°C)	2θ (Degree)	d-spacing, d (Å)	Particle size, D (nm)
RT	7.0	12.5	9.5
	22.4	4.0	
	42.2	2.1	
60	7.1	12.7	18.4
	22.2	7.0	
90	6.9	12.7	22.7
	24.2	3.7	
	41.9	2.2	
120	7.0	12.7	19.2
	22.4	4.0	

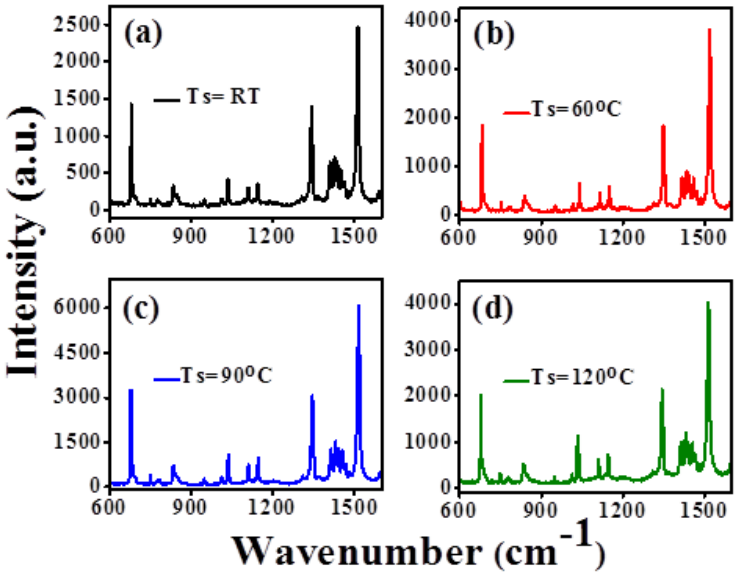

Figure 4.8 Raman spectra of ZnPc thin films deposited on PMMA coated glass substrate at Ts= (a) RT, (b) 60°C, (c) 90°C and (d) 120°C respectively.

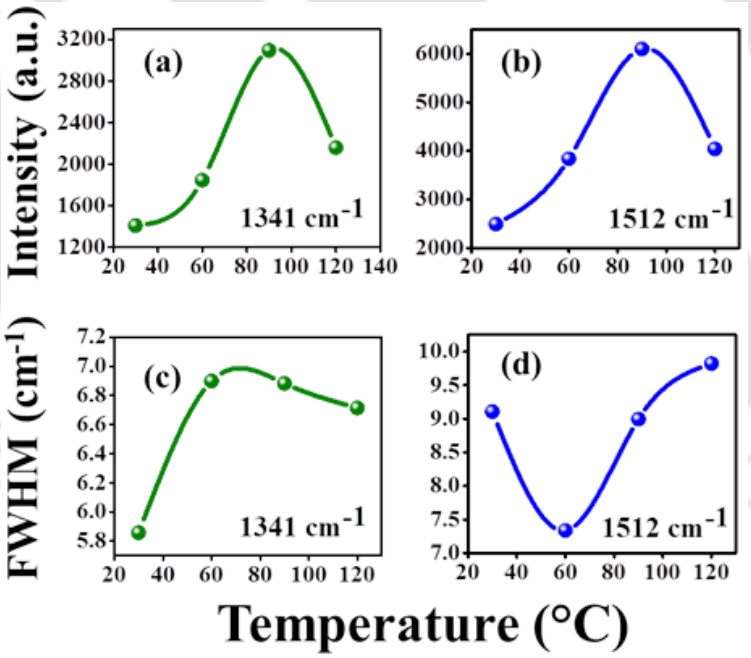

Figure 4.9 Graphical representation of the Ts dependencies of the intensity (a), (b) and FWHM (c), (d) of 1341 and 1512 cm^{-1} Raman modes of ZnPc molecule on PMMA coated glass substrate at Ts= RT, 60°C, 90°C and 120°C respectively.

From Raman spectra (Figure 4.8 and Figure 4.9) it was observed that up to Ts= 90°C, the integral intensities of 1341 cm^{-1} and 1512 cm^{-1} modes which are generally responsible for the stretching and bending vibrations of Zn and N interaction, increased systematically and thereafter it started showing anomalous behaviour for both 1341 cm^{-1} and 1512 cm^{-1} (Figure 4.9a and Figure 4.9b).[10,11]

However, in case of FWHM (Figure 4.9c and Figure 4.9d), a systematic increase in behaviour was observed from RT to 120°C. This observed anomaly in the integral intensity modes indicates that there is a change in planarity of the thin film growth pattern of ZnPc molecule because of the deformation in the symmetry of the molecular structure which is initiated at Ts= 90°C due to the interaction of heavy Zn atom with nitrogen, indicating that the Ts has a strong influence on the growth structure of ZnPc molecule and 90°C is the optimum Ts for ZnPc-OFETs fabrication. The band gap of the ZnPc molecule at 90°C estimated from the Q-band first maxima peak (at 624 nm) [Inset-Figure 4.4c] is ~1.97 eV, whereas, for the second maxima (699 nm) it is ~1.77 eV, which indicated that ZnPc could be easily excited and be responsive to visible light.

4.2.2 Operation Mechanism of PS-OFETs

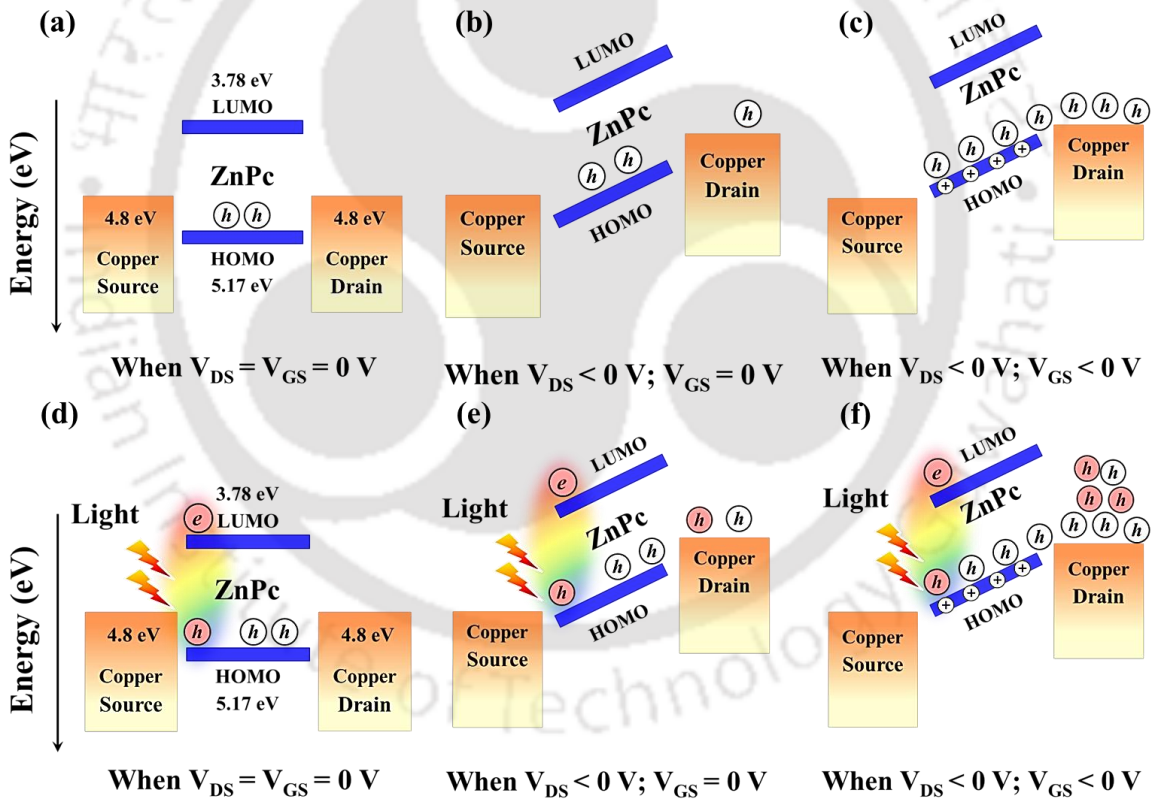

Figure 4.10 Schematic representation of the operation mechanism involved in of ZnPc based p-channel OFETs (a-c) in dark condition and (d-f) in presence of light illumination respectively.

Figure 4.10(a-c) and Figure 4.10(d-f) represent the operation mechanism of ZnPc based PS-OFETs by the simplified energy band diagram under dark and light illumination conditions respectively. The voltage applied between the source to drain and gate to source are represented by V_{DS} and V_{GS} respectively. As the devices were fabricated in

bottom gate top contact configuration, the amount of current flow from source to drain contacts through the ZnPc thin film is strongly dependent on the amount of gate voltage V_{GS}, applied through the gate electrode for a particular V_{DS}. Since the semiconducting layer and the gate electrode are capacitive coupled with each other through the bilayer dielectric system, the charges induced in the semiconductor thin film are generally mobile charges and move with response to the particularV_{DS}.

Figure 4.10a represents the HOMO (~5.17 eV) and LUMO (~3.78 eV) of the ZnPc semiconductor layer with respect to the relative Fermi levels (~4.8 eV) of the Cu source and drain contacts when $V_{DS} = V_{GS} = 0V$, under dark condition. At this condition, the device is in "OFF" state because no current flows from source to drain contacts. When $V_{DS} < 0V$ and $V_{GS} = 0V$ (Figure 4.10b), positively charged holes, initially present in the p-type ZnPc semiconductor, start moving towards the negatively biased drain contact. Since there are no mobile charges present at this condition (since $V_{GS} = 0V$) the current between the source to drain is negligible. When the gate voltage is applied, i.e. $V_{DS} < 0V$ and $V_{GS} < 0\,V$, (Figure 4.10c) mobile charges are induced in the ZnPc semiconductor thin film through the bilayer dielectric system and the transistor becomes in its "ON" state. These mobile charges create a large electric field at semiconductor-dielectric interface which shifted the HOMO and LUMO levels of the semiconductor upwards to match the HOMO to the Fermi level of the Cu drain contact. Since V_{DS} is already less than $0V$ at this condition, more number of positively charged holes will flow through the channel, thereby increasing the drain current.

In case of light illumination on the device, [shown in Figure 4.10(d-f)] these same three mechanisms are expected to take place. The only difference likely to be observed is due to the light illumination when excitons are formed in the semiconductor layer. However, at equilibrium condition i.e. $V_{DS} = V_{GS} = 0V$, there is no current flow from source to drain and only the photo generated charge carriers are present at the semiconductor layer (Figure 4.10d). As $V_{DS} < 0V$ and $V_{GS} = 0V$ (Figure 4.10e), excitons are separated due to the applied V_{DS} and increases the positively charged carrier concentration at the channel. However, again due to the absence of mobile charges, the drain current is less here but more than the similar situation in the dark condition (Figure 4.10b). When both the gate and drain terminals are biased i.e. $V_{DS} < 0V$ and $V_{GS} < 0\,V$, the mobile charges are induced in the channel and the transistor shifted to its "ON" state. The drain current is enhanced in this case (Figure 4.10f) because of the additional holes present in the channel due to the light illumination, which further enhanced the drain current compared to the similar situation in the dark condition (Figure 4.10c).

4.2.3 Device Characteristics

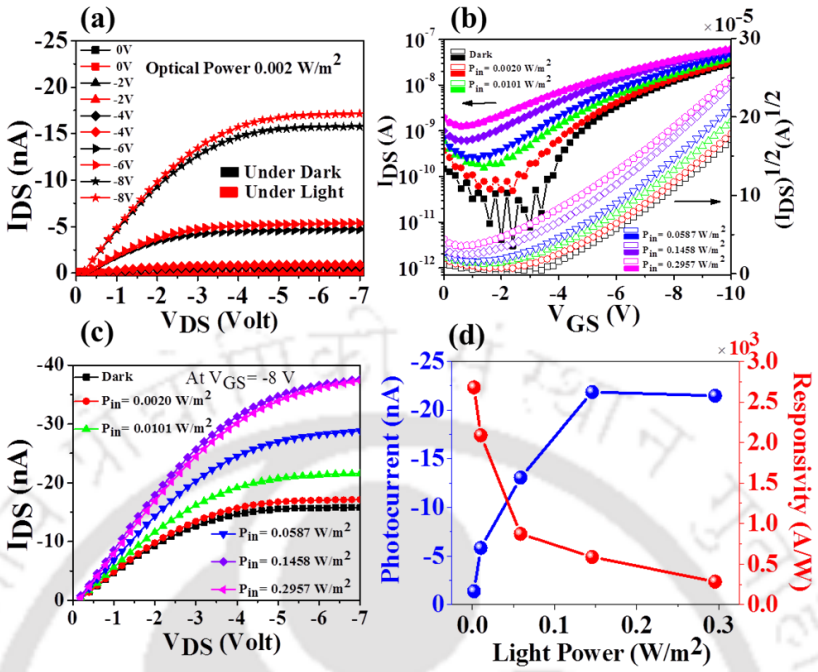

Figure 4.11 (a) Drain characteristic curves of ZnPc based PS-OFETs under dark and light illumination at incident lowest optical power, P_{in}= 0.002 W/m². (b) The transfer characteristics of ZnPc based PS-OFETs under dark and different incident power illumination. (c) Photo current of ZnPc-PS-OFET at V_{GS}= -8V in presence of various optical powers. (d) Responsivity and Photocurrent curves with respect to different incident power at V_{GS}= -8 V.

The photo response characteristics of ZnPc based PS-OFETs are shown in Figure 4.11. The typical channel length (L) and channel width (W) of the devices were kept at 40 µm and 780 µm respectively. Figure 4.11a represents the drain characteristics of the device under the illumination of lowest optical power (P_{in}= 0.002 Wm^{-2}) whereas, Figure 4.11b represents the shift in threshold voltage in the transfer characteristics curve of the device under the irradiation of various optical power. From these drain and transfer characteristics it could be concluded that the device showed significant increase in drain current with low operating voltage, under the illumination of light. The photo-responsivity (R), of the device was calculated by using the Equation (4.2) given below-

$$R = \frac{I_{Ph}}{I_{opt}} = \frac{(I_{DS,illum} - I_{DS,dark}).S^{-1}}{P_{in}} \qquad (4.2)$$

where, I_{Ph} represents the source-to-drain photocurrent, P_{opt} is the incident light power. $I_{DS,dark}$ and $I_{DS,illum}$ are the source-drain current under dark and illumination conditions and P_{in} represents the power of the incident light per unit area respectively. It was observed that the devices showed remarkable photo-responsive behavior, R~ 2679.4 A.W-

[1] at V_{DS}= -7 V; V_{GS}= -8 V under the illumination of very low optical power, P_{in}= 0.002 Wm^{-2} on a small effective sensing area S= 2.54× 10^{-6} cm^2. The photo ON/OFF current ratio of the same device is observed to be 933.56 under the irradiation of highest optical power, P_{in}= 0.2957 Wm^{-2} with the same biasing condition. Moreover, the operating voltage of the device was also very low (-8V), confirming the consumption of electrical power to be very less to operate this device. Figure 4.11c and Figure 4.11d represents the graphical representation of I_{DS} vs. V_{DS} and photocurrent and responsivity curves with respect to different incident power at V_{GS}= -8 V respectively. From Figure 4.11c it was observed that the photo current of ZnPc-PS-OFET at V_{GS}= -8V increases continuously up to the power of 0.1458 Wm^{-2} and with further increase in power (P_{in}= 0.2957 Wm^{-2}), it started decreasing, indicating the maximum limitation of the photocurrent generation of ZnPc based PS-OFET. All the device parameters of the ZnPc based PS-OFETs under dark and various optical power illuminations are summarized in Table 4.2.

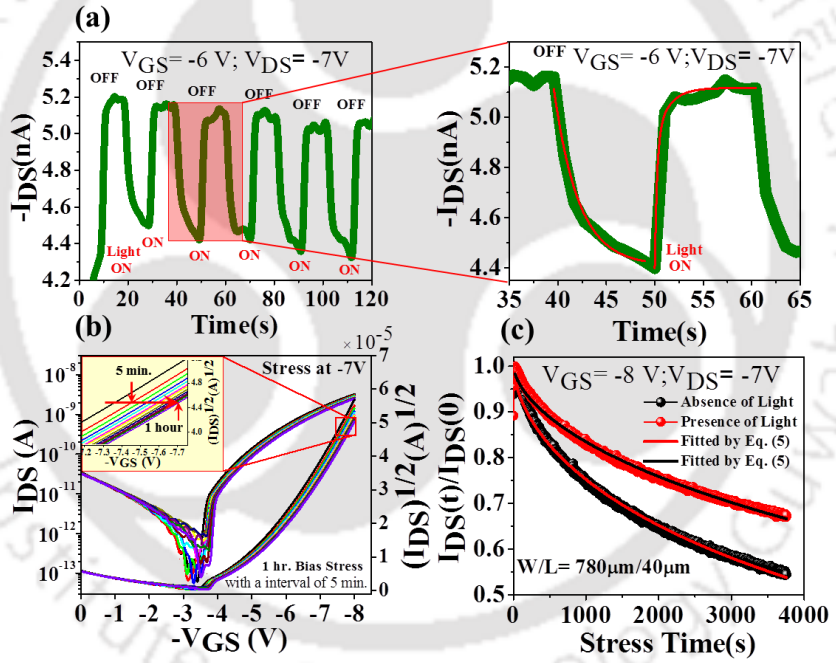

Figure 4.12 (a) The light on-off effect on ZnPc based PS-OFET and the fitted curves of the decay and growth of the IDS under light on-off condition at V_{DS}=-7 V and V_{GS}=-6 V respectively at P_{in}= 0.002 W/m^2. (b) The transfer curves of ZnPc based PS-OFET recorded under dark condition after providing the bias stress (at -7 V) every 5 min up to 1h and (c) represents the time dependence of the normalized drain current $I_{DS}(t)/I_{DS}(0)$ under dark and light illumination gated with Al_2O_3/PMMA bilayer dielectrics system.

To support the proposed mechanism and the observed experimental data we further recorded the rise and decay response of the devices and fitted them by Equation (4.3) and Equation (4.4) to estimate the growth and decay processes of I_{DS} of the device (Figure 4.12a).[30-32]

$$I_{Light_{Growth}} = I_{DS_{Dark}} + A.exp\left(\frac{t}{\tau_1}\right) + B.exp\left(\frac{t}{\tau_2}\right) \quad (4.3)$$

$$I_{Light_{Decay}} = I_{DS_{Dark}} + A.exp\left(\frac{-t}{\tau_1}\right) + B.exp\left(\frac{-t}{\tau_2}\right) \quad (4.4)$$

where, $I_{DS_{Dark}}$ is the dark current, A and B are the scaling constants, t is the time when the light was turned ON or OFF, and τ_1 and τ_2 are the time constants. In these ZnPc based PS-OFETs, the estimated time constants τ_1 and τ_2 are observed as 2.55 sec and 1.46 sec for decay and 1.36 sec and 0.23 sec for growth process respectively, where, time constant τ_1 represents the carrier generation and recombination processes in the semiconductor thin film, and τ_2 is related to the hole trapping and release processes at the interface.[33,34]

For more detailed analysis, the experimental data (Figure 4.12) of I_{DS} was fitted with the stretched-exponential time (t) dependent, Equation 4.5-

$$I_{DS}(t) = I_{DS}(0).exp\left\{-\left(\frac{t}{\tau'}\right)^{\beta}\right\} \quad (4.5)$$

where, β is the stretching parameter related to the barrier energy height for charge trapping ($0 < \beta \leq 1$), τ' is the relaxation time and $I_{DS}(0)$ is the initial maximum drain-source current measured at the beginning of the applied stress.

Table 4.2. Summary of ZnPc based PS-OFETs parameters under dark and various optical power illumination conditions.

Optical Power (W/m^2)	V_{Th} (V)	SS (V/decade)	$N_{trap} \times 10^{12}$ ($eV^{-1} cm^{-2}$)	$\mu \times 10^{-3}$ ($cm^2/V\,s$)	Responsivity (A/W)	Photo I_{ON}/I_{OFF} Ratio
Dark	-4.0	0.2	0.4	3.9	---	---
0.0020	-3.7	1.4	3.6	3.7	2679.4	16.2
0.0101	-3.2	2.8	7.4	3.7	2089.2	88.4
0.0587	-2.7	3.0	8.0	4.0	874.2	173.03
0.1458	-2.1	3.8	10.1	4.2	589.5	502.8
0.2957	-1.3	4.6	12.3	3.3	285.3	933.6

It was observed that the values of β under dark and light illumination are 0.59 and 0.61 and the corresponding relaxation time (τ') values are 8.5×10^3 sec and 1.6×10^4 sec respectively. The larger β and τ' values in presence of light confirms the better stability of the device, which is highly desirable for practical applications of these PS-OFETs.

Generally, an ideal optical sensor device should be cost effective, stable and must be versatile to allow fabrication on any desired substrate. It should not degrade in

presence of light, ambient conditions and have low operating voltage range so that less electrical power is required during device operation. Most of the widely used, stable organic optical sensors, reported till date, are generally fabricated on Si/SiO_2 or ITO based substrate which significantly enhances the overall device cost, and coupled with the higher power consumption and poor flexibility reduces their demand further in the new generation of wearable and flexible electronics.

Table 4.3. Summary of other small molecule based organic photo sensitive transistor with their respective device structure.

Method	Organic Semiconductor	Device structure	Mobility (cm^2 /Vs)	Responsivity (Light source, Intensity)	I_{ph} / I_{dark}	Ref.
Vapor	BPTT	BG/TC (SiO_2)	0.082	82 A/W (380 nm, 1.55 mW/cm^2)	2×10^5	14
	CuPc	BG/TC (SiO_2)	0.02	0.5–2 A/W (365 nm, 1.55 mW/ cm^2)	3×10^3	20
	F_{16}CuPc	BG/TC (P4PMS)	5.3×10^{-4}	1.5 mA/W (White light, 5.66 mW/ cm^2)	22	36
		TG/BC (CL-PVP)	1.05×10^{-4}	1.4 mA/W (White light, 5.98 mW/ cm^2)	79	37
		TG/BC (CL-PVP)	4.6×10^{-4}	2.15 mA/W (White light, 5.66 mW/ cm^2)	300	38
	Pentacene	BG/TC (SiO_2)	0.49	10–50 A/W (365 nm, 1.55 mW/ cm^2)	1.3×10^5	20
		BG/TC (PMMA)	0.01	0.015 A/W (365 nm, 7 mW/ cm^2)	2×10^4	39
	6T	BG/TC (SiO_2)	0.09	1.5–2.4 A/W (365 nm, 1.55 mW/ cm^2)	1.3×10^3	10
	Tetracene	BG/TC (SiO_2)	0.003	NA (364 nm, 0.64 mW/ cm^2)	3×10^3	40
	ABT	BG/TC (SiO_2, OTS)	0.4	1000 A/W (White light, 30 µ W/ cm^2)	800	41
	DPASP	BG/BC (SiO_2, HMDS)	0.67-6.8×10^{-7}	0.1 A/W (White light, 0.96 mW/ cm^2)	100	42
	Spiro-DPSP	BG/BC (SiO_2, HMDS)	1.3×10^{-6}	1 A/W (370 nm, 191 µ W/ cm^2)	5×10^2	12
	Spiro-DPSP 2	BG/BC (SiO_2, HMDS)	2.7×10^{-7}	0.44 A/W (370 nm, 64 µ W/ cm^2)	2.1×10^3	43
	Spiro-4P-CPDT	BG/BC (SiO_2, HMDS)	1 - 2 $\times10^{-4}$	25 A/W (370 nm, 2.4 µ W/ cm^2)	290	22
Vapor/ Solution	Pentacene/PC_{60}BM	BG/BC (ODPA)	0.1- 10^{-3}	NA (469 nm, 3.2 mW/ cm^2)	10^3	44

In this regard, ZnPc single crystal nanobelts based efficient light sensing organic transistor, grown by physical vapor transport process on octadecyltrichlorosilane (OTS) modified Si/SiO_2 substrate with gold (Au) as the top source-drain contact showed high photo-responsivity.[35] Similarly, the light sensing property of CuPc/pentacene based

OFETs deposited on Si/SiO_2 substrate showed photo-responses of 0.5-2 and 10-50 A/W and maximum photo ON/OFF current ratio of 3000 and 1.3×10^5 respectively, under 365 nm UV light.[20] Fluorinated CuPc ($F_{16}CuPc$) based n-type light sensing organic transistor on patterned ITO coated glass substrates, poly(4-phenoxymethyl styrene) (P4PMS) as the polymeric gate dielectric and Au as the top source-drain contacts showed photosensitivity of 1.5 mA/W and photo ON/OFF current ratio of 22.[36] Table 4.3 provides the summary of small molecule based organic photo sensitive transistors with their respective device structure.[37-43] However, due to the extensive use of either ITO or Si/SiO_2 substrates all these devices had very high operating voltage that increased the external electrical power requirement to operate the device. Hence, in this study we could demonstrate the fabrication of ZnPc based PS-OFETs successfully that avoids the use of ITO and Si/SiO_2 which makes the OFETs very cost effective with low bias stress on a glass substrate. This low-cost, low bias stress and electrically stable device is expected to have potential applications in optoelectronic devices and energy efficient sensors.

4.3 Conclusion

In conclusion, the fabrication and characterization of ZnPc based PS-OFETs, on Al_2O_3/PMMA bilayer dielectric system to achieve remarkable light sensitivity under the various power illumination on a small effective sensing area S= 2.54×10^{-6} cm^2 is reported. At the same time, the operating voltage of the device was drastically reduced to -8 V without sacrificing its optical sensing property confirming that the consumption of electrical power to operate the PS-OFET is very less. The bilayer dielectric configuration was used to achieve high drain current and low gate voltage operation of the PS-OFETs to obtain better capacitor coupling at the dielectric-semiconductor interface. Further, the combination of Al_2O_3 (ε~10) and PMMA (ε ~3.5), bilayer dielectric materials offers excellent mechanical and optical properties. Since the aim was to develop low cost and low operating voltage, stable devices, a cost-effective anodic oxidation method was used for the deposition of Al_2O_3 on normal microscope glass substrate by avoiding expensive Si/SiO_2 and ITO substrate. The ZnPc based PS-OFETs having top contact Cu electrode exhibits excellent p-channel behaviour with photo responsivity as high as, R~ 2679.4 $A.W^{-1}$ at V_{DS}= -7 V; V_{GS}= -8 V at P_{in}= 0.002 Wm^{-2} with effective sensing area S= 2.54×10^{-6} cm^2. The photo ON/OFF current ratio of the same device is observed to be 933.6 at P_{in}= 0.2957 Wm^{-2} with the same biasing condition. The device showed remarkable light sensitivity with characteristics carrier relaxation time, τ'~10^4 sec., with optical and

electrical stability having decay of I_{DS} ~20% after 30 min. under constant electrical dc bias stress, V_{DS}= -7 V and V_{GS}= -8 V for 30 min. On the other hand, multiple transfer characteristic scans and bias stress results indicated that these OFETs exhibit better operational stability, indicating potential applications of these transistors in electronic devices and sensors.

4.4 References

[1] Askim, J. R.; Mahmoudiab, M.; Suslick, K. S. Optical Sensor Arrays for Chemical Sensing: the Optoelectronic Nose. *Chem. Soc. Rev.* **2013**, *42*, 8649–8682.

[2] Bilro, L.; Alberto, N.; Pinto J. L.; Nogueira, R. Optical Sensors Based on Plastic Fibers. *Sensors* **2012**, *12*, 12184–12207.

[3] Gomes, H. L.; Stallinga, P.; Dinelli, F.; Murgia, M.; Biscarini, F.; de Leeuw, D. M.; Muck, T.; Geurts, J.; Molenkamp L. W.; Wagner, V. Bias-Induced Threshold Voltages Shifts in Thin-Film Organic Transistors. *Appl. Phys. Lett.* **2004**, *84*, 3184–3186.

[4] Stallinga, P.; Gomes, H. L.; Biscarini, F.; Murgia M.; de Leeuw, D. M.; Electronic Transport in Field-Effect Transistors of Sexithiophene. *J. Appl. Phys.* **2004**, *96*, 5277–5283.

[5] Nelson, S. F.; Lin, Y.-Y.; Gundlach, D. J.; Jackson, T. N. Temperature-Independent Transport in High-Mobility Pentacene Transistors. *Appl. Phys. Lett.* **1998**, *72*, 1854–1856.

[6] Hofmann, O.; Miller, P.; Sullivan, P.; Jones, T. S.; deMello, J. C.; Bradley D. D. C.; deMello, A. J. Thin-Film Organic Photodiodes as Integrated Detectors for Microscale Chemiluminescence Assays. *Sens. Actuators, B* **2005**, *106*, 878–884.

[7] Agostinelli, T.; Campoy-Quiles, M.; Blakesley, J. C.; Speller, R.; Bradley D. D. C.; Nelson, J. A Polymer/Fullerene Based Photodetector with Extremely Low Dark Current for X-Ray Medical Imaging Applications. *Appl. Phys. Lett.* **2008**, *93*, 203305.

[8] Keivanidis, P. E.; Greenham, N. C.; Sirringhaus, H.; Friend, R. H.; Blakesley, J. C.; Speller, R.; Campoy-Quiles, M.; Agostinelli, T.; Bradley D. D. C.; Nelson, J. X-Ray Stability and Response of Polymeric Photodiodes for Imaging Applications. *Appl. Phys. Lett.* **2008**, *92*, 023304.

[9] Du, C. Y.; Guo, Y. L.; Chen, J. M.; Liu, H. T.; Liu, Y.; Ye, S. H.; Lu, K.; Zheng, J. A.; Wu, T.; Liu, Y. Q.; Shuai Z. G.; Yu, G. Design, Synthesis, and Properties of Asymmetrical Heteroacene and Its Application in Organic Electronics. *J. Phys. Chem. C* **2010**, *114*, 10565–10571.

[10] Noh, Y.-Y.; Ghim, J.; Kang, S.-J.; Baeg, K.-J.; Kim D.-Y.; Yase, K. Effect Of Light Irradiation On The Characteristics Of Organic Field-Effect Transistors. *J. Appl. Phys.* **2006**, *100*, 094501.

[11] Liu, X. H.; Dong, G. F.; Duan, L.; Wang L. D.; Qiu, Y. High Performance Low-Voltage Organic Phototransistors: Interface Modification and the Tuning of Electrical, Photosensitive and Memory Properties. *J. Mater. Chem.* **2012**, *22*, 11836–11842.

[12] Saragi, T. P. I.; Pudzich, R.; Fuhrmann T.; Salbeck, J. Organic Phototransistor Based on Intramolecular Charge Transfer in a Bifunctional Spiro Compound. *Appl. Phys. Lett.* **2004**, *84*, 2334–2336.

[13] Mukherjee, B.; Mukherjee, M.; Sim K.; Pyo, S. Solution Processed, Aligned Arrays Of TCNQ Micro Crystals For Low-Voltage Organic Phototransistor. *J. Mater. Chem.* **2011**, *21*, 1931–1936.

[14] Noh, Y.-Y.; Kim, D.-Y.; Yoshida, Y.; Yase, K.; Jung, B.-J.; Lim E.; Shim, H.-K. High-Photosensitivity -Channel Organic Phototransistors Based on a Biphenyl End-capped Fused Bithiophene Oligomer. *Appl. Phys. Lett.* **2005**, *86*, 043501.

[15] Rao M.; Narayan, K. S. Evaluation of Electrode-Semiconductor Barrier in Transparent Top-Contact Polymer Field Effect Transistors. *Appl. Phys. Lett.* **2008**, *92*, 223308.

[16] Pal, T.; Arif M.; Khondaker, S. I. High Performance Organic Phototransistor Based on Regioregular Poly(3-Hexylthiophene). *Nanotechnology* **2010**, *21*, 325201.

[17] Wang, X. H.; Wasapinyokul, K.; De Tan, W.; Rawcliffe, R.; Campbell A. J.; Bradley, D. D. C. Device Physics of Highly Sensitive Thin Film Polyfluorene Copolymer Organic Phototransistors. *J. Appl. Phys.* **2010**, *107*, 024509.

[18] Labram, J. G.; Wöbkenberg P. H.; Bradley D. D. C.; Anthopoulos, T. D. Low-Voltage Ambipolar Phototransistors Based on a Pentacene/$PC_{61}BM$ Heterostructure and a Self-Assembled Nano-Dielectric. *Org. Electron.* **2010**, 11, 1250–1254.

[19] Kang, H.-S.; Choi, C.-S.; Choi, W.-Y.; Kim D.-H.; Seo, K.-S. Characterization Of Phototransistor Internal Gain in Metamorphic High-Electron-Mobility Transistors. *Appl. Phys. Lett.* **2004**, *84*, 3780–3782.

[20] Noh, Y.-Y.; Kim D.-Y.; Yase, K. Highly Sensitive Thin-Film Organic Phototransistors: Effect of Wavelength of Light Source on Device Performance. *J. Appl. Phys.* **2005**, *98*, 074505.

[21] Tang, Q. X.; Li, L. Q.; Song, Y. B.; Liu, Y. L.; Li, H. X.; Xu, W.; Liu, Y. Q.; Hu W. P.; Zhu, D. B. Photoswitches and Phototransistors from Organic Single-Crystalline Sub-micro/nanometer Ribbons. *Adv. Mater.* **2007**, *19*, 2624–2628.

[22] Saragi, T. P. I.; Londenberg J.; Salbeck, J. Photovoltaic and Photoconductivity Effect in Thin-Film Phototransistors Based on a Heterocyclic Spiro-Type Molecule. *J. Appl. Phys.* **2007**, *102*, 046104.

[23] Meixner, R. M.; Gobel, H.; Yildirim, F. A.; Bauhofer W.; Krautschneider, W. Wavelength-Selective Organic Field-Effect Phototransistors Based on Dye-Doped Poly-3-hexylthiophene. *Appl. Phys. Lett.* **2006**, 89, 092110.

[24] Marjanović, N.; Singh, T. B.; Dennler, G.; Günes, S.; Neugebauer, H.; Sariciftci, N. S.; Schwödiauer R.; Bauer, S. Photoresponse of Organic Field-Effect Transistors

Based on Conjugated Polymer/Fullerene Blends. *Org. Electron.* **2006**, *7*, 188–194.

[25] Narayan K. S.; Kumar, N. Light Responsive Polymer Field-Effect Transistor. *Appl. Phys. Lett.* **2001**, *79*, 1891–1893.

[26] Xu, Y. F.; Berger, P. R.; Wilson J. N.; Bunz, U. H. F. Photoresponsivity of Polymer Thin-Film Transistors Based on Polyphenyleneethynylene Derivative with Improved Hole Injection. *Appl. Phys. Lett.* **2004**, *85*, 4219–4221.

[27] Hamilton, M. C.; Martin S.; Kanicki, J. Thin-Film Organic Polymer Phototransistors. *IEEE Trans. Electron Devices* **2004**, *51*, 877–885.

[28] Deen M. J.; Kazemeini, M. H. Photosensitive Polymer Thin-Film FETs Based on Poly(3-octylthiophene). *Proc. IEEE* **2005**, *93*, 1312–1320.

[29] Baeg, K.-J.; Binda, M.; Natali, D.; Caironi M.; Noh, Y.-Y. Organic Light Detectors: Photodiodes and Phototransistors. *Adv. Mater.* **2013**, *25*, 4267–4295.

[30] Chitara, B.; Panchakarla, L. S.; Krupanidhi S. B.; Rao, C. N. R. Infrared Photodetectors Based on Reduced Graphene Oxide and Graphene Nanoribbons. *Adv. Mater.* **2011**, 23, 5419–5424.

[31] Sun, Z. H.; Liu, Z. K.; Li, J. H.; Tai, G.-A.; Lau S.-P.; Yan, F. Infrared Photodetectors Based on CVD-Grown Graphene and PbS Quantum Dots with Ultrahigh Responsivity. *Adv. Mater.* **2012**, *24*, 5878–5883.

[32] Jin, Z. W.; Gao, L.; Zhou Q.; Wang, J. Z. High-Performance Flexible Ultraviolet Photoconductors Based on Solution-Processed Ultrathin ZnO/Au Nanoparticle Composite Films. *Sci. Rep.* **2014**, *4*, 4268.

[33] Liu, Y.-R.; Lai P.-T.; Yao, R.-H. Improvement in the Electrical Performance and Bias-Stress Stability of Dual-Active-Layered Silicon Zinc Oxide/Zinc Oxide Thin-Film Transistor. *Chin. Phys. B* **2012**, *21*, 088503.

[34] Mok, S. M.; Yan F.; Chan, H. L. W. Organic Phototransistor Based on Poly(3-hexylthiophene)/TiO_2 Nanoparticle Composite. *Appl. Phys. Lett.* **2008**, 93, 023310.

[35] Gou, H.; Wang, G. R.; Tong, Y. H.; Tang Q. X.; Liu, Y. C. Electronic and Optoelectronic Properties of Zinc Phthalocyanine Single-Crystal Nanobelt Transistors. *Org. Electron.* **2016**, *30*, 158–164.

[36] Mukherjee, B.; Mukherjee, M.; Choi Y.; Pyo, S. Organic Phototransistor with n-Type Semiconductor Channel and Polymeric Gate Dielectric. *J. Phys. Chem. C* **2009**, *113*, 18870–18873.

[37] Mukherjee, B.; Mukherjee, M.; Choi Y.; Pyo, S. Control over Multifunctionality in Optoelectronic Device Based on Organic Phototransistor. *ACS Appl. Mater. Interfaces* **2010**, *2*, 1614–1620.

[38] Park, J.-E.; Mukherjee, B.; Cho, H.; Kim S.; Pyo, S. Flexible N-channel Organic Phototransistor on Polyimide Substrate. *Synth. Met.* **2011**, *161*, 143–147.

[39] Lucas, B.; El Amrani, A.; Chakaroun, M.; Ratier, B.; Antony R.; Moliton, A. Ultraviolet Light Effect on Electrical Properties of a Flexible Organic Thin Film Transistor. *Thin Solid Films* **2009**, *517*, 6280–6282.

[40] Choi, J.-M.; Lee, J.; Hwang, D. K.; Kim, J. H.; Im S.; Kim, E. Comparative Study of the Photoresponse from Tetracene-Based and Pentacene-Based Thin-Film Transistors. *Appl. Phys. Lett.* **2006**, *88*, 043508.

[41] Guo, Y. L.; Du, C. Y.; Di, C. A.; Zheng, J.; Sun, X. N.; Wen, Y. G.; Zhang, L.; Wu, W. P.; Yu G.; Liu, Y. Q. Field Dependent and High Light Sensitive Organic Phototransistors Based on Linear Asymmetric Organic Semiconductor. *Appl. Phys. Lett.* **2009**, *94*, 143303.

[42] Saragi, T. P. I.; Onken, K.; Suske, I.; Fuhrmann-Lieker T.; Salbeck, J. Ambipolar Organic Phototransistor. *Opt. Mater.* **2007**, *29*, 1332–1337.

5

Influence of Multilayer Dielectric for Photosensitive Organic Field Effect Transistor

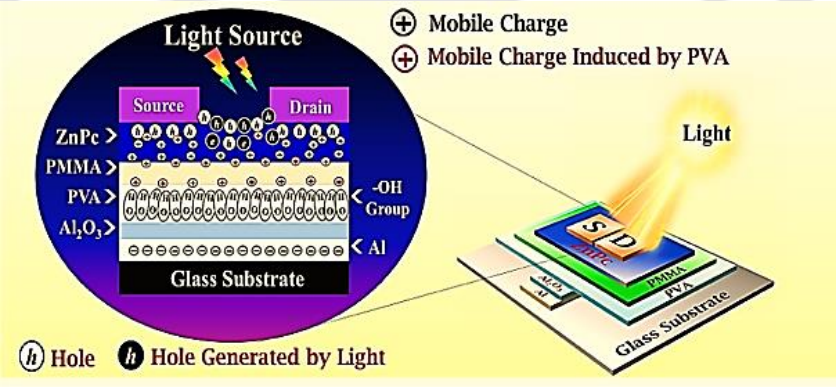

[1] **Dey, A.;** Singh, A.; Das, D.; Iyer, P. K. High-Performance ZnPc Thin Film-Based Photosensitive Organic Field-Effect Transistors: Influence of Multilayer Dielectric Systems and Thin Film Growth Structure. ***ACS Omega*** 2017, *2*, 1241-1248.

5

Influence of Multilayer Dielectric for Photosensitive Organic Field Effect Transistor

Development of highly efficient organic optical sensors is one of the most prominent research theme due to their potential applications in various optoelectronic devices, as low cost active optoelectronic components compared to the conventional inorganic counterparts.[1-8] The widely used optical sensors, such as photo diode, charge-coupled devices etc. consisting of inorganic active materials, although show promising sensitivity, their high fabrication cost, high power consumption and poor flexibility has reduced their demand in the new generation wearable and flexible electronics.[9-15] Thus, for practical applications, it is very vital that an ideal optical sensor should have low operating voltage as possible, high photo responsivity, high optical and electrical stability as well as it should be of low cost and versatile to be fabricated on desired substrate, preferably using economical solution based techniques. In this regard, organic π-conjugated semiconductor based PS-OFETs offers numerous advantages including its unique ability to detect light, low noise, switching capability and signal magnification in a single, low cost manufacturing and flexible device configuration.[16,17] PS-OFET is a three terminal photo sensitive organic electronic component, in which photo generated excitons at the active channel can easily be dissociated through the applied gate bias which provides highly effective and magnified photo detection. However, for the fabrication of highly photo responsive/sensitive OFET several factors have to be considered-(i) the active material should have high and broad absorption spectrum so that maximum number of

carriers can be generated by the incident light, (ii) the mobility of the active material should be superior to obtain easy transportation of the photo generated charge carrier through the channel and (iii) the energy barrier between the active material and the electrodes should be as low as possible so that the charge carriers can be collected for signal efficiently.[18-23] Generally point (i) can be improved through different chemical synthesis protocol by modulating the chemical structure of the active material. However, the low mobility of most organic semiconductors, constrains the development of points (ii) and (iii). Herein, by introducing multilayer dielectric systems and tuning the thin film morphology of the active layer with respect to different substrate temperature (Ts), the process (ii) was modified to realize remarkable improvements in the PS-OFET performance. Among organic semiconductors, porphyrins and phthalocynines are two representative and important macro cycle systems, used as active materials in PS-OFETs due to their wide range of optical absorption spectra and easily tunable electrical and optical properties by which one can modify its thin film growth microstructure.[24,25] Since the dielectric-active material interface and molecular packing of the active layer have a strong influence on the mobility of OFETs it is very important to utilize economical and sustainable materials such as solution processable polymers and clearly understand the growth mechanism of these polymer based dielectric layers in the devices to optimize the thin film growth structure of the deposited active layer prior to device fabrication.[26-39]

Hence, the impact of thin film growth structure and multilayer polymer dielectric systems on the photo response properties of ZnPc based PS-OFETs at various incidents optical powers have been systematically analysed. The combination of inorganic Al_2O_3 and organic non-polar PMMA are used as the bilayer dielectric configuration, whereas in the case of tri-layer dielectric system, bilayer polymer dielectrics, consisting of PMMA as a low-k dielectric polymer, on the top of high-k polar dielectric, PVA have been used along with Al_2O_3 as the third layer. A systematic analysis of the growth nature of ZnPc molecule, deposited on PMMA coated glass substrates at different substrate temperatures (Ts) viz. at room temperature (RT), 60 °C, 90 °C and 120 °C respectively were analysed by various characterization techniques such as, AFM, FESEM, XRD and Raman analysis to optimize the Ts for the best device performance. At 90°C, the fabricated PS-OFET with Al_2O_3/PVA/PMMA tri-layer dielectric configuration showed best p-channel behaviour with enhanced and remarkable photo responsivity of R~9689.39 $A.W^{-1}$ compared to Al_2O_3/PMMA bilayer dielectric system (R~2679.40 $A.W^{-1}$) because of the superior charge transport through the channel by the polarization of dipoles inside the polar-PVA dielectric which increased the charge carrier mobility by one order (μ_h~1.3×10^{-2} $cm^2.V^{-1}.s^{-}$

^{1}) compared to the bilayer dielectric configuration (μ_h~3.9×10^{-3} cm^2.V^{-1}.s^{-1}). The observed specific detectivity, D* and noise equivalent power, NEP values of the bi-layer dielectric system are 6.01 × 10^{13} Jones and 2.655 × 10^{-17} W.Hz$^{-1/2}$ respectively whereas for trilayer dielectric system the observed D* and NEP values are 5.13 × 10^{14} Jones and 1.043 × 10^{-17} W.Hz$^{-1/2}$ respectively. Additionally, the operating voltage of each of the fabricated devices were observed to be exceedingly low (-10V) due to the influence of inorganic high-k Al_2O_3 dielectric layer. The electrical stability of each of the fabricated devices was also investigated by bias stress analysis under both the light and dark conditions in vacuum. To the best of our knowledge, the photo responsivity (R~2679.40 A.W^{-1}) values, reported herein with Al_2O_3/PVA/ PMMA tri-layer dielectric configuration, is the highest among all the thin film based PS-OFETs with remarkably low operating voltage of -10 V. This result suggested that the Al_2O_3/PVA/PMMA configuration along with appropriate Ts for ZnPc deposition generates highly efficient devices, (ITO and Si/SiO_2 free devices), with a benchmark photo responsivity performance of PS-OFETs that are expected to have potential applications in futuristic low-cost and wearable optoelectronics devices.

5.1 Experiments

5.1.1 Materials

ZnPc (99.999% purity), PMMA (M_W=550000 g/mol), aluminium wire (99.999% purity) and copper wire (99.9% purity) were purchased from Sigma Aldrich. Anisole (99% purity) and PVA (M_W~1, 15,000 g/mol) were purchased from Loba Chemie. All the chemicals and materials were used as received, unless otherwise mentioned. Microscope glass slides (thickness ~ 1.2mm) purchased from Jain Scientific Glass Works, India, was used as the device substrate without any surface modification.

5.1.2 Characterization Details

The thin films of ZnPc were deposited by thermal evaporation technique under 10^{-6} mbar of pressure. The thicknesses of the thin films were measured by Veeco Dektak 150 surface profilometer. A Perkin-Elmer Lambda 25 UV-visible spectrophotometer was used to record the UV-visible absorption spectra. AFM images of the thin films were recorded by Agilent 5500-STM instrument. Raman spectra were recorded by HR 800 raman spectrometer. Electrochemical measurements were performed by CH instrument. The

thin film XRD pattern was recorded by a Rigaku TTRAX III with Cu Kα radiation. For PS-OFET measurement, white light irradiation was performed by Oriel DC regulated illuminator connected with Lake Shore fibre optic probes having core diameter ~18µm. The optical power of the illuminated light was measure by both the Tenmars TM-207 power meter and Newport optical power/energy meter (Model 842-PE). All the three terminals opto-electrical properties were characterized by Keithley 4200 semiconductor characterization system with Lake Shore vacuum probe station and Keithley 2400 source meter.

5.1.3. Device Fabrication

The ZnPc based PS-OFETs were fabricated on bi-layer (Al_2O_3/PMMA) and tri-layer (Al_2O_3/PVA/PMMA) dielectric systems with bottom gate top contact configuration. The schematic representations are shown in the next operational mechanism section. For low voltage operation and reduced power consumption, generally, high-k dielectrics are often used in case of OFETs fabrication.[42-47] There are several high-k inorganic dielectric materials that are used in OFETs, such as Al_2O_3, which is one of the most promising material because of its excellent insulating properties and low-cost deposition process.[48-52] In this study, Al_2O_3 is used as high-k inorganic dielectric layer for low voltage operation, which is deposited by anodic oxidation method, followed by the procedure mentioned in the Chapter 2.[53] Since the grown Al_2O_3 thin film inherently has very high surface roughness ($\sigma_{r.m.s.}$ ~11.22 nm), a ~100 nm PMMA (30 mg.mL^{-1} in anisole) film was spun on top of the Al_2O_3 layer and dried for 1 h at 100 °C under inert atmosphere to obtain a smooth surface ($\sigma_{r.m.s.}$ ~1.97 nm) (see Figure 5.1).

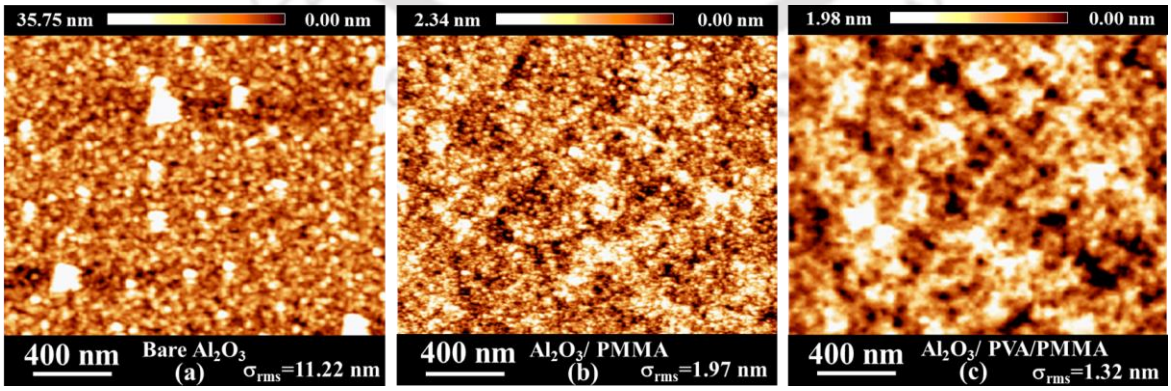

Figure. 5.1 AFM topography images (2µm×2µm) of (a) Bare Al_2O_3, (b) Al_2O_3/PMMA and (c) Al_2O_3/PVA/PMMA dielectric layers respectively.

However, in case of Al_2O_3/PMMA bi-layer dielectric system, though the devices were highly stable and hysteresis free, the drain current was less and the charge transportation through the channel was poor. Hence, high-k polar PVA dielectric was inserted in between PMMA and Al_2O_3 layers so that the polar PVA dielectric could induce more charges into the channel and further the nonpolar PMMA dielectric would prevent the direct interaction of the OH-groups of polar PVA dielectric layer with the active layer molecule. As a result, the enhancement in drain current with superior device stability could be achieved simultaneously. The capacitance density (C_i) of this Al_2O_3/PMMA and Al_2O_3/PVA/PMMA gate insulators were calculated independently from MIM structure of parallel plate capacitor using copper as the top electrode (Figure. 5.2). After the deposition of gate dielectric layers, a 60 nm (±10 nm) ZnPc active material was deposited by thermal deposition under a base pressure of 10^{-6} mbar at Ts = 90°C. Further, Cu source-drain electrodes were thermally deposited at RT (~80 nm) to calculate the three terminal properties of the PS-OFETs.

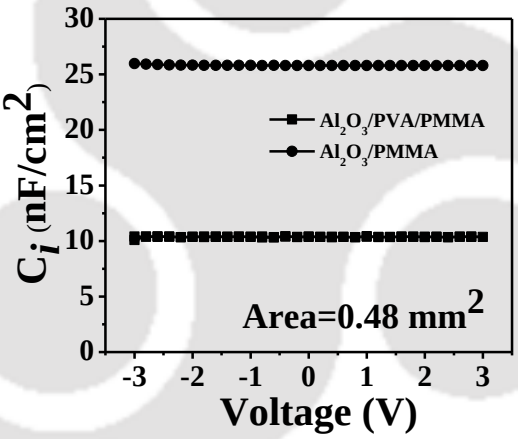

Figure. 5.2 Capacitance density curves of Al_2O_3/PMMA and Al_2O_3/PVA/PMMA gate insulators as a function of voltage at 100 kHz.

5.2 Results and Discussion

5.2.1 Device Characterizations

The photo response characteristics of ZnPc based PS-OFETs with Al_2O_3/PMMA and Al_2O_3/PVA/PMMA gate dielectric configurations under various incident optical power illuminations are shown in Figure 5.3. The typical channel length (L) and channel width (W) of the devices were kept at 40 µm and 780 µm respectively. Figure 5.3a and Figure 5.3c represent the drain characteristics of the devices with bi-layer and tri-layer device

configurations under the illumination of lowest optical power (P_{in}= 0.002 Wm^{-2}) whereas, Figure 5.3b and Figure 5.3d represent the shift in threshold voltage in the transfer characteristic curve of the devices under the irradiation of various optical power. From these drain and transfer characteristics it could be concluded that the device with Al_2O_3/PVA/PMMA configuration showed significant increase in drain current with low operating voltage, under the illumination of light compared to the Al_2O_3/PMMA configuration due to the slow polarization of the dipole in vacuum present at the high-k PVA dielectric that induced more charges at the semiconducting channel of the PS-OFETs.

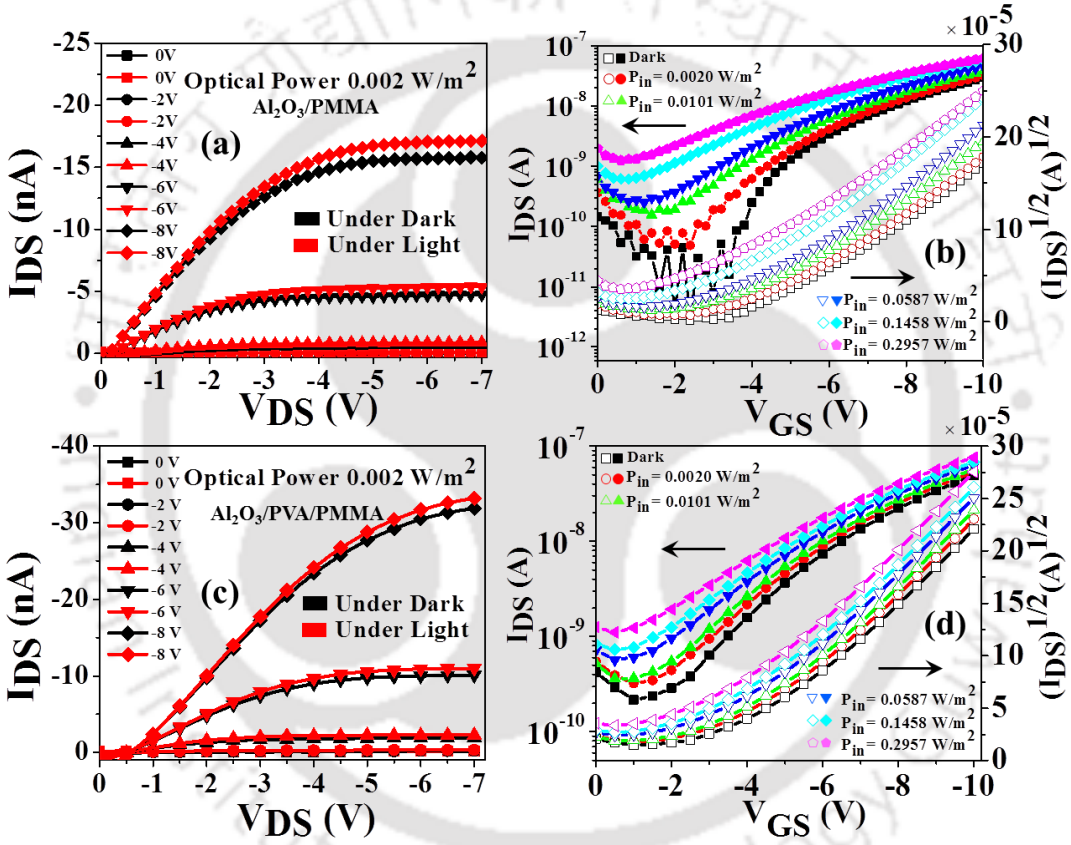

Figure.5.3 Drain characteristic curves of ZnPc based PS-OFETs with (a) Al_2O_3/PMMA and (c) Al_2O_3/PVA/PMMA configuration under dark and illumination at P_{in}= 0.002 Wm^{-2}. The transfer characteristics of ZnPc based PS-OFETs with (b) Al_2O_3/PMMA and (d) Al_2O_3/PVA/PMMA configuration under dark and different incident power illumination.

The photo-responsivity (R), of the device was calculated by using the Equation (5.1)-

$$R = \frac{I_{Ph}}{I_{opt}} = \frac{(I_{DS,illum} - I_{DS,dark}).S^{-1}}{P_{in}} \qquad (5.1)$$

where, I_{Ph} represents the source-to-drain photocurrent, $P_{opt}$is the incident light power. $I_{DS,dark}$ and $I_{DS,illum}$ are the source-drain current under dark and illumination conditions

and P_{in} represents the power of the incident light per unit area respectively. S is signified the effective sensing area of the device.

It was observed that the Al_2O_3/PVA/PMMA devices showed remarkable photo-responsive behaviour, R~9689.39 $A.W^{-1}$ at V_{DS}= -7 V; V_{GS}= -8 V under the illumination of very low optical power, P_{in} = 0.002 Wm^{-2} on a small effective sensing area S = 2.54×10^{-6} cm^2. The photo ON/OFF current ratio of the same device is observed to be 5.8 under the irradiation of highest optical power, P_{in}= 0.2957 Wm^{-2} with the same biasing condition. Moreover, the operating voltage of the device was also incredibly low (-7V), confirming the consumption of very less electrical power to operate this device. All the device parameters of the ZnPc based PS-OFETs under dark and various optical power illuminations with Al_2O_3/PMMA and Al_2O_3/PVA/PMMA dielectric configuration are summarized in Table 5.1.

Table 5.1. Summary of ZnPc based PS-OFETs parameters under dark and various optical power illumination conditions.

Dielectric System	Optical Power (W/m^2)	V_{Th} (V)	SS (V/decade)	$N_{trap}\times10^{12}$ ($eV^{-1}\,cm^{-2}$)	$\mu\times10^{-3}$ (cm^2/Vs)	Responsivity (A/W)	Photo I_{ON}/I_{OFF} Ratio
Al_2O_3/PMMA	Dark	-4.0	0.2	0.4	3.9	---	---
	0.0020	-3.7	1.4	3.6	3.7	2679.4	16.2
	0.0101	-3.2	2.8	7.4	3.7	2089.2	88.4
	0.0587	-2.7	3.0	8.0	4.0	874.2	173.0
	0.1458	-2.1	3.8	10.1	4.23	589.5	502.8
	0.2957	-1.3	4.6	12.3	3.3	285.3	933.6
Al_2O_3/PVA/PMMA	Dark	-3.1	3.0	3.2	12.9	---	---
	0.0020	-3.0	3.5	3.7	14.7	9689.4	1.5
	0.0101	-2.7	3.5	3.7	14.3	3126.9	1.7
	0.0587	-2.4	4.0	4.3	13.8	855.9	2.8
	0.1458	-2.1	4.5	4.8	13.9	465.0	3.6
	0.2957	-2.0	5.0	5.4	15.1	314.4	5.8

5.2.2 Operational Mechanism

Figure 5.4 schematically represents the operation mechanism of ZnPc based PS-OFETs under dark and light illumination conditions with (Figure 5.4a to Figure 5.4f) Al_2O_3/PMMA bi-layer and (Figure 5.4g to Figure 5.4l) Al_2O_3/PVA/PMMA tri-layer device configurations respectively. The voltage applied between the source to drain and gate to source are represented by V_{DS} and V_{GS} respectively. As the devices were fabricated in bottom gate top contact configuration, the amount of current flow from source to drain

contacts through the ZnPc thin film and is strongly dependent on the amount of gate voltage V_{GS}, applied through the gate electrode for a particular V_{DS}. Since the semiconducting layer and the gate electrode are capacitive coupled with each other through the multi-layer dielectric system, the charges induced in the semiconductor thin film are generally mobile charges and move with response to the particular V_{DS}.

Figure.5.4 Schematic representation of the operation mechanism involved in of ZnPc based p-channel OFETs (a-f) with Al_2O_3/PMMA bi-layer and (g-l) Al_2O_3/PVA/PMMA tri-layer device configurations respectively.

Figure 5.4a and Figure 5.4g represent the general schematic of the two different device configurations namely Al_2O_3/PMMA and Al_2O_3/PVA/PMMA respectively. Under dark condition, when $V_{DS}=V_{GS}=0V$ (see Figure 5.4b and Figure 5.4h), both the devices are in "OFF" state because no current flows from source to drain contacts. At this equilibrium condition, when light is illuminated on the channel with a minimum threshold power (Figure 5.4c and Figure 5.4i), excitons are formed in the semiconductor layer. However, as $V_{DS}=V_{GS}=0V$, there is no current flow from source to drain and only the photo generated charge carriers are present at the semiconductor layer. When $V_{DS}<0V$; $V_{GS}=0V$, (Figure 5.4d and Figure 5.4j), positively charged holes, initially presence in the p-type ZnPc semiconductor, start moving towards the negatively biased drain contact. At the same time, the photo generated excitons begin to dissociate due to the applied V_{DS} and increase the positive charge carrier concentration at the channel. Since there are no mobile charges present at this condition (since $V_{GS}=0V$) the total current between the source to drain is negligible at this stage.

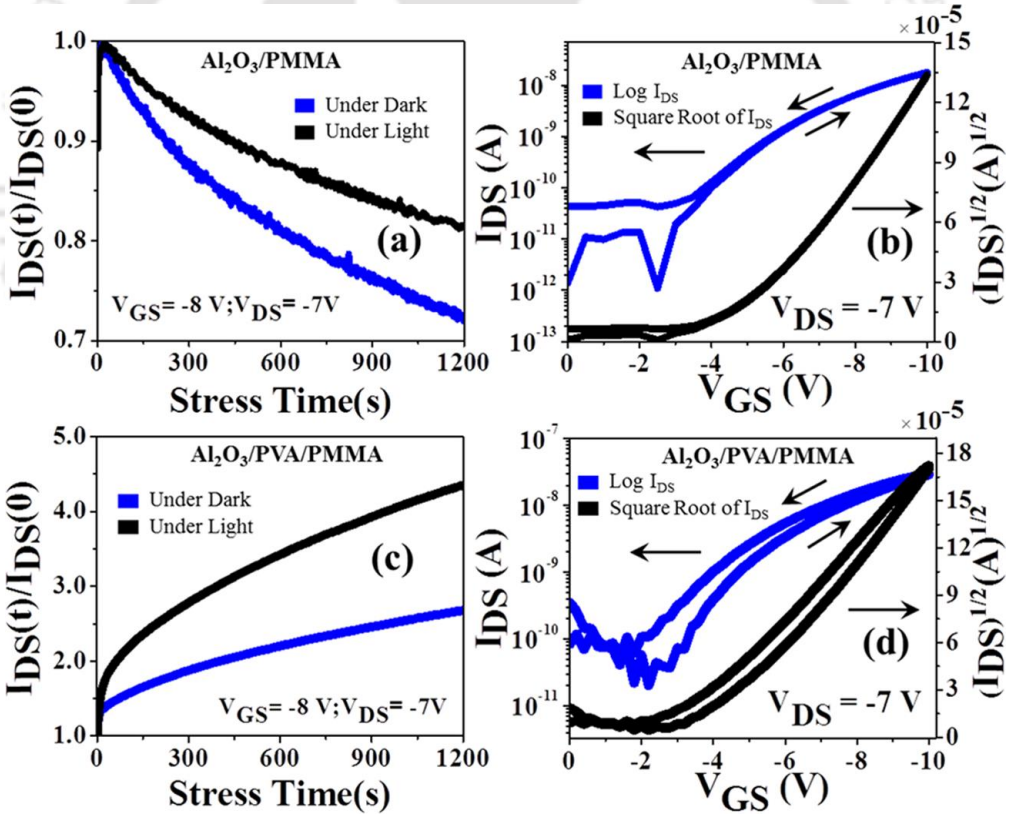

Figure. 5.5 (a, b) and (c, d) Graphical representations of bias stress and hysteresis measurements of ZnPc-PS-OFETs with Al_2O_3/PMMA and Al_2O_3/PVA/PMMA, respectively.

When the gate voltage is applied, i.e. $V_{DS}<0V$ and $V_{GS}<0V$, in case of Al_2O_3/PMMA device configuration (Figure. 5.4e) mobile charges are induced in the ZnPc semiconductor thin film through the bilayer dielectric system and the transistor comes to its "ON" state.

These mobile charges create a large electric field at semiconductor-dielectric interface which shifted the HOMO and LUMO levels of the semiconductor upwards to match the HOMO to the Fermi level of the copper drain contact. Since V_{DS} is already less than 0V at this condition, more number of positively charged holes will flow through the channel, thereby increasing the drain current. Moreover, because of the additional holes present in the channel due to the light illumination, this further enhances the drain current in presence of light compared to the similar situation in the dark condition. When gate voltage deceases from more negative value to less negative value (i.e., gate voltage swept from -10 V to 0 V) with the same condition i.e. V_{DS}<0V and V_{GS}<0V; (Figure. 5.4f) the concentration of mobile charges started to decrease immediately in the PMMA-semiconductor thin film interface which further shifted the HOMO and LUMO levels of the semiconductor downwards to the Fermi level of the copper drain contact. As a result current started to decrease. Since PMMA is a non-polar polymer dielectric, trapping of charges at the semiconductor-dielectric interface becomes less which was also proved by hysteresis analysis (Figure. 5.5b). Similar phenomenon also takes place in case of Al_2O_3/PVA/PMMA tri-layer dielectric configuration. The non-polar PMMA dielectric layer was used here on the top of polar-PVA dielectric, to prevent direct contact of the polar -OH groups in PVA dielectric with the semiconductor thin film so that trapping of charges became less at the PMMA-ZnPc interface compared to PVA-ZnPc. PVA is a high-k dielectric polymer, containing polar -OH groups, that are randomly distributed when V_{GS}= 0V. When the gate voltage is applied i.e., V_{DS}<0V and V_{GS}<0V, (Figure. 5.4k), these –OH groups present at the PVA layer start polarizing slowly and at the maximum V_{GS}, almost all the groups are fully polarized. These polarized -OH groups generate an additional electric field at the PVA and PMMA dielectric interface which can further help to induce more mobile charges at the PMMA-semiconductor thin film interface. These induced mobile charges along with the photo generated charges increase the concentration of holes more at the channel. As a result drain current becomes more at this condition compared to bilayer dielectric configuration (Figure 5.4e). When gate voltage deceases from more negative value to less negative value as in the bilayer dielectric system under the same condition i.e., V_{DS}<0V and V_{GS}<0V; (Figure 5.4l) the same mechanism like Figure 5.4f is expected to take place. However, due to the slow polarization of the hydroxyl group at the PVA dielectric, the polarity of the electric field at the PVA-PMMA changes very slowly. As a result though V_{GS} swept from -10 V to 0 V, at this stage, some positively polarized mobile charges remain at the PMMA-semiconductor thin film interface which opposes the sudden decay of the drain current, resulting in hysteresis of the transfer characteristics (Figure 5.5d).

Further in order to study the operational stability of both the fabricated bi-layer and tri-layer PS-OFETs, the time-dependent decay of I_{DS} in dark and light conditions under a DC bias stress with V_{DS} = -7 V and V_{GS} = -8 V over 1200 sec. (Figure 5.5a and Figure 5.5b) were recorded. It was observed that the decay of drain current in Al_2O_3/PMMA device configuration was very slow compared to Al_2O_3/PVA/PMMA due to lesser trapping of charges at the dielectric-semiconductor interface. Additionally, in case of Al_2O_3/PVA/PMMA, anomalous bias-stress effect was observed due to the slow polarization of the hydroxyl group. Moreover, in both the dielectric configuration, though the charge trap density increases (Table 5.1) in presence of light illumination compared to dark, in the bias stress study lesser decay of I_{DS} was obtained in presence of light compared to the dark condition due to the higher I_{DS} value in presence of light at V_{GS} = -8 V and V_{DS} = -7 V. This is because, after the illumination, the electron hole pairs are generated in the organic semiconductor. The excited electrons are transferred from HOMO to LUMO level. As a result, we observed enhancement in the drain current in presence of light illumination.

To analyse the relaxation characteristics of both the fabricated devices, their rise and decay response were fitted by Equation (5.2) and Equation (5.3) (see Figure 5.6) to estimate the growth and decay processes of I_{DS}.

$$I_{Light_{Growth}} = I_{DS_{Dark}} + A.exp\left(\frac{t}{\tau_1}\right) + B.exp\left(\frac{t}{\tau_2}\right) \quad (5.2)$$

$$I_{Light_{Decay}} = I_{DS_{Dark}} + A.exp\left(\frac{-t}{\tau_1}\right) + B.exp\left(\frac{-t}{\tau_2}\right) \quad (5.3)$$

where, $I_{DS_{Dark}}$ is the dark current, A and B are the scaling constants, t is the time when the light was turned ON or OFF, and τ_1 and τ_2 are the time constants. The time constant τ_1 represents the carrier generation and recombination processes in the semiconductor thin film, and τ_2 is related to the hole trapping and release processes at the interface. In these ZnPc based PS-OFETs, with Al_2O_3/PMMA bilayer dielectric system, the estimated time constants τ_1 and τ_2 are observed as 0.98 sec and 9.59 sec for decay and 0.43 sec for both τ_1 and τ_2 of growth process respectively. For Al_2O_3/PVA/PMMA tri-layer dielectric system, the estimated τ_1 and τ_2 for decay process are observed as 0.87 sec and 5.95 sec and for growth both τ_1 and τ_2 are obtained as 0.43 sec. From all these experimental data, it is clear that the required time for carrier generation and recombination in the semiconductor thin film for both the dielectric system is almost similar whereas the time required for hole trapping and release processes at the interface is much lower for tri-layer dielectric system compared to Al_2O_3/PMMA.

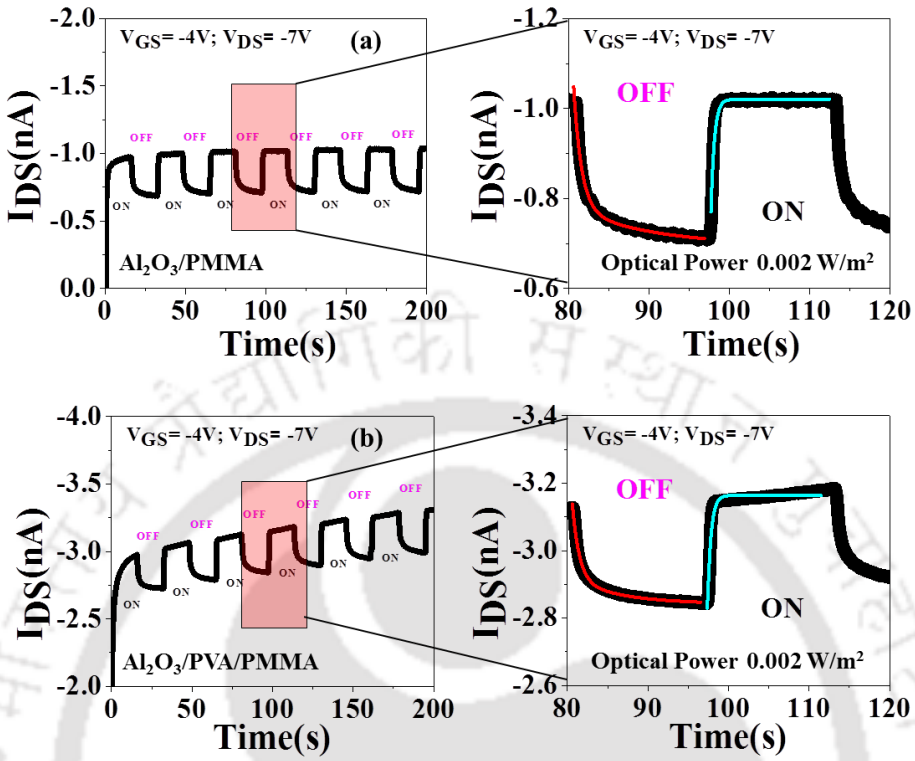

Figure. 5.6 The light on-off effect of ZnPc based PS-OFET and the fitted curves of the decay and growth of the I_{DS} under light on-off condition at V_{DS}=-7V and V_{GS}=-4 V for (a) Al_2O_3/PMMA and (b) Al_2O_3/PVA/PMMA dielectric system respectively.

Generally for an ideal optical sensor it is necessary that the device should be cost effective, stable and be operated under low operating voltage so that less electrical power is required during device operation. Most of the remarkable organic optical sensors, reported till date, are generally fabricated on Si/SiO_2 or ITO based substrate which significantly enhances the overall device cost, and coupled with the higher power consumption. Table 5.2 provides a summary of recent data on high performance PS-OFETs having different device architecture modification for getting efficient device performance.

In this study, the significant influence of thin film growth structure and tri-layer polymer dielectric system on the highest photo response properties with ZnPc based PS-OFETs, at various incident optical powers is reported. At 90°C, the PS-OFET with Al_2O_3/PVA/PMMA configuration showed best p-channel behaviour with enhanced and remarkable photo responsivity of R~9689.39 $A.W^{-1}$ compared to Al_2O_3/PMMA bilayer dielectric system (R~ 2679.40 $A.W^{-1}$) due to superior charge transport through the

channel by the polarization of dipoles inside the polar-PVA dielectric which increases the charge carrier mobility that is one order higher (μ_h~1.3×10^{-2} cm^2.V^{-1}.s^{-1}) compared to bilayer dielectric configuration (μ_h~ 3.9×10^{-3} cm^2.V^{-1}.s^{-1}).

Table 5.2. Summary of recent literature data on high responsive PS-OFETs.

References	Organic Semi-conductor	Device Structure	Operating Voltage	Responsivity, A.W^{-1}/ (Light source, Intensity)	Incident Power Density (W/m^2)	Method
Present Work	ZnPc/ Thin Film	BG/TC (Glass/Al_2O_3 / PVA/PMMA)	-10 V	9689.39/ (White light)	0.0020	Vapor
ACS Appl. Mater. Interfaces 2016, 8, 4894	In_2O_3/D102(Dye)/ Thin Film	BG/TC (Si/SiO_2)	-75 V	2000/ (500 nm)	Not mentioned	Solution
Adv. Sci. 2016, 3, 1500435	DNTT/PLA/ Thin Film	BG/TC (Si/SiO_2)	-60 V	Not mentioned/ (White light)	0.2	Vapor
Nano Lett. 2015, 15, 3787	ZnO quantum dots/ Thin Film	BG/TC (Si/SiO_2)	Not mentioned	10^8/ (335 nm)	1.38 x 10^{-6}	Mono layer Deposition
ACS Appl. Mater. Interfaces 2016, 8, 3744	C5-BTBT:B-upe blend(1:1)/Thin Film	BG/TC (Si/SiO_2)	-60 V	9.7/ (365 nm)	30	Solution
Nature Communications 2015, 6, 8238	$CH_3NH_3PbI_3$:$CH_3NH_3PbI_{3-x}Cl_x$/Thin Film	BG/TC (Si/SiO_2)	±30 V	320/ (400–750 nm)	100 W/m^2	vapour-assisted solution process
ACS Appl. Mater. Interfaces 2015, 7, 11083–11088	Hybrid graphene-P3HT/Thin Film	BG/BC (Si/SiO_2)	120 V	10^5/ (White)	9.7	CVD-Spin coating technique
Chem. Commun., 2015, 51, 12182	Carbazole macromolecule / nanofibers	BG/TC (OTS-Si/SiO_2)	-45 V	12/ (White light)	45.6	Drop-cast method
Adv. Funct. Mater. 2010, 20, 1019	Me-ABT/ micro ribbon	BG/TC (OTS-Si/SiO_2)	-80 V	12 000/ (Not mentioned)	300	Drop-cast method
ACS Nano 2015, 9, 5264	DPPBTSPE/ Nano wire	BG/TC (OTS-Si/SiO_2)	-60 V	1920/ (He-Ne laser)	Not mentioned	Drop-cast method
ACS Nano 2016, 10, 3536	2D CH3NH3PbI3/ Thin Film	BG/TC (Si/SiO_2)	Not mentioned	22/ (405nm laser) 12/(532 nm laser)	5 µW (Area not mentioned)	Drop-cast method
J. Mater. Chem. C, 2015,3, 12083	CZ-BO8/ Thin Film	BG/TC (OTS-Si/SiO_2)	-100 V	665/ (Not mentioned)	Not mentioned	Spin Coating method

J. Phys. Chem. C 2016, 120, 23172	P3HT/ Thin Film	BG/TC (ITO/Azo-e PMMA/PVA)	-80 V	0.0063/ (365 nm)	100	Spin Coating method
Adv. Funct. Mater. 2016, 26, 1445	PQT-12:PEO blend/ Nanofibers	BG/BC (PDMS/OTS -Si/SiO_2)	-100 V	0.93/ (470 nm)	60	Electro spinning Technique
Adv. Mater. 2016, 28, 5200	C8-TBT/Graphene /Thin Film	BG/TC (Si/SiO_2)	-40 V	15700/ (355 nm)	1	Epitaxial Growth Technique
J. Mater. Chem. C, 2015, 3,1942	P(DPP4T-co-BDT)/ Thin Film	BG/TC (OTS-Si/SiO_2)	-60 V	4000/ (White light)	97	Spin Coating method
Chem. Mater. 2015, 27, 2218	PPhTQ/ Thin Film	BG/BC (HMDS-Si/SiO_2)	-80 V	400/ (UV-visible-infrared)	Not mentioned	Drop-casting method
Adv. Mater. 2016, DOI:10.1002/adma.201603969	C8-BTBT / Thin Film	BG/TC (Si/SiO_2)	35 V	10^7/ (660 nm)	2 x 10^{-9}	Off-center spin-coating method
J. Mater. Chem. C, 2016, 4, 5289	Pentacene/ Thin Film	BG/BC (SAM-Si/SiO_2)	-100 V	400 / (365 nm)	0.074	Vapor
ACS Appl. Mater. Interfaces 2016, 8, 14665	ZnON:PBDTT-PP:PC71BM/ Thin Film	BG/BC (Si/SiO_2)	-40 V	170/ (380–940 nm)	0.001	DC sputtering and Spin Coating method
Macromolecules 2012, 45, 1296	PBDT–BBT/ Thin Film	BG/TC (OTS-Si/SiO_2)	-80 V	3.2/ (White light)	55.1	Drop-casting method
Small 2016, 12, No. 23, 3106	HfS_2/ Thin Film	BG/BC (Si/SiO_2)	3 V	0.045/ (473 nm)	650	scotch-tape technique
ACS Appl. Mater. Interfaces 2016, 8, 7291	Ru-complex 1-modified BPEPTCDI/Thin Film	BG/TC (OTS-Si/SiO_2)	100 V	3725/ (450 nm)	0.015	Vapor deposition with drop-cast method
Adv. Mater. 2014, 26, 4683	PDPPTzBT/ Thin Film	BG/BC (OTS-Si/SiO_2 with Ta_2O_3)	150 V	1.0×10^6/ (650 nm)	0.075	Inkjet Printing
J. Mater. Chem. C, 2015, 3, 10734	PBIBDF-BT/ Thin Film	BG/TC (OTS-Si/SiO_2)	-80 V	0.10843 for the p-type 0.038 for the n-type (650 nm)	216.8	Spin Coating method
J. Mater. Chem., 2012, 22, 21673	P3HT and PbS QDs/ Thin Film	BG/TC (HMDS-Si/SiO_2)	-100 V	20000/ (895 nm)	5.85 x 10^{-5}	Spin Coating method
Adv. Funct. Mater. 2013, 23, 629	BPE-PTCDI/ Nano wire	BG/BC (OTS-Si/SiO_2)	100 V	1400/ (635 - 680 nm)	140	Vapor Deposition

Adv. Mater. 2007, 19, 2624	$F_{16}CuP$/ single-nanoribbons	BG/TC (Si/SiO_2)	10 V	Not mentioned (White light)	60	Physical vapor transport process
J. Mater. Chem., 2012, 22, 3192	PTCDI-C8/ Single Crystal	BG/TC (ITO/ CL-PVP)	50 V	7/ (White Light)	75	Capillary tube method
ACS Appl. Mater. Interfaces 2010, 2, 1614	$F_{16}CuPc$/Thin Film	BG/TC (ITO/ P4PMS)	40 V	0.0015/ (White light)	56.6	Thermal vacuum deposition method
J. Phys. Chem. C 2009, 113, 18870	$F_{16}CuPc$/Thin Film	BG/TC (ITO/ P4PMS)	40 V	0.0015/ (White light)	56.6	Thermal vacuum deposition method
J. Phys. Chem. C 2008, 112, 19690	TA-PPE/Thin Film	BG/TC (OTS-Si/SiO_2)	60 V	0.036/ (White light)	57.6	Thermal vacuum deposition method
Adv. Optical Mater. 2016, 4, 264	Blend of C8-BTBT and polystyrene	BG/TC (CLPVP-Si/SiO_2)	-40 V	22000/ (Under UV-Radiation)	0.14	Off-center spin-coating method
Adv. Optical Mater. 2015, 3, 1389	Graphene covered perovskite/ Thin Film	BG/TC (Si/SiO_2)	-60 V	6.0×10^5/ (405 nm)	1.052 nW (spot size: ~500 nm)	CVD and Spin coating technique
Adv. Electron. Mater. 2016, 2, 1600264	P3HT and PDPPTTT/ Thin Film	TG/BC (Glass/PVA/ PMMA)	±40 V	Not mentioned clearly (450 to 795 nm)	Not mentioned	Spin coating technique
Adv. Electron. Mater.2016, DOI:10.1002/aelm.201600430	BODIPY-BF2/ Thin Film	BG/TC (Si/SiO_2)	40 V	11400/ (405 nm)	5 W/m^2	Spin coating technique
Adv. Electron. Mater. 2015, 1, 1500119	Blend of BTBT-C_5 and L-upe/ Thin Film	BG/TC (HMDS-Si/SiO_2)	-60 V	11.1/ (Under UV radiation)	Not mentioned	Spin coating technique

The observed specific detectivity, D* and noise equivalent power, NEP [where, $D^* = RS^{1/2}(2eI_{DS,Dark})^{-1/2}$ and $NEP = (2eI_{DS,Dark})^{1/2}R^{-1}$, e is value of electron charge] values of the bi-layer dielectric system are 6.01×10^{13} Jones and 2.655×10^{-17} $W.Hz^{-1/2}$ respectively whereas for trilayer dielectric system the observed D* and NEP values are 5.13×10^{14} Jones and 1.043×10^{-17} $W.Hz^{-1/2}$ respectively. Additionally, the operating voltage of each of the fabricated devices were observed to be very low (-7V) due to the influence of inorganic high-k Al_2O_3 dielectric layer. The electrical stability of each of the fabricated devices was also investigated by bias stress analysis under both the light and dark condition in vacuum. To the best of our knowledge, the photo responsivity, R, reported here in case of

Al_2O_3/PVA/PMMA tri-layer dielectric configuration, is the highest reported value among all the thin film based PS-OFETs with remarkably low operating voltage of -7 V. This study confirmed that the Al_2O_3/PVA/PMMA tri-layer dielectric configuration is a highly efficient, ITO and Si/SiO_2 free system, which enhances the photo responsivity of PS-OFETs to considerably high level not observed previously in any thin film based OFETs and is expected to have applications in futuristic low-cost and wearable optoelectronics devices.

5.3 Conclusion

In conclusion, "thin film based OFET" with highest photo sensitivity values of R~2679.40 $A.W^{-1}$ have been successfully reported using ZnPc based PS-OFETs. This was achieved by carefully optimizing the multilayer polymer based dielectric systems and the impact of thin film growth structure of the active material to obtain superior photo response properties of ZnPc based PS-OFETs at various incident optical powers. It has been established that the thermally evaporated ZnPc films at 90 °C on PMMA thin-film coated glass substrates at different substrate temperatures exhibited polycrystalline nature as evident from AFM, FESEM, XRD and raman analysis. At 90 °C, the fabricated PS-OFET with Al_2O_3/PVA/PMMA tri-layer dielectric configuration showed p-channel behaviour with enhanced and remarkable photo responsivity of R~9689.39 $A.W^{-1}$, whereas, the Al_2O_3/PMMA bilayer dielectric system showed photo responsivity of R~2679.40 $A.W^{-1}$. This was because of the superior charge transport through the channel by the polarization of dipoles inside the polar-PVA dielectric. Overall this increased the charge carrier mobility by one order (μ_h~1.3×10^{-2} $cm^2.V^{-1}.s^{-1}$) compared to the bilayer dielectric configuration (μ_h~3.9×10^{-3} $cm^2.V^{-1}.s^{-1}$) with very low operating voltage (-7 V) due to the influence of inorganic high-k Al_2O_3 dielectric layer. The electrical stability of each of the fabricated devices was also investigated by bias stress analysis under both the light and dark condition in vacuum. To the best of our knowledge, the photo responsivity, R, reported here in case of Al_2O_3/PVA/PMMA tri-layer dielectric configuration, are the highest among all the thin film based PS-OFETs with remarkably low operating voltage -10 V. This Al_2O_3/PVA/PMMA device on economical glass substrates were devoid of ITO and Si/SiO_2, yet displayed very high photo responsivity in the fabricated PS-OFETs at very low operating voltage and are expected to open newer avenues in the field of electronic devices, energy efficient sensors and futuristic low-cost wearable optoelectronics devices.

5.4 References

[1] Chu, Y.; Wu, X.; Lu, J.; Liu, D.; Du, J.; Zhang, G.; Huang, J. Photosensitive and Flexible Organic Field-Effect Transistors Based on Interface Trapping Effect and Their Application in2D Imaging Array. *Adv. Sci.* **2016**, *3*, 1500435.

[2] Mottram, A. D.; Lin, Y.-H.; Pattanasattayavong, P.; Zhao, K.; Amassian, A.; Anthopoulos, T. D. Quasi Two-Dimensional Dye-Sensitized In2O3 Phototransistors for Ultrahigh Responsivity and Photosensitivity Photodetector Applications. *ACS Appl. Mater. Interfaces* **2016**, *8*, 4894–4902.

[3] Bilro, L.; Alberto, N.; Pinto J. L.; Nogueira, R. Optical Sensors Based on Plastic Fibers. *Sensors* **2012**, *12*, 12184–12207.

[4] Askim, J. R.; Mahmoudiab, M.; Suslick, K. S. Optical Sensor Arrays for Chemical Sensing: the Optoelectronic Nose. *Chem. Soc. Rev.* **2013**, *42*, 8649–8682.

[5] Shao, D.; Gao, J.; Chow, P.; Sun, H.; Xin, G.; Sharma, P.; Lian, J.; Koratkar, N. A.; Sawyer, S. Organic–Inorganic Heterointerfaces for Ultrasensitive Detection of Ultraviolet Light. *Nano Lett.* **2015**, *15*, 3787–3792.

[6] Ljubic, D.; Smithson, C. S.; Wu, Y.; Zhu, S. Effect of Polymer Binders on UV-Responsive Organic Thin-Film Phototransistors with Benzothienobenzothiophene Semiconductor. *ACS Appl. Mater. Interfaces* **2016**, *8*, 3744–3754.

[7] Li, F.; Ma, C.; Wang, H.; Hu, W.; Yu, W.; Sheikh, A. D.; Wu, T. Ambipolar Solution-Processed Hybrid Perovskite Phototransistors. *Nat. Commun.* **2015**, *6*, 8238.

[8] Huisman, E. H.; Shulga, A. G.; Zomer, P. J.; Tombros, N.; Bartesaghi, D.; Bisri, S. Z.; Loi, M. A.; Koster, L. J. A.; Wees, B. J. V. High Gain Hybrid Graphene–Organic Semiconductor Phototransistors. *ACS Appl. Mater. Interfaces* **2015**, *7*, 11083–11088.

[9] Gomes, H. L.; Stallinga, P.; Dinelli, F.; Murgia, M.; Biscarini, F.; de Leeuw, D. M.; Muck, T.; Geurts, J.; Molenkamp L. W.; Wagner, V. Bias-Induced Threshold Voltages Shifts in Thin-Film Organic Transistors. *Appl. Phys. Lett.* **2004**, *84*, 3184–3186.

[10] Huang, Y.; Zheng, W.; Qiu, Y.; Hu, P. Effects of Organic Molecules with Different Structures and Absorption Bandwidth on Modulating Photoresponse of MoS_2 Photodetector. *ACS Appl. Mater. Interfaces* **2016**, *8*, 23362–23370.

[11] Yang, J.; Kwak, H.; Lee, Y.; Kang, Y.-S.; Cho, M.-H.; Cho, J. H.; Kim, Y.-H.; Jeong, S.-J.; Park, S.; Lee, H.-J.; Kim, H. MoS2–InGaZnO Heterojunction

Phototransistors with Broad Spectral Responsivity. *ACS Appl. Mater. Interfaces* **2016**, *8*, 8576–8582.

[12] Sun, Z.; Chang, H. Graphene and Graphene-like Two-Dimensional Materials in Photodetection: Mechanisms and Methodology. *ACS Nano* **2014**, *8*, 4133–4156.

[13] Rim, Y. S.; Yang, Y. M.; Bae, S.-H.; Chen, H.; Li, C.; Goorsky, M. S.; Yang, Y. Ultrahigh and Broad Spectral Photodetectivity of an Organic–Inorganic Hybrid Phototransistor for Flexible Electronics. *Adv. Mater.* **2015**, *27*, 6885–6891.

[14] Spina, M.; Lehmann, M.; Náfrádi, B.; Bernard, L.; Bonvin, E.; Gaál, R.; Magrez, A.; Forró, L.; Horváth, E. Microengineered $CH_3NH_3PbI_3$ Nanowire/Graphene Phototransistor for Low-Intensity Light Detection at Room Temperature *Small* **2015**, *11*, 4824–4828.

[15] Pang, Y.; Xue, F.; Wang, L.; Chen, J.; Luo, J.; Jiang, T.; Zhang, C.; Wang, Z. L. Tribotronic Enhanced Photoresponsivity of a MoS_2 Phototransistor. *Adv. Sci.* **2016**, *3*, 1500419.

[16] Stallinga, P.; Gomes, H. L.; Biscarini, F.; Murgia M.; de Leeuw, D. M.; Electronic Transport in Field-Effect Transistors of Sexithiophene. *J. Appl. Phys.* **2004**, *96*, 5277–5283.

[17] Nelson, S. F.; Lin, Y.-Y.; Gundlach, D. J.; Jackson, T. N. Temperature-Independent Transport in High-Mobility Pentacene Transistors. *Appl. Phys. Lett.* **1998**, *72*, 1854–1856.

[18] Dong, H.; Bo, Z.; Hu, W. High Performance Phototransistors of a Planar Conjugated Copolymer. *Macromol. Rapid Commun.* **2011**, *32*, 649–653.

[19] Lee, M. Y.; Hong, J.; Lee, E. K.; Yu, H.; Kim, H.; Lee, J. U.; Lee, W.; Oh, J. H. Highly Flexible Organic Nanofiber Phototransistors Fabricated on a Textile Composite for Wearable Photosensors. *Adv. Funct. Mater.* **2016**, *26*, 1445–1453.

[20] Liu, X.; Luo, X.; Nan, H.; Guo, H.; Wang, P.; Zhang, L.; Zhou, M.; Yang, Z.; Shi, Y.; Hu, W.; Ni, Z.; Qiu, T.; Yu, Z.; Xu, J.-B.; Wang, X. Epitaxial Ultrathin Organic Crystals on Graphene for High-Efficiency Phototransistors. *Adv. Mater.* **2016**, *28*, 5200–5205.

[21] Ma, L.; Yi, Z.; Wang, S.; Liu, Y.; Zhan, X. Highly Sensitive Thin Film Phototransistors Based on a Copolymer of Benzodithiophene and Diketopyrrolopyrrole. *J. Mater. Chem. C* **2015**, *3*, 1942–1948.

[22] Li, M.; An, C.; Marszalek, T.; Guo, X.; Long, Y.-Z.; Yin, H.; Gu, C.; Baumgarten, M.; Pisula, W.; Müllen, K. Phenanthrene Condensed Thiadiazoloquinoxaline Donor–Acceptor Polymer for Phototransistor Applications. *Chem. Mater.* **2015**, *27*, 2218–2223.

[23] Zhang, Y.; Yuan, Y.; Huang , J. Detecting 100 fW cm^{-2} Light with Trapped Electron Gated Organic Phototransistors. *Adv. Mater.* **2017**, *29*, 1603969.

[24] Umeyama, T.; Takamatsu, T.; Tezuka, N.; Matano, Y.; Araki, Y.; Wada, T.; Yoshikawa, O.; Sagawa, T.; Yoshikawa, S.; Imahori, H. Synthesis and Photophysical and Photovoltaic Properties of Porphyrin–Furan and –Thiophene Alternating Copolymers. *J. Phys. Chem. C* **2009**, *113*, 10798–10806.

[25] Senthilarasu, S.; Hahn, Y. B.; Lee, S.-H. Structural Analysis of Zinc Phthalocyanine (ZnPc) Thin Films: X-Ray Diffraction Study. *J. Appl. Phys.* **2007**, *102*, 043512.

[26] Dong, H.; Wang, C.; Hu, W. High Performance Organic Semiconductors for Field-Effect Transistors. *Chem. Commun.* **2010**, *46*, 5211–5222.

[27] Zhang, H.; Chen, H.; Ma, W.; Hui, J.; Meng, S.; Xu, W.; Zhu, D.; Guo, X. Photocontrol of Charge Injection/Extraction at Electrode/Semiconductor Interfaces for High-Photoresponsivity Organic Transistors. *J. Mater. Chem. C* **2016**, *4*, 5289—5296.

[28] Rim, Y. S.; Ok, K.-C.; Yang, Y. M.; Chen, H.; Bae, S.-H.; Wang, C.; Huang, Y.; Park, J.-S.; Yang, Y. Boosting Responsivity of Organic–Metal Oxynitride Hybrid Heterointerface Phototransistor. *ACS Appl. Mater. Interfaces* **2016**, *8*, 14665–14670.

[29] Liu, Y.; Wang, H.; Dong, H.; Tan, J.; Hu, W.; Zhan, X. Synthesis of a Conjugated Polymer with Broad Absorption and Its Application in High-Performance Phototransistors. *Macromolecules* **2012**, *45*, 1296–1302.

[30] Xu, K.; Huang, Y.; Chen, B.; Xia, Y.; Lei, W.; Wang, Z.; Wang, Q.; Wang, F.; Yin, L.; He, J. Toward High-Performance Top-Gate Ultrathin HfS_2 Field-Effect Transistors by Interface Engineering. *Small* **2016**, *12*, 3106–3111.

[31] Liu, X.; Lee, E. K.; Kim, D. Y.; Yu, H.; Oh, J. H. Flexible Organic Phototransistor Array with Enhanced Responsivity via Metal–Ligand Charge Transfer. *ACS Appl. Mater. Interfaces* **2016**, *8*, 7291–7299.

[32] Wang, H.; Cheng, C.; Zhang, L.; Liu, H.; Zhao, Y.; Guo, Y.; Hu, W.; Yu, G.; Liu, Y. Inkjet Printing Short-Channel Polymer Transistors with High-Performance and Ultrahigh Photoresponsivity. *Adv. Mater.* **2014**, *26*, 4683–4689.

[33] Wang, Q.; Zhu, M.; Wu, D.; Zhang, G.; Wang, X.; Lu, H.; Wang, X.; Qiu, L. Phototransistors Based on a Donor–Acceptor Conjugated Polymer with a High Response Speed. *J. Mater. Chem. C* **2015**, *3*, 10734—10741.

[34] Sun, Z.; Li, J.; Yan, F. Highly Sensitive Organic Near-Infrared Phototransistors Based on Poly (3-hexylthiophene) and Pbs Quantum Dots. *J. Mater. Chem.* **2012**, *22*, 21673–21678.

[35] Tang, B. Q.; Li, L.; Song, Y.; Liu, Y.; Li, H.; Xu, W.; Liu, Y.; Hu, W.; Zhu, D. Photoswitches and Phototransistors from Organic Single-Crystalline Sub-micro/nanometer Ribbons. *Adv. Mater.* **2007**, *19*, 2624–2628.

[36] Yu, H.; Bao, Z.; Oh, J. H. High-Performance Phototransistors Based on Single-Crystalline n-Channel Organic Nanowires and Photogenerated Charge-Carrier Behaviors. *Adv. Funct. Mater.* **2013**, *23*, 629–639.

[37] Mukherjee, B.; Sim, K.; Shin, T. J.; Lee, J.; Mukherjee, M.; Ree, M.; Pyo, S. Organic Phototransistors Based on Solution Grown, Ordered Single Crystalline Arrays of a π-Conjugated Molecule. *J. Mater. Chem.* **2012**, *22*, 3192–3200.

[38] Mukherjee, B.; Mukherjee, M.; Choi, Y.; Pyo, S. Control Over Multifunctionality in Optoelectronic Device Based on Organic Phototransistor. *ACS Appl. Mater. Interfaces* **2010**, *2*, 1614–1620.

[39] Mukherjee, B.; Mukherjee, M.; Choi, Y.; Pyo, S. Organic Phototransistor with n-Type Semiconductor Channel and Polymeric Gate Dielectric. *J. Phys. Chem. C* **2009**, *113*, 18870–18873.

[40] Tackley, D. R.; Dent, G.; Smith, W. E. IR and Raman Assignments for Zinc Phthalocyanine from DFT Calculations. *Phys. Chem. Chem. Phys.* **2000**, *2*, 3949-3955.

[41] Basova, T. V.; Kolesov, B. A. Raman Polarization Studies of the Orientation of Molecular Thin Films. *Thin Solid Films* **1998**, *325*, 140–144.

[42] Cho, S. W.; Jeong, J. G.; Park, S. H.; Cho, M.-H.; Jeong, K.; Whang, C.-N.; Yi, Y. The Characteristics and Interfacial Electronic Structures of Organic Thin Film Transistor Devices with Ultrathin $(HfO_2)_x$ $(SiO_2)_{1-x}$ Gate Dielectrics. *Appl. Phys. Lett.* **2008**, *92*, 213302.

[43] Majewski, L. A.; Schroeder, R.; Grell, M. One Volt Organic Transistor. *Adv. Mater.* **2005**, *17*, 192–196.

[44] Dong, H.; Li, H.; Wang, E.; Nakashima, H.; Torimitsu, K.; Hu, W. Phototransistors of a Rigid Rod Conjugated Polymer. *J. Phys. Chem. C* **2008**, *112*, 19690–19693.

[45] Yuan, Y.; Huang, J. Ultrahigh Gain, Low Noise, Ultraviolet Photodetectors with Highly Aligned Organic Crystals. *Adv. Opt. Mater.* **2015**, *4*, 264.

[46] Wang, Y.; Zhang, Y.; Lu, Y.; Xu, W.; Mu, H.; Chen, C.; Qiao, H.; Song, J.; Li, S.; Sun, B.; Cheng, Y.-B.; Bao, Q. Hybrid Graphene–Perovskite Phototransistors with Ultrahigh Responsivity and Gain. *Adv. Opt. Mater.* **2015**, *3*, 1389.

[47] Nam, S.; Han, H.; Seo, J.; Song, M.; Kim, H.; Anthopoulos, T. D.; McCulloch, I.; Bradley, D. D. C.; Kim, Y. Ambipolar Organic Phototransistors with p-Type/n-Type Conjugated Polymer Bulk Heterojunction Light-Sensing Layers. *Adv. Electron. Mater.* **2016**, *2*, 1600264.

[48] Koo, J. B.; Ku, C. H.; Lim, S. C.; Kim, S. H.; Lee, J. H. Hysteresis and Threshold Voltage Shift of Pentacene Thin-Film Transistors and Inverters with Al_2O_3 Gate Dielectric. *Appl. Phys. Lett.* **2007**, *90*, 133503.

[49] Li, F.; Chen, Y.; Ma, C.; Buttner, U.; Leo, K.; Wu, T. High-Performance Near-Infrared Phototransistor Based on n-Type Small-Molecular Organic Semiconductor. *Adv. Electron. Mater.* **2017**, *3*, 1600430.

[50] Ljubic, D.; Smithson, C. S.; Wu, Y.; Zhu, S. Highly UV-Sensitive and -Responsive Benzothiophene/Dielectric Polymer Blend-Based Organic Thin-Film Phototransistor. *Adv. Electron. Mater.* **2015**, *1*, 1500119.

[51] Zhang, Y.; Wang, M.; Collins, S. D.; Zhou, H.; Phan, H.; Proctor, C.; Mikhailovsky, A.; Wudl, F.; Nguyen, T. Q. Enhancement of the Photoresponse in Organic Field-Effect Transistors by Incorporating Thin DNA Layers. *Angew. Chem. Int. Ed.* **2014**, *53*, 244–249.

[52] Hwang, H.; Kim, H.; Nam, S.; Bradley, D. D. C.; Ha, C. -S.; Kim, Y. Organic Phototransistors with Nanoscale Phase-Separated Polymer/Polymer Bulk Heterojunction Layers. *Nanoscale* **2011**, *3*, 2275-2279.

[53] Dey, A.; Singh, A.; Kalita, A.; Das, D.; Iyer, P. K. High Performance, Low Operating Voltage n-Type Organic Field Effect Transistor based on Inorganic-Organic Bilayer Dielectric System. *J. Phys.: Conf. Ser.* **2016**, *704*, 012017(1-8).

6

Effect of Hybrid Dielectric System for Ultralow Operated n-type Organic Field Effect Transistor

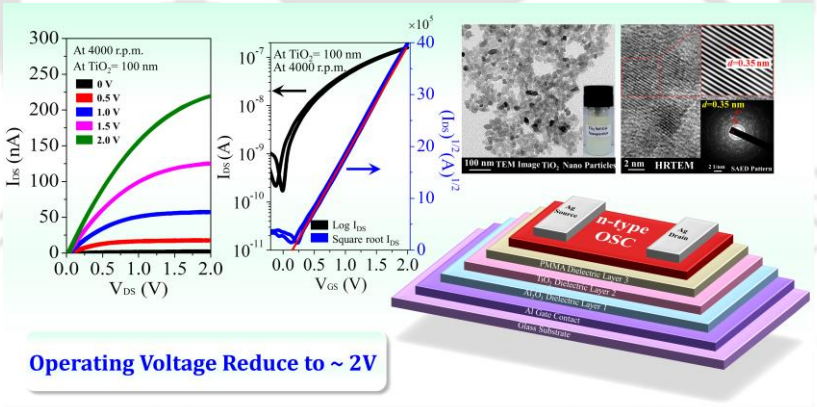

[1] **Dey, A.;** Singh, A.; Iyer, P. K. Method for the Fabrication of Low Cost, Reduced Bias Stress Multi-layers Dielectric System Ultralow Operated n-type Organic Field Effect Transistors, 2017, **Patent**, Ref. No. 201731046914, App. No. TEMP/E-1/47853/2017-KOL.

[2] **Dey, A.;** Singh, A.; Iyer, P. K. Cost Effective Tri-layers Dielectric System for Ultralow Operating Voltage, Electrically Stable n-channel Organic Field Effect Transistors. **Communicated**.

6

Effect of Hybrid Dielectric System for Ultralow Operated n-type Organic Field Effect Transistor

Organic field effect transistors are one of the most attractive electronic components of organic electronics which are expected to be the best alternative of inorganic transistors in near future with its additional qualities like low-cost, easy fabrication, mechanical flexibility and biocompatibility under very low voltage of operation.[1-4] However, to achieve these targets practically, especially for n-channel OFETs, more efforts are needed in reducing the operating voltage of the device and on its electrical stability so that it can be efficiently used as a stable, low-powered electronic components for the next generation of electronics market. Generally, most of the reported OFETs are found to be operated under large operating voltage range due to the high band gap of the organic semiconductors and low k-value of gate insulator, which restricted there use towards low cost portable electronic applications.[5-7] Hence, an OFET, which will be applicable for real-life application, like radio frequency identification (RFID) tag, display, smart card, chemo- and bio-sensor, electro-optical switch, e-skin etc., should have low operational voltage with high electrical stability and longer lifetime. To overcome this major problem, high-k dielectric materials are one of the popular choices for the researcher to achieve excellent OFET performance under low voltage operational range.[8-12] Along with the higher k-value, the surface morphology, thickness, roughness and crystallinity of dielectric materials also show strong influence on device performance.[13-15] Generally in OFET, the semiconductor-dielectric layer interface is responsible to regulate the charge conveyance and the high-k

dielectric material is responsible for the operational voltage of the devices.[16-18] In this regard, highly doped silicon dioxide (SiO_2) is traditionally used as dielectric material for OFET fabrication because of its stable dielectric strength. But due to the low k-value, the operating voltage of SiO_2 based OFETs are observed to be higher which further increases the consumption of power. Additionally with this, the device having SiO_2 as gate insulating layer, show poor stability under continuous electrical operation due to the trapping of charge carriers from the gate bias-induced conduction channel into localized electronic states, which is also known as the bias stress effect.[19, 20] Similarly, there are several other high-k organic, inorganic and hybrid gate insulating materials that have been mentioned in literature to achieve efficient OFET performance. Among them PVA, PMMA, Polystyrene (PS), Polyvinyl phenol (PVP), Bis-benzocyclobutene (BCB) etc., are widely used organic dielectric materials for OFET fabrication.[21-23] Though these materials have very good film forming probability, the capacitance value possesses by these are not high enough to accumulate large number of charge carriers at the semiconductor-dielectric interface and therefore does not able to reduce the operating voltage below 3V. Furthermore, if the operating voltage is not reduces to 3V, it limited OFETs application especially in case of biosensor, display, smart card, etc. There are several other inorganic and hybrid dielectrics materials, like Ta_2O_5, Al_2O_3, TiO_2, ZrO_2, HfO_2, Gd_2O_3, $(HfO_2)_{0.25}(SiO_2)_{0.75}$, Ta_2O_5+HMDS, HfO_2/Si_3N_4 etc., have been used in OFETs to achieved low operating voltage.[24-26] Though this material possesses very high dielectric strength, but due to the costly deposition techniques and high surface roughness their application is restricted for OFET fabrication.

Herein, we reported a very simple, highly stable, cost effective and compatible to flexible substrate, inorganic-organic hybrid tri-layer dielectric system for the fabrication of ultra-low operating voltage n-channel organic field effect transistor. Two types of inorganic dielectric layers, namely Al_2O_3 (first dielectric layer) and TiO_2 nanoparticles (NPs) (second dielectric layer) are use in this study. Al_2O_3 is deposited by low-cost anodic oxidation method whereas TiO_2 NPs are synthesized by simple sol-gel technique and spin coated on the top of Al_2O_3. PMMA, an organic dielectric material, is chosen as the third dielectric layer which is also deposited by spin coating method. In this study, each of the dielectric layers has their own significance like Al_2O_3 is used to make a thin barrier layer in between TiO_2 and Al gate contact. It is also used to block the gate leakage current up to 5 μA. TiO_2 sol-gel NPs layer is used to accumulate more number of charge carriers in the semiconductor-dielectric interface so that it can fill the trap energy level and can reduce the threshold voltage, V_{Th} and operating voltage of the device. Further PMMA was used as

a buffer layer in between TiO_2 and the active semiconducting layer so that it can modify the TiO_2 surface and prevents the degradation of n-type semiconductor by protecting direct contact of it's with the oxygen molecule of TiO_2. Before the device fabrication, the synthesized TiO_2 sol-gel NPs were systematically examined by various characterization techniques like UV-Vis spectroscopy, XRD, FESEM and TEM from which it was observed that the average particle size of TiO_2 NPs is ~ 15 nm and is highly polycrystalline in nature. To check the effect of this ordered, high-k dielectric material on the performance of PDI-C8 and NDI-CY2 based n-channel OFETs, four different types of OFETs with different device architecture were designed where the thickness of Al_2O_3 and PMMA were kept constant for all the devices and only the thickness of TiO_2 was modulated very carefully in nanoscale range by varying the r.p.m. value viz., 2000, 3000, 4000 and 5000 respectively. It has been observed that at 4000 r.p.m. (~100 nm of TiO_2) the devices with top contact Ag electrodes exhibit excellent and highest n-channel behaviour with electron mobility values with high current on/off ratio ~10^4 and ultra-low operating voltage of 2V. The electrical stability of the devices were also analysed by bias stress instability study during long term operation under vacuum condition. Moreover it was also observed that this tri-dielectric system showing similar suitable gate dielectric property in case of flexible and transparent substrate with same ultra-low operational voltage. This high performance OFET device having operating voltage ~2V, with optimum TiO_2 NPs dielectric contained hybrid tri-layer dielectric system is expected to have diverse applications in next generation of portable electronics.

6.1 Experiments

6.1.1 Materials

For the synthesis of TiO_2 sol-gel NPs, titanium (IV) isopropoxide (97% purity), glacial acetic acid and isopropanol were purchased from Sigma Aldrich and used without further purification. For OFET fabrication, PMMA (M_W=550000 g/mol), silver (99.999% purity) and aluminium wire (99.999% purity) were purchased from Sigma Aldrich. Citric acid monohydrate (99.5% purity) was purchased from Alfa Aesar and used as weak electrolyte for Al_2O_3 deposition by anodization method. Anisole was purchased from Loba Chemie (99% purity) and used as received for making PMMA dielectric solution. Microscope glass slides (thickness 1-1.2mm) purchased from Jain Scientific Glass Works, India, was used as one of the device substrate without any surface modification.

Polyethylene terephthalate (PET) flexible substrate were also purchased from Sigma Aldrich, India. All the chemical and materials were used as received, unless otherwise mentioned. The n-type semiconductors namely, PDI-C8 was purchased from Sigma Aldrich and NDI-CY2 molecule was synthesized following the procedure reported in Chapter 3.

6.1.2 Characterization Details

The thin film of PDI-C8 and NDI-CY2 were deposited by thermal evaporation technique by Excel instrument. Laurell and Spin 150 spin coaters were used for the deposition of TiO_2 sol-gel and PMMA dielectric thin films. After the deposition the thicknesses of all the films were measured by Veeco Dektak 150 surface profilometer. The UV-Visible absorption spectra of the synthesized TiO_2 sol-gel and PDI-C8 were characterized by Jaz UV-Vis spectrophotometer. The TEM image of TiO_2 dielectric nanoparticles was characterized by Tecnai G2 F20 S-twin JEOL 2100 transmission electron microscope. Agilent 5500-STM instrument was used for the AFM analysis. The thin film XRD pattern was recorded by a Rigaku TTRAX III with Cu Kα radiation. Finally, the electrical properties were characterized by Keithley 4200 semiconductor characterization system and 2400 source meter.

6.2 Results and Discussion

6.2.1 Synthesis and Growth Structure of TiO_2 Sol-Gel

Colloidal high-k TiO_2 dielectric is synthesized by using simple Sol-Gel method. A solution of Titanium (IV) isopropoxide in isopropanol was added to a solution of water and glacial acetic acid which was placed in an ice bath prior to the addition for about 30 min. After the addition, the mixture was constantly stirred and a cloudy white precipitate was observed. The precipitate was then placed in a water bath at 80°C with constant stirring to obtain a gel like entity which became milky on cooling down. This colloidal solution obtained was placed in a sealed glass flask and kept in a vacuum oven at 200°C for 12 hours and then cooled to the room temperature to obtain white colloidal TiO_2 solution.

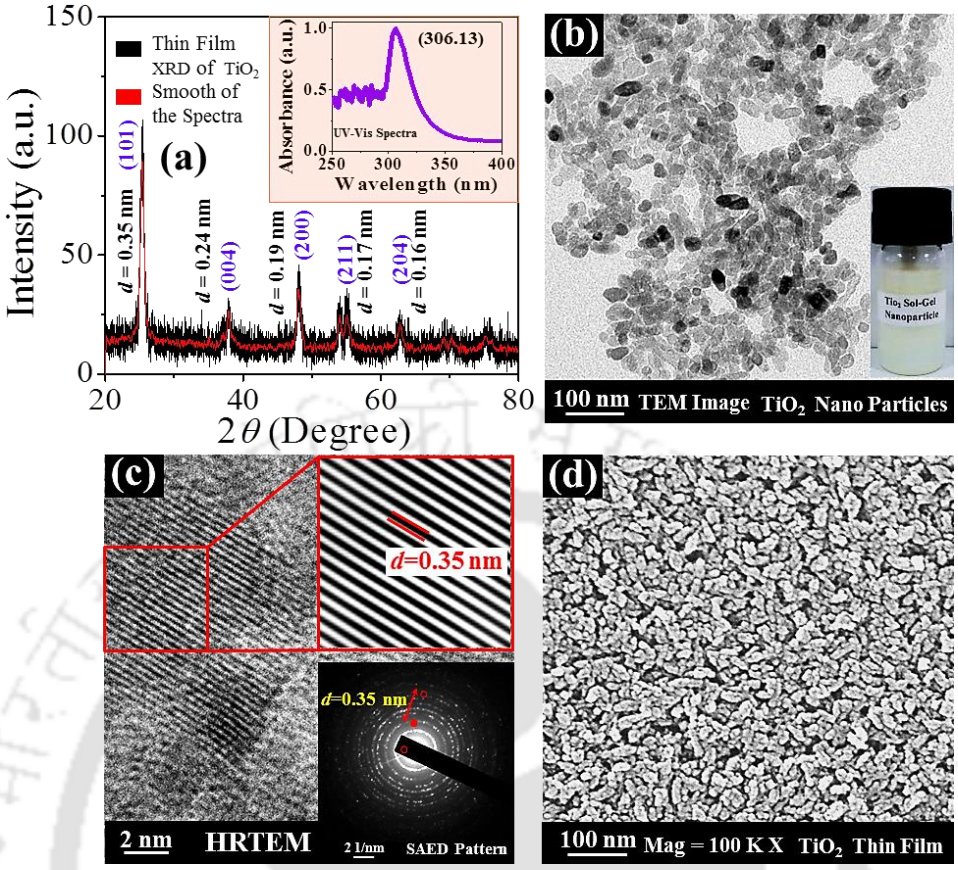

Figure 6.1 (a) Thin film XRD spectra of TiO_2 sol-gel NPs. Inset: thin film UV-Vis absorption spectra. (b) TEM image of TiO_2. Inset: Synthesizes TiO_2 sol-gel NPs. (c) HRTEM spectra of TiO_2 NPs. Inset: SAED pattern. Showing d-spacing, d= 0.35 nm. (d) FESEM image of TiO_2 over anodized Al_2O_3 dielectric layer.

The solution obtained was stable for a month and could be used after stirring. The end product was a white solution of TiO_2 with a bluish ting. The synthesized TiO_2 sol-gel nanoparticle was characterized by various experimental techniques which are shown in Figure 6.1. The crystalline nature of TiO_2 thin film was confirmed by using high power (18 kW) X-ray diffractometer. Figure 6.1(a) displays both the UV-vis absorption spectra (λ_{max} =306.13 nm) and XRD patterns of TiO_2 thin film. It is evident that the sharp diffraction peaks observed in the regions from 2θ= 20° to 80° support the formation of small size, polycrystalline, pure anatase phase of the TiO_2 (JCPDS card no. 21-1272) nanoparticle. The crystalline size (D) of TiO_2 NPs was calculated by using the well-known Debye-Scherer formula, for respective different diffraction peak positions. The highest particle size at 2θ= 25° is calculated as ~16.4 nm which also has good agreement with the size observed in case of TEM analysis [>15 nm, shown in Figure 6.1(b)]. To further investigate the crystalline nature, we investigate the HRTEM images and SAED patterns of TiO_2 sol gel which are shown in Figure 6.1(c). Closer observation of the HRTEM image

reveals that, the interplanar spacing is about 0.35 nm, which is exactly matching with the value calculated from the XRD peak at 2θ = 25°. The polycrystalline nature of TiO_2 is also confirmed by SAED patterns as shown in the inset of Figure 6.1(c). Figure 6.1(d) represent the FESEM image of TiO_2 thin film deposited on anodized Al_2O_3 layer. As the film is very rough in nature and visible cracks are observed, this analysis revels that without any additional buffer layer modification, bare TiO_2 thin film is not suitable for smoother active layer thin film deposition.

6.2.2 Thin Film Growth Structure of Active Layer Materials

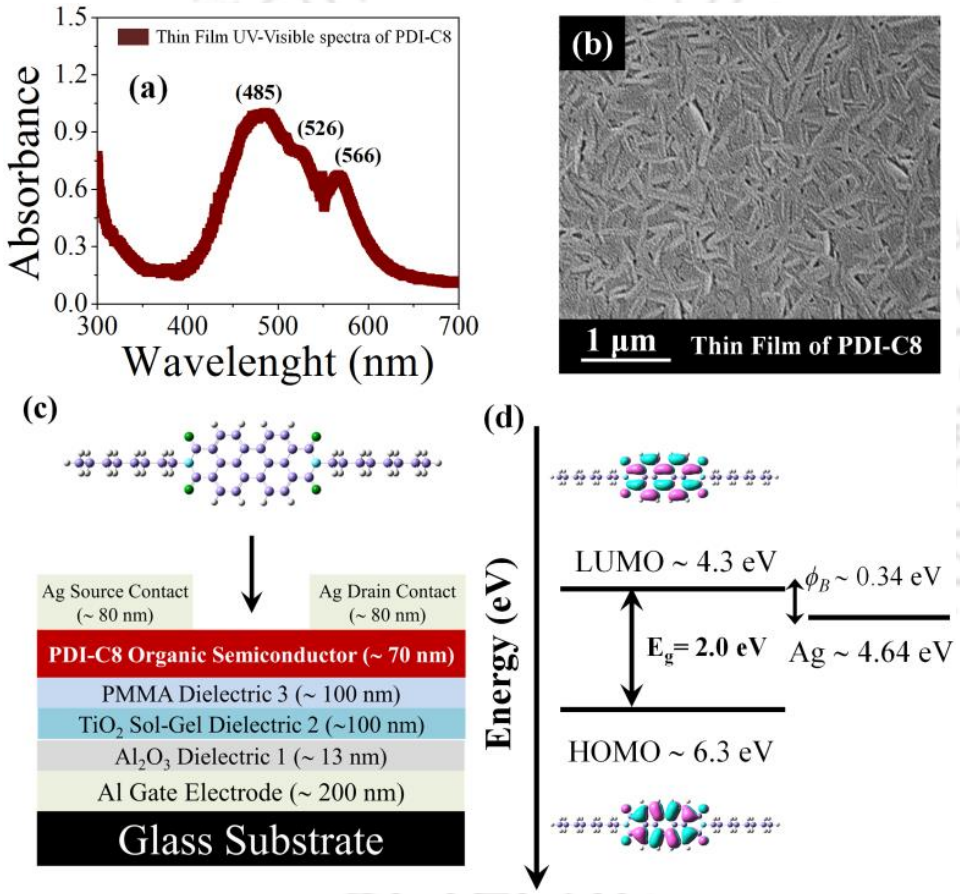

Figure 6.2 (a) Thin film UV-Vis absorption spectra of PDI-C8 molecule (b) FESEM image of PDI-C8 deposited at 90°C substrate temperature on PMMA dielectric layer. (c) Schematic of the fabricated OFETs device with PDI-C8 as active layer (d) Illustration of energy level diagram of PDI-C8 molecule with Ag electrode under zero bias condition.

The thin film growth natures of both the active layer molecules were standardized systematically prior to the device fabrication. The morphology of NDI-CY2 was already discussed in detail in the chapter 3. Before the device fabrication, the PDI-C8 molecule is characterized by different characterization techniques which are presented in Figure 6.2.

From Figure 6.2 (a) it has been observed that when PDI-C8 is deposited upon TiO_2/PMMA coated glass substrate, the thin film UV-Vis spectra of the molecule shows mainly three characteristics peak at 485 nm, 526 nm and 566 nm wavelengths range. These three peaks subsequently signify the (S0-S2), (S0-S1) and (S0-S0) transitions of PDI-C8 molecule.[27] Figure 6.2(b) represents the FESEM image of PDI-C8 on TiO_2/PMMA dielectric substrate. From this it was observed that at 90°C substrate temperature (Ts) the molecule form densely packed thin film with larger grains (~ 0.5 µm in size) which is highly suitable for OFET fabrication. Figure 6.2(c) and 6.2(d) represent the schematic of tri-layer dielectric contained PDI-C8 based OFET device architecture and the illustration of energy level diagram of the molecule with Ag electrodes under equilibrium condition.

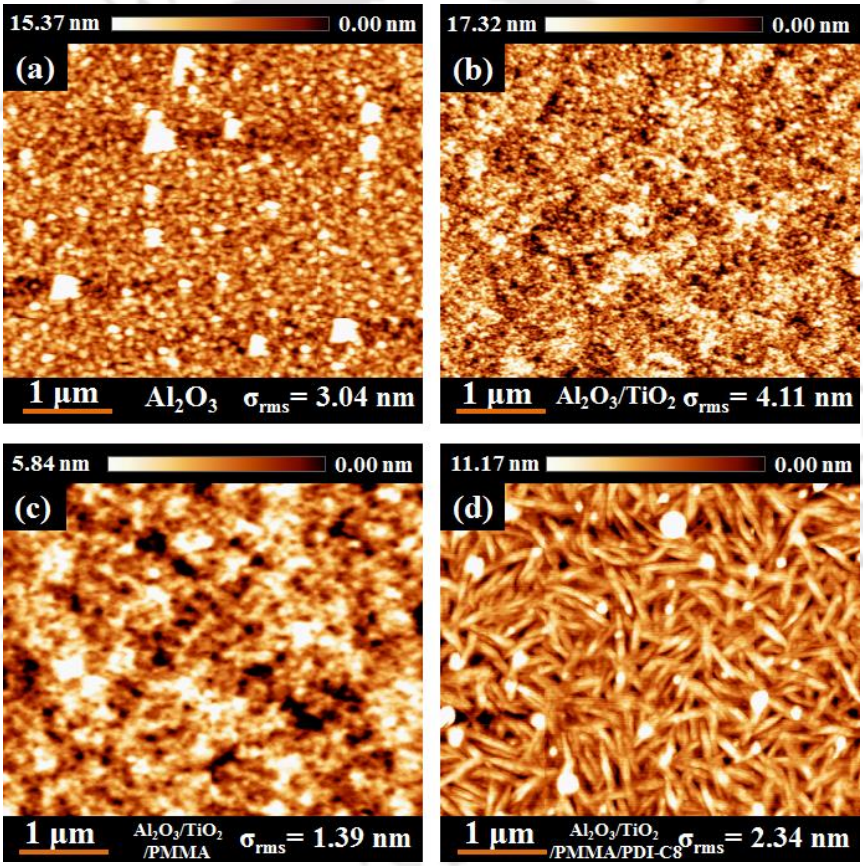

Figure 6.3 Layer-by-layer AFM imagers of (a) anodized Al_2O_3 (b) Al_2O_3/TiO_2 sol-gel (c) Al_2O_3/TiO_2 sol-gel/PMMA and (d) Al_2O_3/TiO_2 sol-gel/PMMA/ PDI-C8 at 90°C substrate temperature deposited on glass substrate.

The layer-by layer AFM images of the PDI-C8 based OFET are shown in Figure 6.3. It has been observed that the r.m.s. surface roughness of bare Al_2O_3 [~3.04 nm, Figure 6.3(a)] and Al_2O_3/TiO_2 [~4.11 nm, Figure 6.3(b)] are quite high but after PMMA coating it reduces to ~1.39 nm [Figure 6.3(c)]. Further, after the deposition of PDI-C8 it again

slightly increases to ~2.34 nm due to the micro fibred film formation of PDI-C8 [Figure 6.3(d)].

6.2.3 Device Fabrication and Characterization

The n-type OFETs were fabricated with bottom gate top contact configuration on tri-layer (Al_2O_3/TiO_2/PMMA) dielectric systems. In this study, two types of substrates were used-(a) Microscope glass substrate and (b) PET substrate to check the compatibility of the inorganic-organic hybrid dielectric layers. All the substrates are initially cut into 1 cm × 2.5 cm dimension and then clean by the following methods, mentioned below-

1) The glass substrates were cleaned by dipping in acidic piranha solution (3:1 ratio of H_2SO_4: H_2O_2) for 1 hour. After that they are vigorously washed by de-ionized water for 8-10 times to remove the acidic layer on the substrate surface and then dried at 100°C on hot plate.
2) The PET substrates are first clean with detergent for 2-3 times and then washed by de-ionized water for several times. Followed by this all the flexible substrates are dried separately by N_2 air flash under room temperature.

After cleaning the glass and PET substrates, >200 nm Al-gate was thermally deposited through the shadow mask. Nearly 13 nm of the upper surface of these thermally deposited Al films were then electrochemically oxidized to grow the first barrier type inorganic Al_2O_3 dielectric layer followed by our previously reported anodic oxidation method.[28] Anodization is a very good, effective and solution based technique to grow metal oxide films with nanometer control. In addition, this process can yield a high-quality metal-oxide insulator at room temperature with very low cost and less time. The function of this barrier type Al_2O_3 dielectric layer [σ_{rms} ~3.04 nm, Figure 6.3(a)] is to reduce the gate leakage up to 5 μA and to prevent the direct contact of the second inorganic dielectric layer to the gate electrode.

The second inorganic dielectric layer, i.e., the sol-gel solution of TiO_2 was then spin coated on the Al_2O_3 coated substrate with different r.p.m. (i.e., 2000, 3000, 4000 and 5000) for 1 min and baked at 110°C on the hot plate. Note that before the spin coating, the sol was vigorously stirred overnight in a hot plate to get uniform thin film. As the roughness of these crystalline TiO_2 films are observed very high [σ_{rms}~4.11 nm, see Figure 6.3(b)], to reduce it, a very thin, PMMA polymer dielectric layer, i.e., the third dielectric

layer, were coated [3% (w/v) in anisole at 3000 rpm] on the top of these TiO_2 layers which further reduces the surface roughness of the TiO_2 layers reduced very significantly (σ_{rms} ~1.39 nm) which were also confirmed in layer-by-layer AFM analysis (Figure 6.3). After the deposition of the inorganic-organic tri-layer dielectric layers, the PDI-C8 and NDI-CY2 small molecule (~70 nm) were deposited on the top of the dielectric layers by thermal evaporation technique under 10^{-6} mbar of pressure at 90°C and 60°C substrate temperatures respectively. Finally, ~80 nm of the source-drain silver/aluminium contacts were deposited at RT above the semiconductor layer through the shadow mask in order to calculate the three terminal properties of the devices.

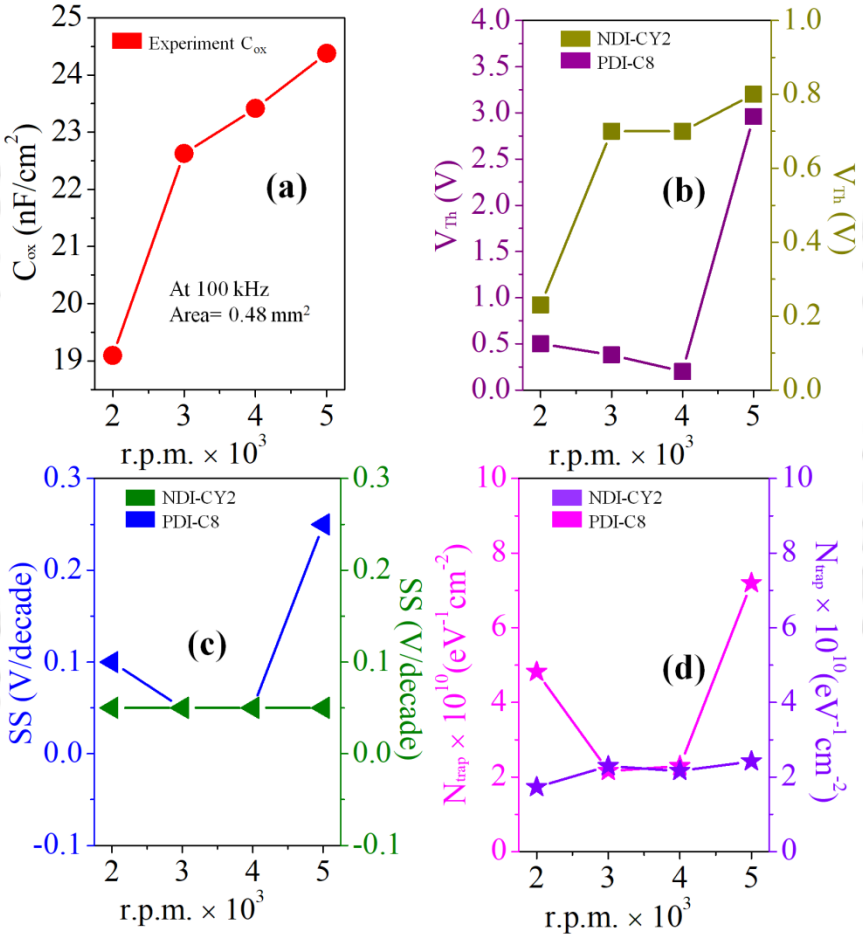

Figure 6.4 Graphical presentation of (a) capacitance density at 100 kHz and variation of (b) V_{Th} (c) SS and (d) trapped charge density with respect to TiO_2 deposition speed (r.p.m) of PDI-C8 based Al_2O_3/TiO_2/PMMA contained organic field effect transistors.

From Figure 6.4 (a) it was observed that the overall capacitance density (C_{ox}) of the tri-layer dielectric layer increases systematically on increasing the r.p.m value. Though the V_{Th} values also show systematic decrement with the decrease in TiO_2 thickness [Figure 6.4(b)], at 5000 r.p.m. it increased again. Similar anomalous behaviour was also observed

in the drain and transfer characteristics (Figure 6.5 and Figure 6.6). From Figure 6.5, it was observed that the drain current increases up to 3000 r.p.m. and reached maximum at 4000 r.p.m and then started to decrease at 5000 rpm. This is because, at 2000 and 3000 r.p.m., due to the high thickness of the second dielectric layer, less numbers of charges were able to accumulate at the channel. At 4000 r.p.m. the thickness of TiO_2 and PMMA becomes almost equal (~ 100 nm) and since TiO_2 is a high-k dielectric material compared to PMMA, the dominancy of TiO_2 becomes more in this case. As a result I_{DS} increases. Further decreasing the thickness of TiO_2 (~50 nm at 5000 r.p.m.), the dominancy of PMMA becomes more since all the dielectrics are connected with each other with a series combination. As a result due to very less influence of TiO_2, the OFETs in this case are exhibiting higher operating voltages and V_{Th} values, which further decrease the charge carrier mobility.

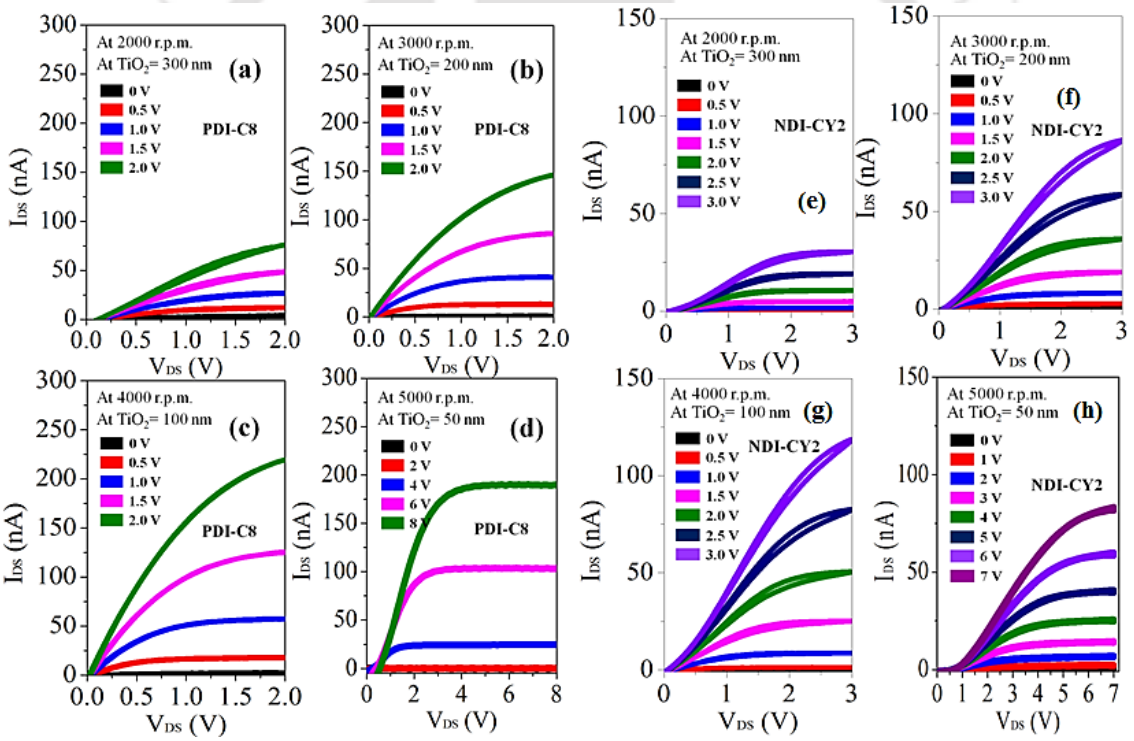

Figure 6.5 Drain Characteristics of PDI-C8 (a-d) and NDI-CY2 (e-h) based OFET with respect to different TiO_2 deposition speed (r.p.m).

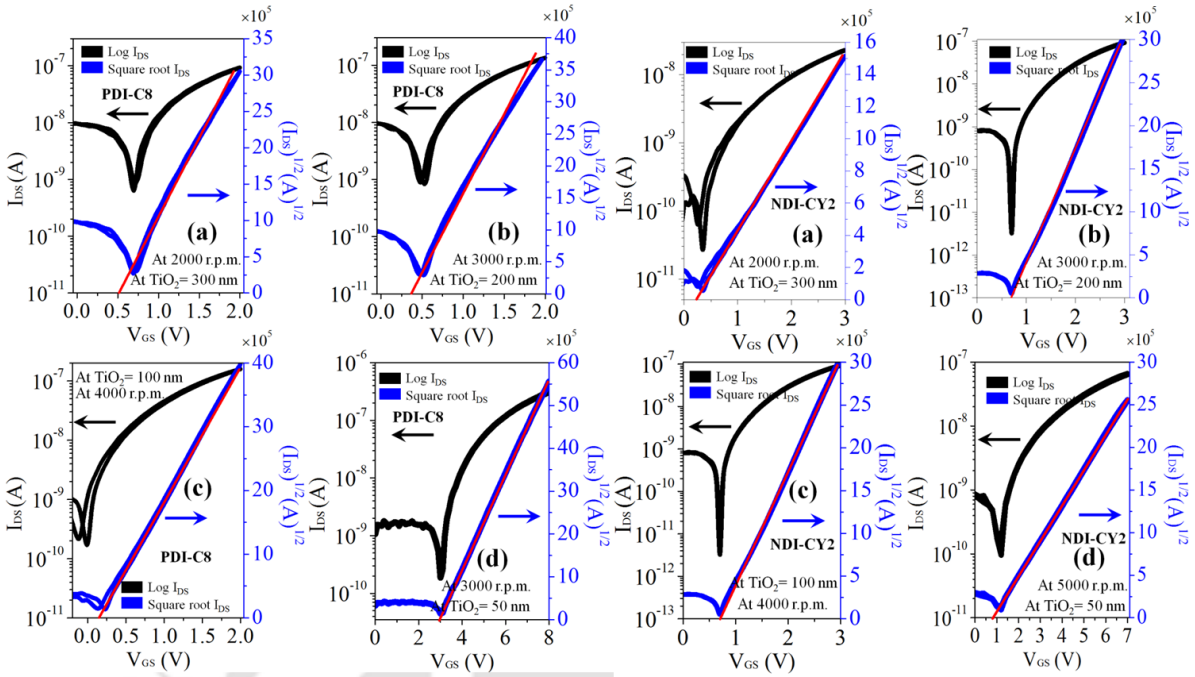

Figure 6.6 Transfer Characteristics of PDI-C8 (a-d) and NDI-CY2 (e-h) based OFET with respect to different TiO_2 deposition speed (r.p.m).

These results are also supported by Figure 6.4(c) and Figure 6.4(d). As the influence of TiO_2 decreases the trap density increases in case of 5000 r.p.m. The detail OFETs performances of the fabricated devices on all different r.p.m. of TiO_2 are summarized in Table 6.1.

Table 6.1. Summary of the device performance of hybrid tri-layer dielectrics contained PDI-C8 and NDI-CY2 based ultra-low operating voltage n-channel organic field effect transistors.

Substrate	Molecule	r.p.m.	C_{ox} (nF/cm²)	V_{Th} (V)	μ (cm²/Vs)	I_{ON}/I_{OFF} Ratio	$N_{trap} \times 10^{10}$ (eV^{-1} cm^{-2})	SS (V/decade)
Glass	PDI-C8	2000	17.3	0.5	0.20	10^3	4.8	0.1
		3000	21.9	0.4	0.25	10^3	2.3	0.05
		4000	22.9	0.2	0.30	10^4	2.2	0.05
		5000	24.2	3.0	0.03	10^3	7.2	0.25
	NDI-CY2	2000	17.3	0.2	0.02	10^3	1.7	0.05
		3000	21.9	0.7	0.07	10^3	2.3	0.05
		4000	22.9	0.7	0.10	10^4	2.2	0.05
		5000	24.2	0.8	0.01	10^2	2.4	0.05
PET	PDI-C8	4000	21.1	0.2	0.27	10^3	2.0	0.05
	NDI-CY2	4000	21.1	0.7	0.09	10^4	2.1	0.05

Further in order to check the electrical stability of the devices under tri-layer dielectric system, the time-dependent decay of I_{DS} under a DC bias stress with V_{DS}= V_{GS}= 2 for PDI-C8 and V_{DS}= V_{GS}= 3 for NDI-CY2 over 1200 sec [Figure 6.7] are recorded. It was observed that the decay of drain current, I_{DS} at 2000, 3000 and 4000 r.p.m. are very less (~5-10%). But at 5000 r.p.m. decay of I_{DS} is more (~30%).

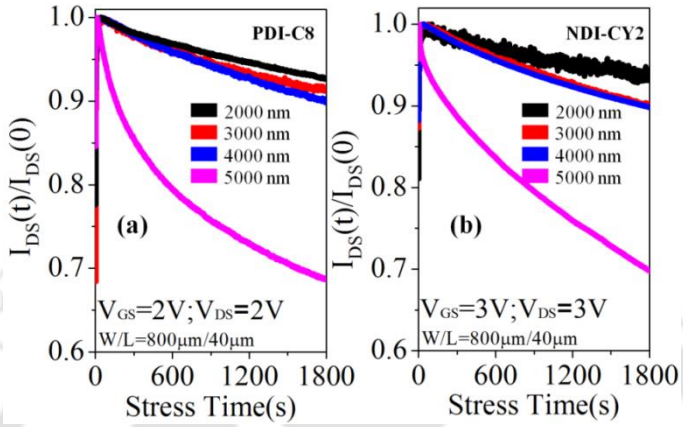

Figure 6.7 Graphical representations of the time dependence of the normalized drain current I_{DS} (t)/I_{DS} (0) of (a) PDI-C8 and (b) NDI-CY2 with Al_2O_3/TiO_2/PMMA tri-layer dielectrics system with respect to different TiO_2 deposition speed.

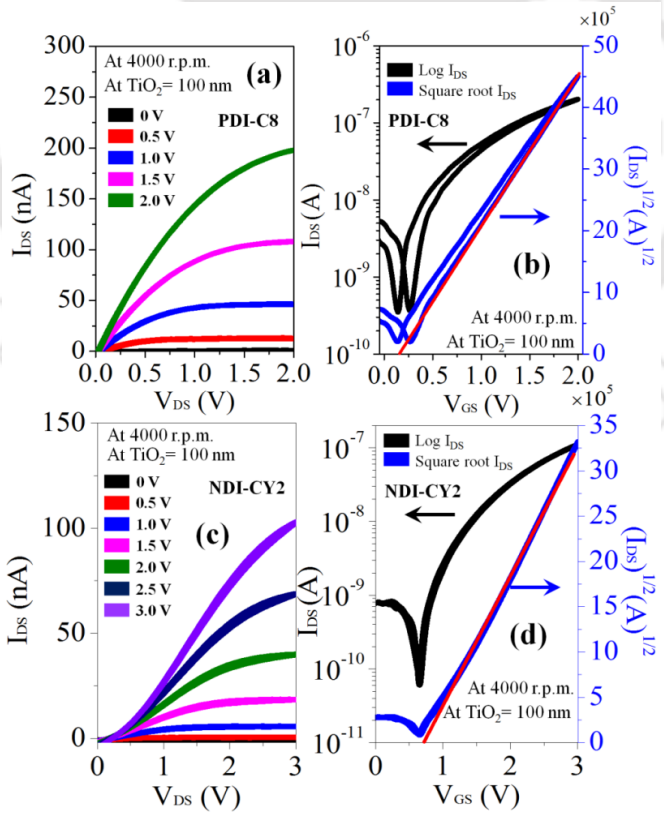

Figure 6.8 (a, c) Drain and (b, d) transfer characteristic of the fabricated OFET devices gated with Al_2O_3/TiO_2/PMMA tri-layer dielectrics system on flexible PET substrate.

This is because of higher trapping of charges at the dielectric-semiconductor interface. Again in order to check the compatibility of this dielectric material in flexible substrate we fabricated the same devices on PET substrate followed by the procedure mentioned in the device fabrication method. It has been observed that this device configuration is also compatible with flexible substrate showing the same performance as observed in case of glass substrate [Figure 6.8]. From the overall performances of the device it can be strongly concluded that this device with the new dielectrics architecture is one of the best and stable device configuration for ultra-low operating voltage, n-type organic field effect transistor.

Generally for real-life application, the main criteria of an OFET are that it should be cost effective, stable and must be operated under low operating voltage so that less electrical power is required during device operation. Most of the remarkable low-operated organic FETs, reported till date, have generally used very costly dielectric materials or very expensive techniques for the deposition of the dielectric layer. Further, in most of the cases p-type semiconductors are chosen for the demonstration since it is very challenging to get highly stable OFET device containing n-type material under low-voltage operation compared to p-types. In this regard, pentacene and CuPc based p-type OFETs based on amorphous film of strontium titanate (STO) perovskite material, show a much better gate dielectric property with operating voltage ~-6V on Si-substrate.[29] Similarly, Pentacene based p-type OFET with hybrid bilayer dielectric system containing zirconium dioxide (high-k dielectric) and amorphous fluoropolymer, CYTOP (low-k dielectric) also showed very low operating voltage (-3V).[30] Very low operational voltage (-4V) was also achieved for same pentacene-OFET by using two layers of cross-linked PVP dielectric.[31] Researchers also synthesized new cross-linkable random copolymers of PMMA (PAZ 12) and used them to fabricated low-voltage pentacene-OFET.[32] Recently, cross-linked PMMA was further used for the fabrication of TIPS-TPDO-tetraCN-Based n-type OFET with operating voltage of 5V.[33]

In this study, the significant influence of low-cost Al_2O_3/TiO_2/PMMA tri-layer hybrid dielectric system for the ultra-low operation of electrically stable n-channel OFETs is demonstrated. Two types of inorganic dielectrics, namely Al_2O_3 and TiO_2 are use in this study. Al_2O_3 is deposited by low-cost anodic oxidation method whereas TiO_2 is synthesized by simple sol-gel technique and spin coated on the top of Al_2O_3 first dielectric layer. PMMA, an organic dielectric material, is chosen as the third dielectric layer which is also deposited by spin coating method. By keeping the thickness of Al_2O_3 and PMMA

constant, the thickness of TiO_2 is varied and their effects on the performance of n-type small molecule based OFETs are systematically analysed. It has been observed that ~100 nm thickness of TiO_2 layer is the optimum thickness and along with top contact Ag electrode the device exhibited the best n-channel behaviour with very low operating voltage of 2V. With this optimum condition, the device showed the highest electron mobility value (μ_e= 0.3 $cm^2.V^{-1}.s^{-1}$ for PDI-C8 and μ_e= 0.1 $cm^2.V^{-1}.s^{-1}$ for NDI-CY2), compared to other thickness of TiO_2, with threshold voltages V_{Th}= 0.2 V (PDI-C8), V_{Th}= 0.7 V (NDI-CY2) and current on/off ratio ~10^4. The electric stability of all the devices were analysed by bias stress instability study by applying constant V_{GS}=V_{DS}=2V (PDI-C8) and V_{GS}=V_{DS}=3V (NDI-CY2) for half an hour under vacuum condition. Only ~10% decrements of I_{DS} were observed in this stress experiment which denotes the high stability of the device. Furthermore, this low-cost dielectric architecture was found compatible with flexible PET substrate and shows ultra-low operating voltage. This high performance, electrically stable, n-channel OFET device having ultra-low operating voltage, with tri-layer dielectric system is expected to have diverse applications in next generation of portable electronics.

6.3 Conclusion

In conclusion, the influence of cost effective inorganic-organic tri-layer hybrid dielectric system for the ultra-low operation of n-channel organic field effect transistors are demonstrated. Al_2O_3 and TiO_2 were used as two inorganic dielectrics and PMMA was used as organic dielectric material. By keeping the thickness of Al_2O_3 and PMMA as constant, the thickness of synthesized sol-gel TiO_2 was varied and their effects on the performance of n-channel PDI-C8 and NDI-CY2 based OFETs were systematically analysed. It has been observed that at ~100 nm thickness of TiO_2 the device showed its best n-channel behaviour with remarkable low operating voltage of 2V (PDI-C8) and 3V (NDI-CY2) due to the better capacitor coupling which results in maximum number of accumulating charge at the channel. The n-type based OFETs with top contact Ag/Al electrode at this optimum condition shows the highest electron mobility value (μ_e= 0.3 $cm^2.V^{-1}.s^{-1}$ for PDI-C8 and μ_e= 0.1 $cm^2.V^{-1}.s^{-1}$ for NDI-CY2), compared to other thickness of TiO_2, with threshold voltages V_{Th}= 0.2 V (PDI-C8), V_{Th}= 0.7 V (NDI-CY2) and current on/off ratio ~10^4. The electrical stability of the devices are analysed by applying constant V_{GS}=V_{DS}=2V (PDI-C8) and V_{GS}=V_{DS}=3V (NDI-CY2) for half an hour under vacuum condition which shows only ~10% decrements of I_{DS}. These tri-layer dielectrics are also

found compatible with flexible PET substrate and show almost same device performance like in glass substrate with ultra-low operating voltage. This ultra-low operating voltage n-channel OFET device with Al_2O_3/TiO_2/PMMA tri-layer dielectric system is expected to have diverse applications in the future for portable organic electronics application.

6.4 References

[1] Chua, L.-L.; Zaumseil, J.; Chang, J.-F.; Ou, E. C.-W.; Ho, P. K.-H.; Sirringhaus, Friend, H.; R. H. General Observation of n-Type Field-Effect behaviour in Organic Semiconductors. *Nature* **2005**, *434*, 194–198.

[2] Hardigree, J. F. M.; Howard E. K. Through Thick and Thin: Tuning the Threshold Voltage in Organic Field-Effect Transistors. *Acc. Chem. Res.* **2014**, *47*, 1369–1377.

[3] Hlaing, H.; Kim C.-H.; Carta F.; Nam, C.-Y.; Barton R.A.; Petrone, N.; Hone, J.; Kymissis, I. Low-Voltage Organic Electronics based on a Gate-Tunable Injection Barrier in Vertical Graphene-Organic Semiconductor Heterostructures. *Nano Lett.* **2015**, *15*, 69–74.

[4] Dey, A.; Singh, A.; Das, D.; Iyer, P. K. High-Performance ZnPc Thin Film-based Photosensitive Organic Field-Effect Transistors: Influence of Multilayer Dielectric Systems and Thin Film Growth Structure. *ACS Omega* **2017**, *2*, 1241–1248.

[5] Dey, A.; Kalita, A.; Iyer, P. K. High-Performance n‑Channel Organic Thin-Film Transistor based on Naphthalene Diimide. *ACS Appl. Mater. Interfaces* **2014**, *6*, 12295–12301.

[6] Shukla, D.; Nelson, S. F.; Freeman, D. C.; Rajeswaran, M.; Ahearn, W. G.; Meyer, D. M.; Carey, J. T. Thin-Film Morphology Control in Naphthalene-Diimide-based Semiconductors: High Mobility n-Type Semiconductor for Organic Thin-Film Transistors. *Chem. Mater.* **2008**, *20*, 7486–7491.

[7] Xu, X.; Yao, Y.; Shan, B.; Gu, X.; Liu, D.; Liu, J.; Xu, J.; Zhao, N.; Hu, W.; Miao, Q. Electron Mobility Exceeding 10 $cm^2 V^{-1} s^{-1}$ and Band-Like Charge Transport in Solution-Processed n-Channel Organic Thin-Film Transistors. *Adv. Mater.* **2016**, *28*, 5276–5283.

[8] Wang, C.-Y.; Fuentes-Hernandez, C.; Liu, J.-C.; Dindar, A.; Choi, S.; Youngblood, J. P.; Moon, R. J.; Kippelen, B. Stable Low-Voltage Operation Top-Gate Organic Field-Effect Transistors on Cellulose Nanocrystal Substrates. *ACS Appl. Mater. Interfaces* **2015**, *7*, 4804–4808.

[9] Dey, A.; Singh, A.; Das, D.; Iyer, P. K. Photosensitive Organic Field Effect Transistors: The Influence of ZnPc Morphology and Bilayer Dielectrics for Achieving a Low Operating Voltage and Low Bias Stress Effect. *Phys. Chem. Chem. Phys.* **2016**, *18*, 32602–32609.

[10] Held, M.; Schießl, S. P.; Miehler, D.; Gannott, F.; Zaumseil, J. Polymer/Metal Oxide Hybrid Dielectrics for Low Voltage Field-Effect Transistors with Solution-Processed, High-Mobility Semiconductors. *Appl. Phys. Lett.* **2015**, *107*, 083301(1-4).

[11] Sagade, A. A.; Rao, K. V.; George, S. J.; Datta, A.; Kulkarni, G. U. A Charge Transfer Single Crystal Field Effect Transistor Operating at Low Voltages. *Chem. Commun.* **2013**, *49*, 5847–5849.

[12] Hung, C.-C.; Wu, H.-C.; Chiu, Y.-C.; Tung, S.H.; Chen, W.-C. Crosslinkable High Dielectric Constant Polymer Dielectrics for Low Voltage Organic Field-Effect Transistor Memory Devices. *J. Polym. Sci., Part A: Polym. Chem.* **2016**, *54*, 3224–3236.

[13] Seong, H.; Baek, J.; Pak, K.; Im, S. G. A Surface Tailoring Method of Ultrathin Polymer Gate Dielectrics for Organic Transistors: Improved Device Performance and the Thermal Stability Thereof. *Adv. Funct. Mater.* **2015**, *25*, 4462–4469.

[14] Liang, J.; Li, L.; Chen, D.; Hajagos, T.; Ren, Z.; Chou, S. Y.; Hu, W.; Pei, Q. Intrinsically Stretchable and Transparent Thin-Film Transistors based on Printable Silver Nanowires, Carbon Nanotubes and an Elastomeric Dielectric. *Nat. Commun.* **2015**, *6*, 7647(1-10).

[15] Luzio, A.; Ferré, F. G.; Fonzo, F. D.; Caironi, M. Hybrid Nanodielectrics for Low-Voltage Organic Electronics. *Adv. Funct. Mater.* **2014**, *24*, 1790–1798.

[16] Jang, M.; Park, J. H.; Im, S.; Kim, S. H.; Yang, H. Critical Factors to Achieve Low Voltage- and Capacitance-based Organic Field-Effect Transistors. *Adv. Mater.* **2014**, *26*, 288–292.

[17] Shi, L.; Xu, X.; Ma, M.; Li, L. High-Performance, Low-Operating Voltage, and Solution-Processable Organic Field-Effect Transistor with Silk Fibroin as the Gate Dielectric. *Appl. Phys. Lett.* **2014**, *104*, 023302(1-4).

[18] Liu, A.; Liu, G. X.; Zhu, H. H.; Xu, F.; Fortunato, E.; Martins, R.; Shan, F. K. Fully Solution-Processed Low-Voltage Aqueous In_2O_3 Thin-Film Transistors Using an Ultrathin ZrO_x Dielectric. *ACS Appl. Mater. Interfaces* **2014**, *6*, 17364–17369.

[19] Bobbert, P. A.; Sharma, A.; Mathijssen, S. G.; Kemerink, M.; de Leeuw, D. M. Operational Stability of Organic Field-Effect Transistors. *Adv. Mater.* **2012**, *24*, 1146–1158.

[20] Ng, T. N.; Daniel, J. H.; Sambandan, S.; Arias, A.-C.; Chabinyc, M. L.; Street, R. A. Gate Bias Stress Effects due to Polymer Gate Dielectrics in Organic Thin-Film Transistors. *J. Appl. Phys.* **2008**, *103*, 044506(1-5).

[21] Kumar, S.; Dhar A. Low Operating Voltage n-Channel Organic Field Effect Transistors using Lithium Fluoride/PMMA Bilayer Gate Dielectric. *Mater. Res. Bull.* **2015**, *70*, 590–594.

[22] Ye, X.; Lin, H.; Yu, X.; Han, S.; Shang, M.; Zhang, L.; Jiang, Q.; Zhong, J. High Performance Low-Voltage Organic Field-Effect Transistors Enabled by Solution Processed Alumina and Polymer Bilayer Dielectrics. *Synth. Met.* **2015**, *209*, 337–342.

[23] Ortiz, R. P.; Facchetti, A.; Marks, T. J. High-k Organic, Inorganic, and Hybrid Dielectrics for Low-Voltage Organic Field-Effect Transistors. *Chem. Rev.* **2010**, *110*, 205–239.

[24] Facchetti, A.; Yoon, M.-H.; Marks, T. J. Gate Dielectrics for Organic Field-Effect Transistors: New Opportunities for Organic Electronics. *Adv. Mater.* **2005**, *17*, 1705–1725.

[25] Park, Y. M.; Desai, A.; Salleo, A.; Jimison, L. Solution-Processable Zirconium Oxide Gate Dielectrics for Flexible Organic Field Effect Transistors Operated at Low Voltages. *Chem. Mater.* **2013**, *25*, 2571–2579.

[26] Amin, A. Y.; Khassanov, A.; Reuter, K.; Meyer-Friedrichsen, T.; Halik, M. Low-Voltage Organic Field Effect Transistors with a 2-Tridecyl[1]benzothieno[3,2-b][1]benzothiophene Semiconductor Layer. *J. Am. Chem. Soc.* **2012**, *134*, 16548–16550.

[27] Balakrishnan, K.; Datar, A.; Oitker, R.; Chen, H.; Zuo, J.; Zang, L. Nanobelt Self-Assembly from an Organic n-Type Semiconductor: Propoxyethyl-PTCDI. *J. Am. Chem. Soc.* **2005**, *127*, 10496-10497.

[28] Dey, A.; Singh, A.; Kalita, A.; Das, D.; Iyer, P. K. High Performance, Low Operating Voltage n-Type Organic Field Effect Transistor based on Inorganic-Organic Bilayer Dielectric System. *J. Phys.: Conf. Ser.* **2016**, *704*, 012017(1-8).

[29] Yadav, S.; Ghosh, S. Amorphous Strontium Titanate Film as Gate Dielectric for Higher Performance and Low Voltage Operation of Transparent and Flexible Organic Field Effect Transistor. *ACS Appl. Mater. Interfaces* **2016**, *8*, 10436–10442.

[30] Ha T.-J. Low-Voltage and Hysteresis-Free Organic Thin-Film Transistors Employing Solution-Processed Hybrid Bilayer Gate Dielectrics. *Appl. Phys. Lett.* **2014**, *105*, 043305(1-3).

[31] Yi, M.; Guo, Y.; Guo, J.; Yang, T.; Chai, Y.; Fan, Q.; Xie, L.; Huang, W. The Mechanical Bending Effect and Mechanism of High Performance and Low-Voltage Flexible Organic Thin-Film Transistors with a Cross-Linked PVP Dielectric Layer. *J. Mater. Chem. C* **2014**, *2*, 2998–3004.

[32] Simas, E. R.; Kang, E. S. H.; Gassmann, A.; Katholing, E.; Janietz, S.; von Seggern, H. Cross-Linkable Random Copolymers as Dielectrics for Low-Voltage Organic Field-Effect Transistors. *J. Mater. Chem. C* **2015**, *3*, 9217–9223.

[33] Jung, S.; Albariqi, M.; Gruntz, G.; Al-Hathal, T.; Peinado, A.; Garcia-Caurel, E.; Nicolas, Y.; Toupance, T.; Bonnassieux, Y.; Horowitz, G. A TIPS-TPDO-tetraCN-based n-Type Organic Field-Effect Transistor with a Cross-linked PMMA Polymer Gate Dielectric. *ACS Appl. Mater. Interfaces* **2016**, *8*, 14701–14708.

7

Rapid Detection of Gram Positive and Gram Negative Bacteria using n-Type Organic Field Effect Transistor

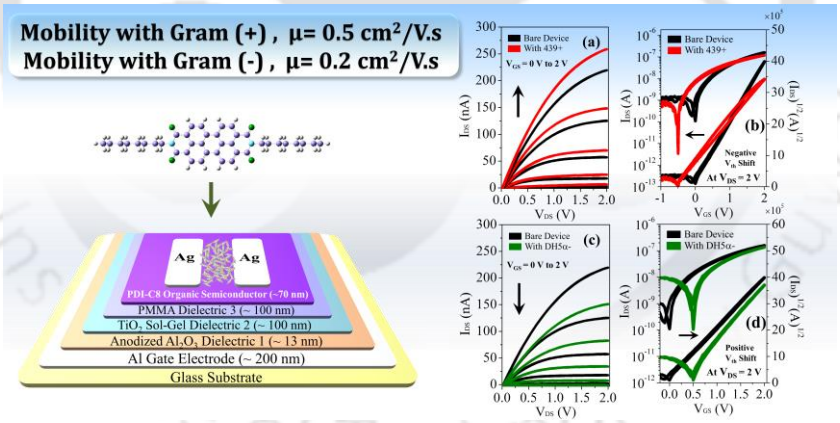

[1] **Dey, A.;** Singh, A.; Dutta, D.; Ghosh, S. S.; Iyer, P. K. Method for the Detection of Gram Positive and Gram Negative Bacteria by Ultra-low Operating Voltage n-type Organic Field Effect Transistor, 2017, **Patent**, Ref. No. 201831000478, App. No. TEMP/E-1/462/2018-KOL.

[2] **Dey, A.;** Singh, A.; Dutta, D.; Ghosh, S. S.; Iyer, P. K. Rapid and Facile Label-Free Bacteria Detection using Hybrid Tri-Layer Dielectrics Contained Ultra-low Operated n-Type Organic Field Effect Transistor. **Communicated**.

7

Rapid Detection of Gram Positive and Gram Negative Bacteria using n-Type Organic Field Effect Transistor

Organic Field Effect Transistors have received great deal of attention since the past few decades because of their potential use in various chemical and biological sensing applications.[1-4] A transistor-based biosensor normally has high demand because of its high sensitivity since the single device can sense the analyte as well as can amplify its response.[5-7] In addition, organic materials are more compatible with biological elements, which is very essential for an effective sensor device. Compared to other inorganic biosensor, the low cost, flexible and easy to fabricate OFET seems to be one of the ideal disposable sensing devices which can deliver accurate results in the new generation of flexible electronics. [8-11] Among the biosensors, bacteria sensor is one of the most challenging since bacterial contamination is a major health hazard especially in the context of food safety, environmental monitoring, and pharmaceutical industry. It assumes even greater significance in case of pathogens as the presence of even a single cell may lead to serious health risk. Thus, rapid quantification of bacteria is imperative for clinical diagnosis, food safety, therapeutic strategies, and for reducing potential infections.[12-14] But the sensing of bacteria or other living cells are generally detected by organic electro-chemical transistors (OECTs) in literature since it can be easily fabricated and mainly operated under low operating voltage. On the other hand the main disadvantage of OECT is slower response time compared to OFETs and it cannot be easily handled since it contains electrolytic solution.[15] This study successfully overcomes the

disadvantages of OFET over OECT, by reducing the operating voltage toward very low (~2V) with the help of hybrid tri-layer dielectrics system.

Here, two different inorganic dielectrics namely Al_2O_3 and TiO_2 and one polymer dielectric, namely, PMMA were used to form hybrid tri-layer dielectric system. Each of the individual dielectric layer of this system has significant contribution for reducing the operational voltage of PDI-C8 based n-type OFET used for bacteria detection. The first low-k inorganic dielectric layer (Al_2O_3) was used to prevent the gate leakage up to 5 μA whereas the second high-k inorganic dielectric TiO_2 was synthesized by low cost sol-gel method and used to reduce the operating voltage of the OFET and simultaneously help to improve the sensitivity of the device by improving its mobility by the induction of more charges in the active channel through the entire dielectric layer. Since mobility depends upon the active layer surface morphology, smoothness of the second dielectric surface was vital, together with a biocompatible, low-k PMMA dielectric that was used as a third dielectric layer, before the active layer deposition. This dielectric material was also chosen in such a way in combination of these three dielectrics, that the second dielectric TiO_2 becomes more dominant layer compared to the other two. The structure of this n-type OFET was standardized step-by-step prior to the bacteria detection as mentioned in Chapter 6. The average electron mobility (μ_e) and threshold voltage (V_{Th}) of the PDI-C8 based OFET was observed to be 0.3 $cm^2V^{-1}s^{-1}$ and 0.2 V respectively without bacteria. The electrical stability of the bare device was also investigated at $V_{GS}=V_{DS}=2V$ under vacuum, from which it was found that the device showed high electrical stability with a decay of I_{DS} ~10% after 30 min. Further it was observed that this low cost, solution processable, dielectric system is compatible with any desired substrate like glass, PET/OHP plastic sheet etc. For sensing bacteria, it has been found that due to the interaction between the surface charges of bacteria cell wall and the charge carriers in the channel, the device is successfully able to detect and distinguish the gram positive and gram negative bacteria. In presence of gram positive bacteria the average μ_e increases with reduced V_{Th} whereas in the presence of gram negative bacteria the average μ_e decreases with increased V_{Th}. This study is the first report of OFET based bacteria sensor having detection limit 10^3 cfu/mL for both the types of bacteria, with remarkably ultra-low operating voltage of 2 V, on low-cost glass substrates without indium tin oxide or/and Si/SiO_2.

7.1 Experiments

7.1.1 Materials

Titanium (IV) isopropoxide (97% purity), glacial acetic acid, isopropanol and polyethylene terephthalate (PET) were purchased from Sigma Aldrich and used without further purification for the preparation of TiO_2 sol-gel. For device fabrication, N, N′-dioctyl-3, 4, 9, 10-perylenedicarboximide (PDI-C8), PMMA (M_W=550000 g/mol), silver (99.999% purity) and auminium wire (99.999% purity) were also purchased from Sigma Aldrich and used as received, unless otherwise mentioned. Citric acid monohydrate (99.5% purity), purchased from Alfa Aesar was used as weak electrolyte in Al anodization method. Anisole (99% purity) was purchased from Loba Chemie. Glass microscopic slides (thickness 1-1.2mm) were used as one of the device substrate without any surface modification, purchased from Jain Scientific Glass Works, India.

7.1.2 Characterization Details

The semiconducting active layer of PDI-C8 was deposited by thermal evaporation method using Excel instrument. TiO2 sol-gel and PMMA dielectric thin films were deposited by spin coating method using Laurell and Spin 150 spin coaters. Veeco Dektak 150 surface profilometer were used to measure the thicknesses of all the after the deposition. For characterizing the synthesized TiO2 sol-gel, Jaz UV-Vis spectrophotometer, Tecnai G2 F20 S-twin JEOL 2100 transmission electron microscope and Agilent 5500-STM instrument were used for recording UV-Visible absorption spectra, TEM image and AFM analysis respectively. The thin film XRD pattern of TiO2 was recorded by a Rigaku TTRAX III with Cu Kα radiation. Keithley 2400 source meter was for anodic oxidation of Al. Finally, all the electrical properties and sensing study were done by using Keithley 4200 semiconductor characterization system.

7.1.3 Device Fabrication Method

The bacteria sensing PDI-C8 based ultra-low operated OFETs were fabricated with bottom gate top contact configuration with hybrid tri-layer (Al_2O_3/TiO_2/PMMA) dielectric systems [Figure 7.1]. For fabricating the devices, at the very beginning microscope glass substrates were cut into 1 cm × 2.5 cm dimension and then cleaned by dipping in acidic piranha solution (1:3 ratio of H_2O_2:H_2SO_4) for 1 h. After 1 h all the substrates

were vigorously washed by de-ionized water 8-10 times to remove the acidic layer and dried at 100°C on hot plate. After cleaning, >200 nm Al-gate was thermally deposited through the shadow mask. Nearly 13 nm of the upper surface of these thermally deposited Al films were then electrochemically oxidized to grow the first barrier type inorganic Al_2O_3 dielectric layer followed by our previously mentioned anodic oxidation method.[16-18]

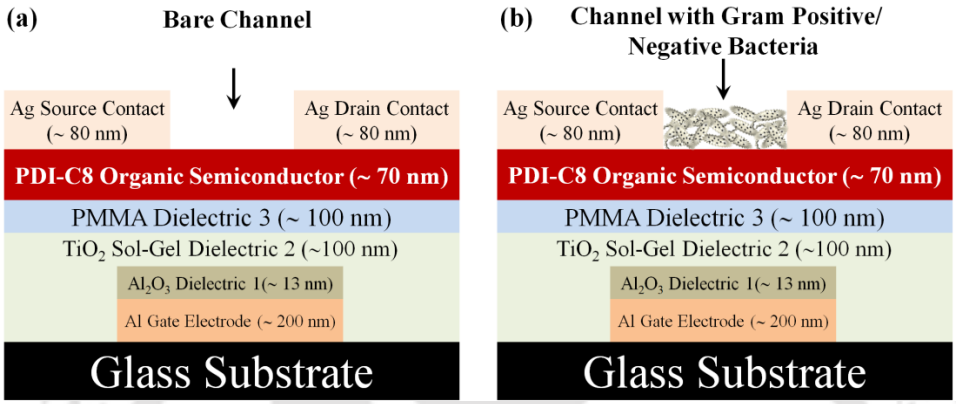

Figure 7.1 Schematic representation of the ultra-low operated n-type OFETs (a) Bare Device and (b) Device with bacteria at the channel.

The function of this barrier type Al_2O_3 dielectric layer is to reduce the gate leakage up to 5 μA and to prevent the direct contact of the second inorganic high-k TiO_2 dielectric layer to the gate electrode. Next the second inorganic dielectric, colloidal solution of high-k TiO_2 was synthesised one night before to the device fabrication by using simple sol-gel method as mentioned in Chapter 6. The solution was then spun on Al_2O_3 coated glass substrate at 4000 r.p.m. for 1 min and then baked at 110°C on the hot plate. To reduce roughness of the TiO_2 sol-gel layer, a very thin, PMMA polymer dielectric layer, i.e., the third dielectric layer, was coated [3% (w/v) in anisole, 3000 r.p.m.]. Due to this polymer dielectric layer the roughness of the top surface of TiO_2 layers reduced very significantly. Following this, a 70 nm (±10 nm) of PDI-C8 were deposited on the top of the hybrid tri-layer dielectric layers by thermal evaporation technique at 90°C substrate temperature with a base pressure of 10^{-6} mbar. Finally, ~80 nm of the source-drain silver contacts were deposited at RT above the semiconductor layer through the shadow mask in order to calculate the three terminal properties of the devices. After these steps all the bare device properties of the OFET device was recorded and analysed which are systematically explained in the "Results and Discussion" section.

7.1.4 Bacterial Culture

In this study for bacteria sensing two different types of gram positive bacteria, namely, enterococcus faecalis (439+) and bacillus cereus (1305+) and gram negative bacteria, namely, escherichia coli (DH5α-) and pseudomonas aeruginosa (2488-) were taken. The gram positive bacteria were grown in BHI (brain heart infusion) media at 37°C at 180 r.p.m. for 12 h. The gram negative pseudomonas aeruginosa (2488-) was grown in NB (nutrient broth) medium whereas the escherichia coli (DH5α-) cells were grown in LB (Luria-Bertani) medium under same conditions. Following this the bacteria were serially diluted (10^{-1}, 10^{-2}, 10^{-3} and 10^{-4}) and 100 µL of each sample was spread on agar plates and incubated at 37 °C overnight to obtain colonies.

7.1.5 Bacterial Cell Wall Lysis

For removing the bacterial cell wall, 1 mg/mL solution of chicken egg white lysozyme was prepared and out of this solution 50 µg/mL working solution was made. A 50 µL of this was added to 1 mL of each of both gram positive and gram negative bacteria culture and incubated for 30 min at 37 °C. Then the suspension was centrifuged at 10000 r.p.m. for 1 min and supernatant was removed. The pellet was then re-dispersed for further measurements.

7.2 Results and Discussion

7.2.1 Operation Mechanism

Figure 7.2a-c and Figure 7.2d-i represent the operation mechanism of PDI-C8 based ultra-low operated n-type OFETs by the simplified energy band diagram in absence and presence of bacteria in the channel of the device respectively. V_{DS} and V_{GS} represent the voltage applied between source-to-drain and gate-to-source respectively. Since the fabricated OFETs have top contact bottom gate architecture, the flow of current from source-to-drain through the PDI-C8 active layer is directly dependent on the applied voltage between gate-to-source V_{GS}, for a constant value of V_{DS}. As the PDI-C8 active layer and the Al-gate contact are capacitive coupled with each other with the help of hybrid tri-layer dielectric system, the externally injected charges in the active layer thin film are

generally mobile charges which moves with respect to the particular value of V_{DS}. Figure 7. 2a-c represent the operation mechanism of bare PDI-C8 based OFET device in which

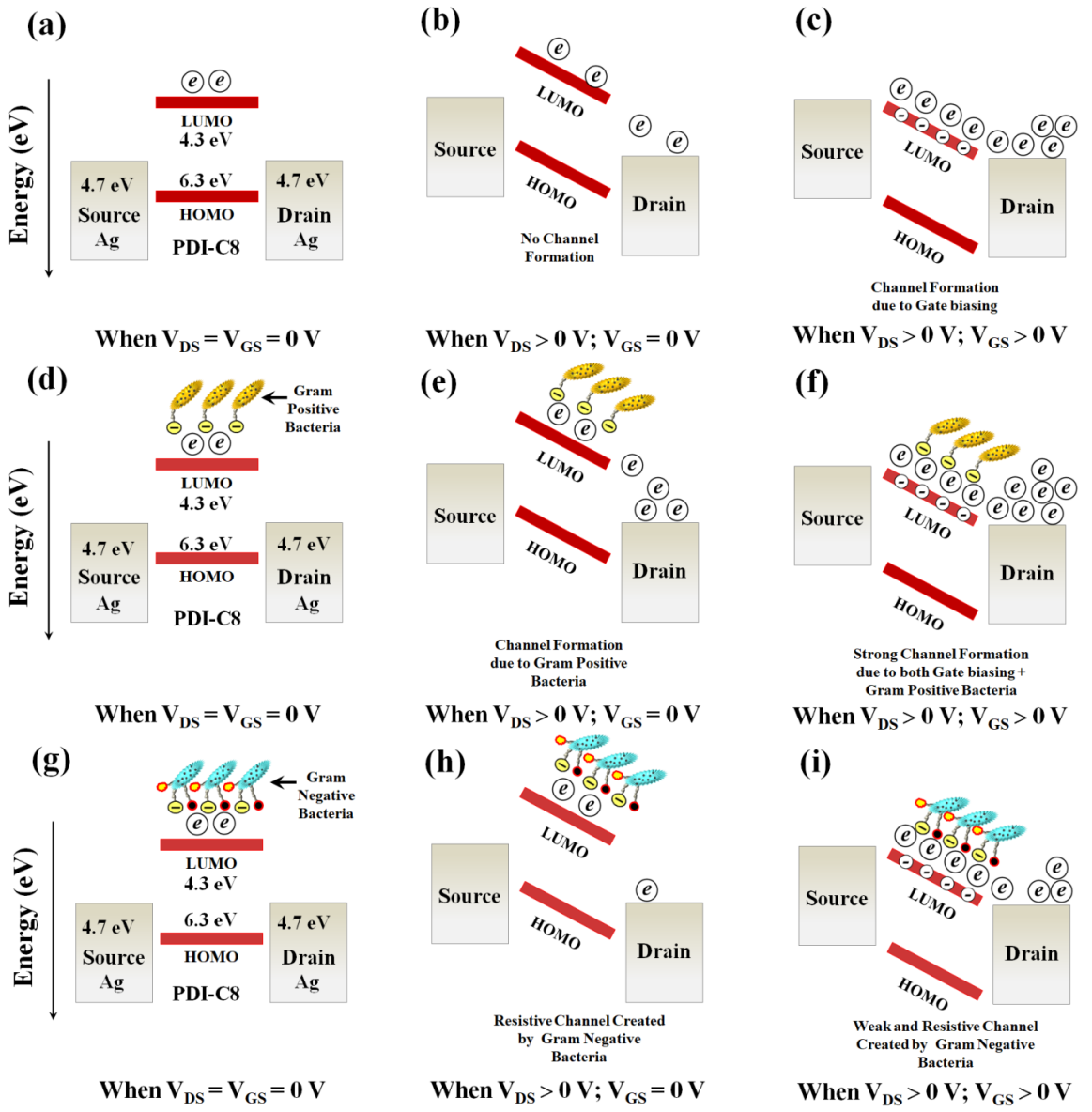

Figure 7.2 Schematic representation of the operation mechanism involved in ultra-low operated PDI-C8 based n-type OFETs. (a–c) represent the bare device operational mechanism whereas (d-f) and (g-i) represents the operational mechanism of the same device in presence of Gram positive and Gram negative bacteria in the channel respectively.

Figure 7.2a represents the equilibrium condition of the device when V_{DS}= V_{GS}= 0V. At this condition, the device is in its "OFF" condition since at this stage no current is flowing from source-to-drain. In Figure 7.2b, i.e., when V_{DS}> 0V and V_{GS}= 0V, negatively charged electrons which are initially present in PDI-C8 active layer, started to move towards positively biased drain electrode. Since V_{GS}= 0V, at this stage no channel is able to formed

due to the absence of mobile charges, as a result the source-to-drain current becomes negligible. When the gate-to-source voltage is applied along with the applied source-to-drain voltage, i.e. V_{DS}> 0V and V_{GS}> 0V as shown in Figure 7.2c, the channel is formed in the PDI-C8 active layer due to the induction of mobile charges with the help of the hybrid tri-layer dielectric system and the transistor becomes in its "ON" state. These induced mobile charges generate an enormous electric field at semiconductor-dielectric interface which shifted the HOMO and LUMO levels of PDI-C8 downwards to match the LUMO to the Fermi level of Ag drain contact. Since V_{DS} is already greater than 0V at this stage, more number of electrons will flow through the channel, as a result of which drain current increases. In presence of gram positive bacteria, the negatively charged wall teichoic acid creates an additional channel on the top of the semiconducting active layer [Figure 7.2d-f]. As a result, higher drain current is obtained even in absence of the external gate bias compared to the bare device [Figure 7.2e]. With the same condition, in presence of gate bias [Figure 7.2f], the drain current further increases due to the collective effect of both the channels created by the negatively charged gram positive bacteria and the external gate bias, which is much higher compared to the similar situation in absence of gram positive bacteria [Figure 7.2f and Figure 7.2c].

Further, in case of gram negative bacteria, though the surface of the bacteria is also negatively charged like the gram positive one, decrement in drain current was observed in the output of the n-type OFETs [Figure 7. 2g-i]. This may be due to the difference in the outer cell wall of both the bacteria. As it is already known that, the outer cell wall of gram negative bacteria contained several biological entities like lipid, proteins, lipopolysaccharides etc. compared to the gram positive bacteria which mainly contained the teichoic acid. Therefore, the outer layer of the cell wall of gram positive bacteria are much well-arranged compared to the gram negative one. Hence, when gram negative bacteria are present in the channel of n-type OFETs, instead of increasing the output current, it decreases the drain current by creating some obstacles in the channel which further forms some resistive path to the flow of electrons from source-to-drain, as a result of which drain current decreases at this stage compared to the bare device [Figure 7.2i and Figure 7.2c].

7.2.2 Device Characterizations

Before bacteria sensing, the bare device properties of hybrid tri-layer dielectric contained PDI-C8 based OFET was analysed systematically. It has been observed that at

4000 r.p.m. the devices with top contact Ag electrodes exhibit excellent n-channel behaviour electron mobility, μ_e= 0.3 $cm^2.V^{-1}.s^{-1}$, threshold voltages V_{th}= 0.2 V and current on/off ratio ~10^4 with an operating voltage of only 2V, which is due to the better capacitor coupling among the tri-layer dielectric materials at the optimum thickness of TiO_2 which further helps to accumulate maximum number of charge at the channel at very low gate bias. The electrical stability of the bare device was also investigated at V_{GS}=V_{DS}=2V under vacuum, from which it was found that the device shows high electrical stability with a decay of I_{DS} ~10% after 30 min. From the overall performances of the device it can be strongly concluded that this ultra-low operated, highly stable n-type OFET can be easily used for bio sensing application.

After completing the systematic analysis of the bare device, for the immobilization of the gram positive and gram negative bacteria in the channel, both the analyte were taken in de-ionized water media and 1 µL of each of the solution was drop cast on the effective channel and vacuum dried under dark to evaporate the water. For the confirmation of the presence of bacteria on the channel, FESEM image was taken after the immobilization [Figure 7.3]. The devices were again characterized by Keithley 4200-SCS semiconductor parameter analyser under dark and vacuum condition in presence of the bacteria.

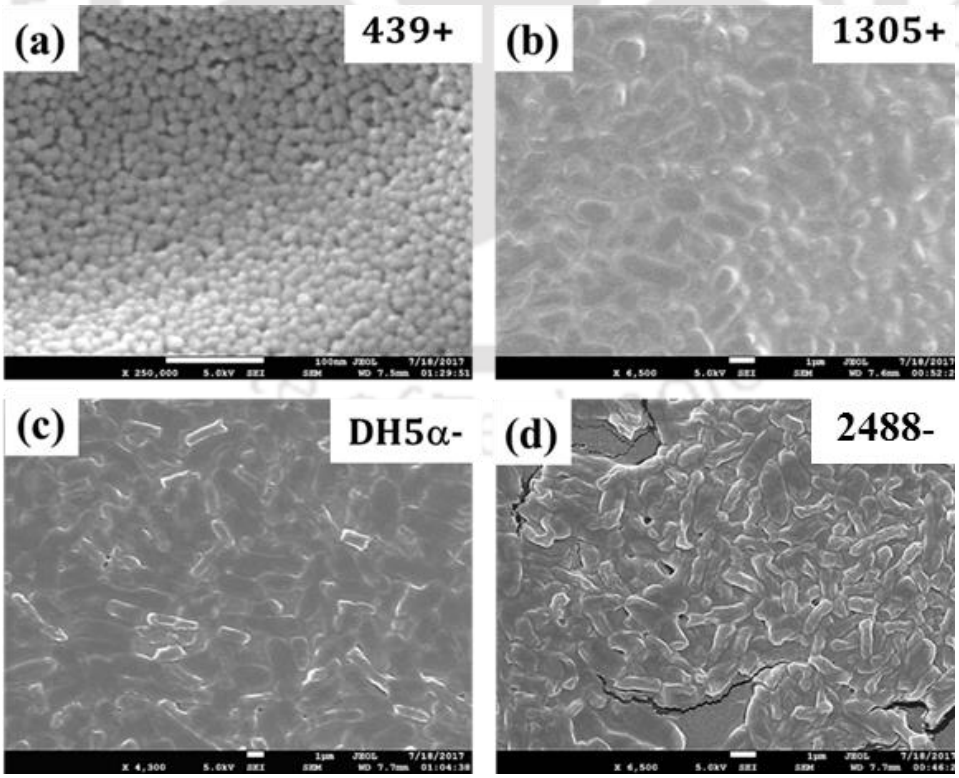

Figure 7.3 FESEM images of the Bacteria layers (with 10^{-3} dilution) on 40 µm channels of n-type OFETs.

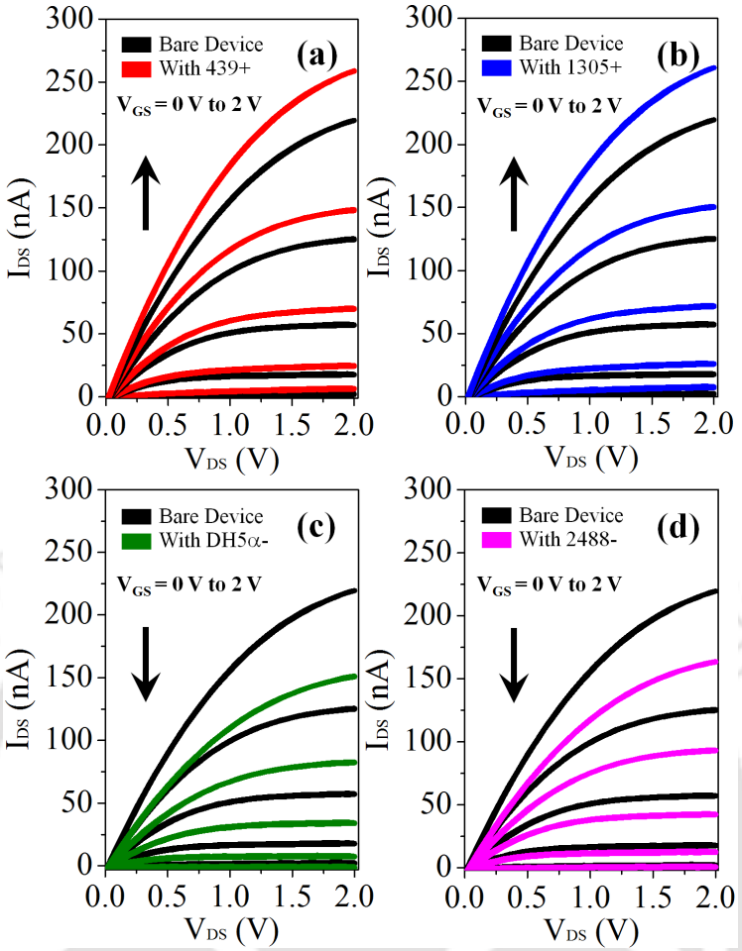

Figure 7.4 Drain Characteristics of the fabricated n-type OFET based Bacteria sensors.

Figure 7.4 described the drain characteristics of the fabricated devices. The black line signifies the characteristics of the bare device, whereas the coloured line signifies the device properties in presence of bacteria. From Figure 7.4a and Figure 7.4b it was observed that drain current of the OFETs increased in the presence of gram positive bacteria possibly due to the presence of negatively charged teichoic acid in bacterial cell wall, which may further create an additional channel along with the original channel of the OFETs and helps to increase the flow rate of charge carrier in the channel. As a result, drain current increases. Further, though the gram negative bacteria are also negatively charged, we observed completely opposite behaviour from Figure 7.4c and Figure 7.4d. The may be due to unsymmetrical cell wall structure of gram negative bacteria compared to gram positive, which is expected to create more resistive path along the channel as a result of which drain current decreases. Figure 7.5 described the transfer characteristics of the fabricated devices. Similar to Figure 7.4, in the Figure 7.5 also the black line signifies the characteristics of the device without the bacteria whereas the coloured line signifies the device properties in the presence of bacteria.

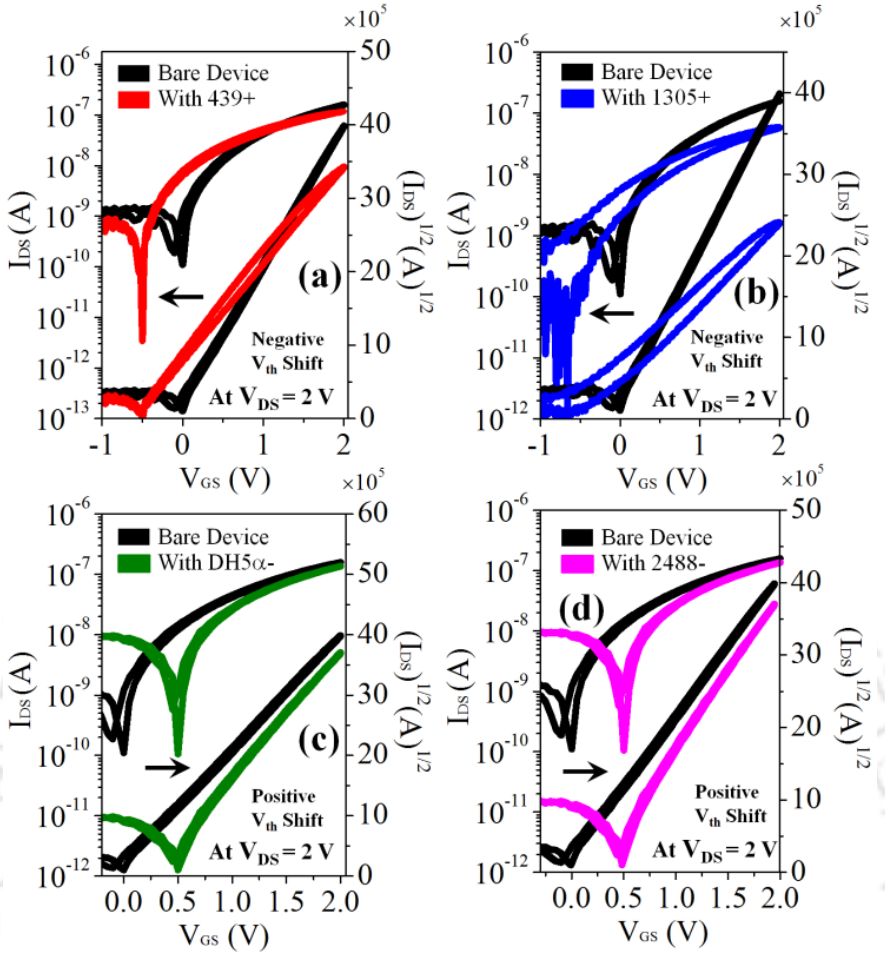

Figure 7.5 Transfer Characteristics of the fabricated n-type OFET based Bacteria sensors.

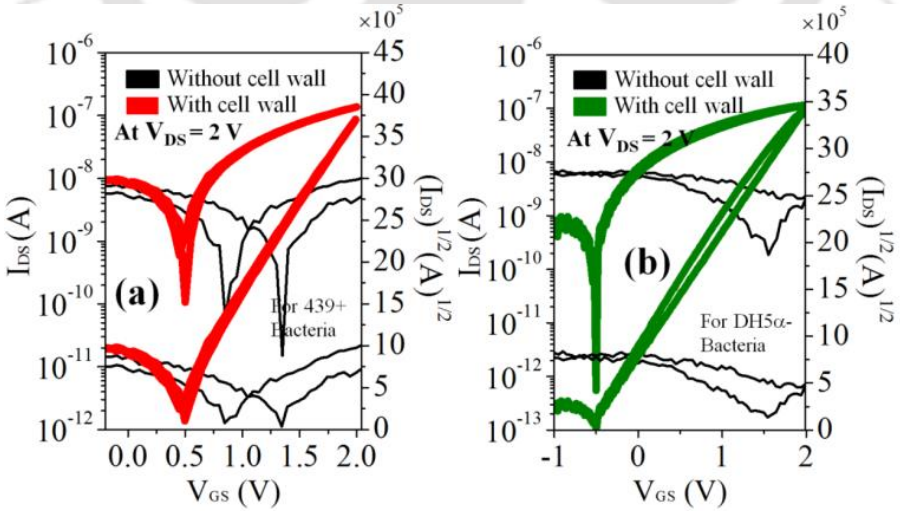

Figure 7.6 Transfer Characteristics of the fabricated n-type OFET based Bacteria sensors with and without bacteria cell wall.

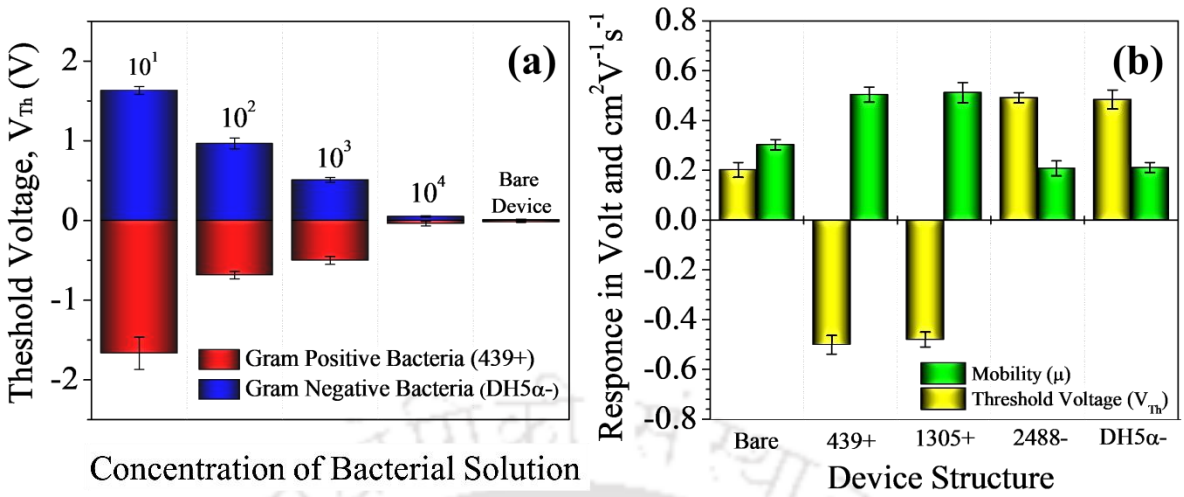

Figure 7.7 (a) Threshold voltage shift of the fabricated n-type OFET based Bacteria sensors with different concentration of bacteria solution. (b) Graphical representation of standard deviations of mobility and threshold voltage of all the fabricated devices.

Figure 7.4 and Figure 7.5 actually supported the assumptions which already explain in Figure 7.3. Due to the symmetrical structure of the gram positive bacteria and the presence of negatively charged teichoic acid in the cell wall, the overall charge density increases at the channel of the OFETs. As a result The V_{Th} values of Figure 7.5a and Figure 7.5b shifted towards more negative, whereas due to the decrement of charge density at the channel in presence of gram negative bacteria, the V_{Th} values of Figure 7.5c and Figure 7.5d shifted towards more positive.

To prove this assumption, the cell walls of both bacteria were removed according to the method described in the experimental section and then immobilised in the channel following the same method as mentioned above. It has been found that without the cell wall the device showed no output properties [Figure 7.6]. This experiment strongly reveals that the deflections in the OFETs properties in presence of bacteria were obtained only due to the interaction of the cell wall of the bacteria. Further to determine the sensitivity of the device, 1 μL of bacteria solution with different concentrations (viz., serial dilutions of 10^{-1}, 10^{-2}, 10^{-3} and 10^{-4}) were immobilised in the channel. It has been found that the device is able to detect both the types of the bacteria up to 10^3 cfu/mL [Figure 7.7a]. Fig. 7b graphically represents the standard deviation curve of the mobility and threshold voltage of all the fabricated devices (~25 devices). Table 7.1 describes all the results obtained in the whole process which also implies that the limit of detection through this method is quite compatible compared to some other available costly techniques.

Table 7.1 Device parameters of OFETs based bacteria sensor.

Molecule	With/without Bacteria		Theoretical Capacitance per unit area (nF/cm^2)	Experimental Capacitance per unit area (nF/cm^2)	Vth (V)	μ (cm^2/Vs)	I_{ON}/I_{OFF} Ratio	Limit of Detection (LOD) $cfu.mL^{-1}$
PDI-C8	Bare		23.09	22.93	0.20 (± 0.03)	0.30 (± 0.02)	10^4	----
	With gram positive bacteria	439	23.09	22.93	-0.50 (± 0.04)	0.50 (± 0.03)	10^5	2.3×10^3
		1305	23.09	22.93	-0.47 (± 0.03)	0.52 (± 0.04)	10^5	2.7×10^3
	With gram negative bacteria	2488	23.09	22.93	0.49 (± 0.02)	0.21 (± 0.03)	10^3	2.4×10^3
		DH5α	23.09	22.93	0.52 (± 0.03)	0.22 (± 0.02)	10^3	2.8×10^3

There are various types of biosensors like optical, mechanical, electrochemical, potentiometric, amperometric and impedimetric which are widely mentioned in literature for bacterial detection. In this regard, *escherichia coli* was detected using surface-enhanced Raman scattering in buffer medium with LOD 10^3 cfu/mL.[19-32] Further, the same *escherichia coli* bacteria was detected mechanically using quartz crystal microbalance in buffer medium with LOD 10^6 cells/mL.[23] Again by using potentiometric stripping analysis with the help of Glassy carbon electrode, *sulfate-reducing bacteria* was detected with a LOD ~10^7 cfu/mL. Using impedimetric biosensor[26] *escherichia coli* was detected using biotinyl antibody bio receptor with LOD ~10^8 cfu/mL.[30] Table 7.2 provides a summary of some of these methods which were successfully able to detect different types of bacteria. But these methods are either time-consuming, expensive or require specialist equipment and proficient operators. In this study, we have reported ultra-low operated OFET based biosensor which is one of the simple, facile and low-cost biosensor which is successfully used for the label-free detection of gram positive and gram negative bacteria.

Table 7.2 Summary of recent literature data on OFETs based bacteria sensor.

Method	Target analyte(s)	Transducer Signal	Sensor assembly	Bioreceptor(s)	LOD	Analyte(s)	Ref.
Optical Biosensor	Salmonella enterica, Listeria monocytogenes, Escherichia coli O157:H7	Fluorescence	Antibodies linked via biotin/avidin to optical fibers	Polyclonal antibody for capture, fluorescent monoclonal antibody or aptamer against surface protein InlA as reporter	10^3 cfu/ml	Artificially contaminated meat samples	19, 20
	Escherichia coli	Surface plasmon resonance	Bacteriophage covalently bound to SiO_2 optical fibers	T4 bacteriophage	10^3 cfu/ml	Bacteria in buffer	21
	Shewanella oneidensis	Surface-enhanced Raman scattering	Silver nanoparticles sandwiched by analyte binding on optical fiber tip	NA	10^6 cells/ml	Bacteria in buffer	22
Method	Target analyte(s)	Transducer Signal	Sensor assembly	Bioreceptor(s)	LOD	Analyte(s)	Ref.
Mechanical biosensors	E. coli O157:H7	Quartz crystal microbalance	Antibody for capture and antibodyfunctionalized nanoparticles for signal enhancement	Anti-E. coli antibody	10^6 cells/ml	Bacteria in buffer	23
	Bacillus anthracis	Quartz crystal microbalance	Protein A/antibody-functionalized SAM on gold	Anti-B. anthracis antibody	1×10^3 cfu or spores/ml	Vegetative cells and spores	24
	Vibrio cholerae O1 Microcantilever	Microcantilever / Dynamic Force Microscopy	Antibody-functionalized SAM on gold	Anti-V. cholera antibody (monoclonal)	1×10^3 cfu/ml	Bacteria in buffer	25
Method	Bacterium	Transducer	Technique	Bioreceptor	LOD	Comments	Ref.
Potentiometric Biosensor	Sulfate-reducing bacteria	Glassy carbon electrode	Potentiometric stripping analysis	None	2.3×10 to 2.3×10^7 cfu/ml	Need bacterial processing	26
	Staphylococcus aureus	Single-walled carbon nanotubes	electron motive force	Aptamer	8×10^2 cfu/ml	Bacterium-spiked pig skin	27
Method	Bacterium	Transducer	Technique	Bioreceptor	LOD	Comments	Ref.
Amperometric Biosensor	E. coli	Photolithographic gold	Immunomagnetic/amperometric in flow cells	Antibody	55 cells/ml in PBS, 100 cells/ml in milk	No contact of biocomponent with sensor	28
	Heat-killed E. coli	Saturated calomel electrode	Amperometric detection of secondary antibody with glucose oxidase	Biotinyl antibody	3×10^1 to 3.2×10^6 cfu/ml, down to 15 cfu/ml	Labeling needed but tested in synthetic stool	29
Method	Bacterium	Transducer	Chemistry	Bioreceptor	LOD	Ref.	

Impedimetric electrochemical biosensors	E. coli	7% gold-tungsten plate wire	Polyethyleneamine-streptavidin	Biotinyl antibody	10^3–10^8 cfu/ml	30
	E. coli	Screen-printed carbon microarrays	ethyl(dimethylaminopropyl) carbodiimide/ N-hydroxysuccinimide	Bacteriophage	10^4 cfu/ml for 50µl samples	31
	Sulfate-reducing bacteria	ITO	Chitosan-reduced grapheme sheet	Bioimprint of bacteria	1.0×10^4 to 1.0×10^8 cfu/ml	32

A combination of inorganic-organic hybrid tri-layer dielectric system was introduced in the study to reduce the operating voltage of the device ~2V. To achieve this, two different inorganic dielectrics namely Al_2O_3 and TiO_2 and one polymer dielectric, namely, PMMAwere used to form hybrid tri-layer dielectric system. Each of the individual dielectric layer of this system has significant contribution for reducing the operational voltage of PDI-C8 based n-type OFET used for bacteria detection. The structure of this n-type OFET was standardized step-by-step prior to the bacteria detection. The average electron mobility (μ_e) and threshold voltage (V_{Th}) of the PDI-C8 based OFET was observed to be 0.3 $cm^2V^{-1}s^{-1}$ and 0.2 V respectively without bacteria. The electrical stability of the bare device was also investigated at $V_{GS}=V_{DS}=2V$ under vacuum, from which it was found that the device is showing high electrical stability with a decay of I_{DS} ~10% after 30 min. For sensing bacteria, it has been found that due to the interaction between the surface charges of bacteria cell wall and the charge carriers in the channel, the device could successfully detect and distinguish the gram positive and gram negative bacteria. In presence of gram positive bacteria the average μ_e increases from 0.3 $cm^2V^{-1}s^{-1}$ to 0.5 $cm^2V^{-1}s^{-1}$ with reduced V_{Th} (0.2 V to -0.5 V) whereas in the presence of gram negative bacteria the average μ_e decreases from 0.3 $cm^2V^{-1}s^{-1}$ to 0.2 $cm^2V^{-1}s^{-1}$ with increased V_{Th} from 0.2 V to 0.5 V. This study is the first report of OFET based bacteria sensor having detection limit 10^3 cfu/mL for both the types of bacteria, with remarkably ultra-low operating voltage of 2 V, on low-cost glass substrates without using ITO or/and Si/SiO_2.

7.3 Conclusion

In conclusion, a simple, facile and low-cost ultra-low operated n-type OFET based biosensor which successfully detects gram positive and gram negative bacteria has been demonstrated. A combination of two different inorganic dielectrics namely Al_2O_3 and TiO_2 and one polymer dielectric, namely, PMMA were used to form hybrid tri-layer dielectric

system, the function of which was to reduce the operating voltage of the fabricated OFET device ~2V. Each of the individual dielectric layers of this system has significant effect on reducing the operational voltage of n-type PDI-C8 based OFET for bacteria detection. A step-by-step structural standardization of the device was performed prior to the sensing application. The average electron mobility (μ_e) and threshold voltage (V_{Th}) of the bare PDI-C8-OFET was observed to be 0.3 $cm^2V^{-1}s^{-1}$ and 0.2 V respectively. The electrical stability of the bare device was also investigated by bias stress analysis at $V_{GS}=V_{DS}=2V$ under vacuum. For bacterial sensing, initially the bacteria was grown and diluted by following standard protocol and then immobilized on the channel of the OFETs followed by vacuum drying under dark conditions. It has been observed that due to the interaction between the surface charge of bacteria cell wall and the charge carriers in the channel, the device is successfully able to detect and distinguish the gram positive and gram negative bacteria. In presence of gram positive bacteria the average μ_e increases from 0.3 $cm^2V^{-1}s^{-1}$ to 0.5 $cm^2V^{-1}s^{-1}$ with reduced V_{Th} (0.2 V to -0.5 V) whereas in presence of gram negative bacteria the average μ_e decreases from 0.3 $cm^2V^{-1}s^{-1}$ to 0.2 $cm^2V^{-1}s^{-1}$ with increased V_{Th} from 0.2 V to 0.5 V. The sensing mechanism was confirmed by repeating the same study by removing the bacterial cell wall. To the best of our knowledge, this study is the first report of OFET based bacteria sensor having detection limit 10^3 cfu/mL for both the types of bacteria, with remarkably ultra-low operating voltage of 2 V, on low-cost glass substrates without using ITO or/and Si/SiO_2.

7.4 References

[1] Janata, J.; Josowicz, M. Conducting Polymers in Electronic Chemical Sensors. *Nat. Mater.* **2003**, *2*, 19-24.

[2] Sun, Z.; Li, J.; Liu, C.; Yang, S.; Yan, F. Enhancement of Hole Mobility of Poly (3-Hexylthiophene) Induced by Titania Nanorods in Composite Films. *Adv. Mater.* **2011**, *23*, 3648-3652.

[3] Yan, F.; Tang, H. Application of Thin-Film Transistors in Label-Free DNA Biosensors. *Expert Rev. Mol. Diagn.* **2010**, *10*, 547-549.

[4] Berggren, M.; Richter-Dahlfors, A. Organic Bioelectronics. *Adv. Mater.* **2007**, *19*, 3201-3213.

[5] Owens, R. M.; Malliaras, G. G. 2010. Organic Electronics at the Interface with Biology. *MRS Bull.* **2010,** *35*, 449-456.

[6] Zhang, Q.; Subramanian, V. DNA Hybridization Detection with Organic Thin Film Transistors: Toward Fast and Disposable DNA Microarray Chips. *Biosens. Bioelectron.* **2007**, *22*, 3182-3187.

[7] Bartic, C.; Campitelli, A.; Borghs, S. Field-Effect Detection of Chemical Species with Hybrid Organic/Inorganic Transistors. *Appl. Phys. Lett.*, **2003**, *82*, 475-477.

[8] Jagannathan, L.; Subramanian, V. DNA Detection using Organic Thin Film Transistors: Optimization of DNA Immobilization and Sensor Sensitivity. *Biosens. Bioelectron.* **2009**, *25*, 288-293.

[9] Zhang, Q.; Jagannathan, L.; Subramanian, V. Label-Free Low-Cost Disposable DNA Hybridization Detection Systems using Organic TFTs. *Biosens. Bioelectron.* **2010**, *25*, 972-977.

[10] Scarpa, G.; Idzko, A. L.; Yadav, A.; Martin, E.; Thalhammer, S.; Toward Cheap Disposable Sensing Devices for Biological Assays. *IEEE Trans. Nanotechnol.* **2010**, *9*, 527-532.

[11] Khan, H. U.; Jang, J.; Kim, J. J.; Knoll, W. Effect of Passivation on the Sensitivity and Stability of Pentacene Transistor Sensors in Aqueous Media. *Biosens. Bioelectron.* **2011**, *26*, 4217-4221.

[12] Lin, P.; Yan, F.; Yu, J.; Chan, H. L.; Yang, M. The Application of Organic Electrochemical Transistors in Cell-Based Biosensors. *Adv. Mater.* **2010**, *22*, 3655-3660.

[13] Lin, P.; Luo, X.; Hsing, I.; Yan, F. Organic Electrochemical Transistors Integrated in Flexible Microfluidic Systems and Used for Label-Free DNA Sensing. *Adv. Mater.* **2011**, *23*, 4035-4040.

[14] Krishnamoorthy, K.; Gokhale, R. S.; Contractor, A. Q.; Kumar, A.; Novel Label-free DNA Sensors based on Poly (3, 4-ethylenedioxythiophene). *Chem. Commun.* **2004**, *7*, 820-821.

[15] Bolin, M. H.; Svennersten, K.; Nilsson, D.; Sawatdee, A.; Jager, E. W.; Richter-Dahlfors, A.; Berggren, M.; Active Control of Epithelial Cell-Density Gradients Grown Along the Channel of an Organic Electrochemical Transistor. *Adv. Mater.* **2009**, *21*, 4379-4382.

[16] Dey, A.; Singh, A.; Kalita, A.; Das, D.; Iyer, P. K. High Performance, Low Operating Voltage n-Type Organic Field Effect Transistor based on Inorganic-Organic Bilayer Dielectric System. *J. Phys.: Conf. Ser.* **2016**, *704*, 012017(1-8).

[17] Dey, A.; Singh, A.; Das, D.; Iyer, P. K. Photosensitive Organic Field Effect Transistors: The Influence of ZnPc Morphology and Bilayer Dielectrics for Achieving a Low Operating Voltage and Low Bias Stress Effect. *Phys. Chem. Chem. Phys.* **2016**, *18*, 32602-32609.

[18] Dey, A.; Singh, A.; Das, D.; Iyer, P. K. High-Performance ZnPc Thin Film-based Photosensitive Organic Field-Effect Transistors: Influence of Multilayer Dielectric Systems and Thin Film Growth Structure. *ACS Omega* **2017**, *2*, 1241-1248.

[19] Ohk, S. -H.; Bhunia, A. K. Multiplex Fiber Optic Biosensor for Detection of Listeria Monocytogenes, Escherichia coli O157: H7 and Salmonella Enterica from Ready-to-eat Meat Samples. *Food Microbiol.* **2013**, *33*, 166-171.

[20] Ohk, S. -H.; Koo, O. K.; Sen, T.; Yamamoto, C. M.; Bhunia, A. K. Antibody-aptamer Functionalized Fibre-optic Biosensor for Specific Detection of Listeria Monocytogenes from Food. *J. Appl. Microbiol.* **2010**, *109*, 808-817.

[21] Tripathi, S. M.; Bock, W. J.; Mikulic, P.; Chinnappan, R.; Ng, A.; Tolba, M.; Zourob, M. Long Period Grating based Biosensor for the Detection of Escherichia coli Bacteria. *Biosens. Bioelectron.* **2012**, *35*, 308-312.

[22] Yang, X.; Gu, C.; Qian, F.; Li, Y.; Zhang, J. Z. Highly Sensitive Detection of Proteins and Bacteria in Aqueous Solution using Surface-Enhanced Raman Scattering and Optical Fibers. *Anal. Chem.* **2011**, *83*, 5888-5894.

[23] Jiang, X.; Wang, R.; Wang, Y.; Su, X.; Ying, Y.; Wang, J.; Li, Y. Evaluation of Different Micro/Nanobeads used as Amplifiers in QCM Immunosensor for More Sensitive Detection of E. Coli O157: H7. *Biosens. Bioelectron.* **2011**, *29*, 23-28.

[24] Hao, R.; Wang, D.; Zhang, X. E.; Zuo, G. Wei, H.; Yang, R.; Zhang, Z., Cheng, Z.; Guo, Y.; Cui, Z.; Zhou, Y. Rapid Detection of Bacillus Anthracis using Monoclonal Antibody Functionalized QCM Sensor. *Biosens. Bioelectron.* **2009**, *24*, 1330-1335.

[25] Sungkanak, U.; Sappat, A.; Wisitsoraat, A.; Promptmas, C.; Tuantranont, A.; Ultrasensitive Detection of Vibrio Cholerae O1 using Microcantilever-based Biosensor with Dynamic Force Microscopy. *Biosens. Bioelectron.* **2010**, *26*, 784-789.

[26] Wan, Y.; Zhang, D.; Hou, B. Selective and Specific Detection of Sulfate-reducing Bacteria using Potentiometric Stripping Analysis. *Talanta*, **2010**, *82*, 1608-1611.

[27] Zelada-Guillén, G. A.; Sebastián-Avila, J. L.; Blondeau, P.; Riu, J.; Rius, F.X. Label-free Detection of Staphylococcus Aureus in Skin using Real-time Potentiometric Biosensors based on Carbon Nanotubes and Aptamers. *Biosens. Bioelectron.* **2012**, *31*, 226-232.

[28] Laczka, O.; Maesa, J. M.; Godino, N.; del Campo, J.; Fougt-Hansen, M.; Kutter, J. P.; Snakenborg, D.; Muñoz-Pascual, F. X.; Baldrich, E. Improved Bacteria Detection by Coupling Magneto-immunocapture and Amperometry at Flow-Channel Microband Electrodes. *Biosens. Bioelectron.* **2011**, *26*, 3633-3640.

[29] Li, Y.; Fang, L.; Cheng, P.; Deng, J.; Jiang, L., Huang, H.; Zheng, J.; An Electrochemical Immunosensor for Sensitive Detection of Escherichia coli O157: H7 using C60 Based Biocompatible Platform and Enzyme Functionalized Pt Nanochains Tracing Tag. *Biosens. Bioelectron.* **2013**, *49*, 485-491.

[30] Lu, L.; Chee, G.; Yamada, K.; Jun, S. Electrochemical Impedance Spectroscopic Technique with a Functionalized Microwire Sensor for Rapid Detection of Food borne pathogens. *Biosens. Bioelectron.* **2013**, *42*, 492-495.

[31] Shabani, A.; Zourob, M.; Allain, B.; Marquette, C. A.; Lawrence, M. F.; Mandeville, R. Bacteriophage-modified Microarrays for the Direct Impedimetric Detection of Bacteria. *Anal. Chem.* **2008**, *80*, 9475-9482.

[32] Qi, P.; Wan, Y.; Zhang, D. Impedimetric Biosensor based on Cell-mediated Bioimprinted Films for Bacterial Detection. *Biosens. Bioelectron.* **2013**, *39*, 282-288.

8

Epilogue

Due to the influential motivation and demand of recent day technology for highly efficient sensor device, this thesis mainly focusses to introduce different methods to reduce the operational voltage of both p-channel and n-channel OFET and use them for different types of sensor applications. The entire thesis essentially paves attention in device engineering of OFETs by modulating the gate dielectric layers with combination of inorganic and organic dielectric materials.

At the very beginning, the thesis discussed the fabrication and characterization of a low cost, n-type OFET on glass substrate using PVA gate dielectric material. Here, a conjugated molecule NDI-OD2 has been synthesized in a single step from commercial materials and then characterized by different standard characterization techniques. It has been observed that this NDI-OD2 molecule when processed by solution method, forms rod-shaped crystalline microstructures, whereas, when thermally deposited, it assumes the formation of smooth 2D films. The chemical as well as physical properties and theoretical calculations of this molecule have been studied and the effect of the C-18 alkyl chain unit has been discussed. The OFET consisting of NDI-OD2 exhibits excellent performance parameters such as high electron mobility (μ_e =~1.0 $cm^2V^{-1}s^{-1}$) and I_{on}/I_{off} ratio. After demonstrating the high performance of NDI-OD2-based OFET devices fabricated with biocompatible PVA dielectric, it has also been demonstrated that these devices can be degraded because of the presence of this PVA dielectric when exposed to a

high-moisture environment. In this study, a conceptually important feature and futuristic aspect that the n-channel OFET devices can also be biodegraded irreversibly is demonstrated. This concept of developing a low cost and biodegradable OFET device with biocompatible PVA dielectric with excellent electron mobility is expected to have diverse applications in disposable electronic tags, biomedical devices, and food industry packing.

In the next step, another new concept was demonstrated where the fabrication and characterization of low operating voltage, electrically stable n-type OFET using inorganic-organic bilayer dielectric system is discussed. In this study two different derivatives of NDI were synthesized, namely NDIOD2 and NDI-CY2 in a single step and characterized by different characterization techniques before the device fabrication. The bilayer systems contain two different device configurations namely Al_2O_3/PVA and Al_2O_3/PMMA in order to reduce the operating voltage and improve the device performance. The high capacitance, pinhole-free Al_2O_3 gate insulator was deposited by electrochemical oxidation or anodization method with a constant current density of 0.06 mA cm^{-2} and a voltage of 10 V in a 0.001 M citric acid monohydrate electrolyte solution at room temperature using a square-shaped platinum mesh as counter electrode to form a ~13 nm thick Al_2O_3 layer over the aluminum film gate electrode. It was observed that the devices with Al_2O_3/PMMA bilayer dielectric system and top contact aluminum electrodes exhibit excellent n-channel behavior for both the molecule under vacuum compared to the other structures and operating under a very low voltage (7V). All these devices demonstrate highly stable electrical behavior under multiple scans and low threshold voltage instability in vacuum condition even after 7 days. This low operating voltage, high performance OFET device with bilayer dielectric system is expected to have diverse applications in the next generation of OFET technologies.

In the next step the application of inorganic-organic bilayer dielectric contained low operating voltage OFETs were demonstrated. This inorganic-organic bilayerdielectric concept was successfully used to fabricate highly efficient photo sensitive organic field effect transistors (PS-OFETs). PS-OFETs based on morphology controlled ZnPc layer, with inorganic-organic bilayer gate dielectrics system, fabricated on glass substrate showed remarkable efficiency as light sensors at various incident optical powers. The ITO as well as Si/SiO_2 free low cost PS-OFET devices, show low bias stress, reduced operating voltage device with Al_2O_3/PMMA as bilayer gate dielectrics and Cu as top contacts exhibit excellent p-channel behavior with a remarkable photo responsivity of 2679.40 $A.W^{-1}$ and photo ON/OFF current ratio 933.56 with a very low operating voltage (0 to -7 V) that are not observed previously. The bias stress effect of the device was investigated under both

light and dark condition in vacuum. It was observed that the effect of the stress is extremely small in presence of light (decay of I_{DS}~ 20% after 30 min) compared to the dark, with characteristic carrier relaxation time τ'~10^4 sec. This device with high electrical stability at ambient conditions and low threshold voltage under constant electrical bias stress is expected to have potential applications in optoelectronic devices and energy efficient sensors.

Furthermore, in the next chapter the key impact and the significance of multilayer polymer based dielectric system on the remarkable photo response properties of ZnPc based PS-OFETs, at various incidents optical powers is discussed. The combination of inorganic Al_2O_3 and organic non-polar PMMA are used as the bilayer dielectric configuration, whereas, in case of tri-layer dielectric system, bilayer polymer dielectrics, consisting of PMMA as a low-k dielectric polymer, on top of high-k polar dielectric, PVA) have been fabricated along with Al_2O_3 as the third layer. At 90°C, the fabricated PS-OFET with Al_2O_3/PVA/PMMA tri-layer dielectric configuration showed best p-channel behavior with enhanced and remarkable photo responsivity of R~9689.39 $A.W^{-1}$ compared to Al_2O_3/PMMA bilayer dielectric system (R~2679.40 $A.W^{-1}$) due to the polarization of dipoles inside the polar-PVA dielectric which increases the charge transport through channel. The charge carrier mobility of the device also improved by one order (μ_h~1.3×10^{-2} $cm^2.V^{-1}.s^{-1}$) compared to bilayer dielectric configuration (μ_h~ 3.5×10^{-3} $cm^2.V^{-1}.s^{-1}$). The observed specific detectivity, D* and noise equivalent power, NEP values of the bilayer dielectric system are 6.01×10^{13} Jones and 2.655×10^{-17} $W.Hz^{-1/2}$ respectively whereas for tri-layer dielectric system the observed D* and NEP values are 5.13×10^{14} Jones and 1.043×10^{-17} $W.Hz^{-1/2}$ respectively. Additionally, the operating voltage of each of the fabricated devices were also very low (-7V) due to the influence of inorganic high-k Al_2O_3 dielectric layer. The electrical stability of all the fabricated devices was also investigated by bias stress analysis under both light and dark condition in vacuum. To the best of our knowledge, the photo responsivity (R) reported here with Al_2O_3/PVA/PMMA tri-layer dielectric configuration, is the highest reported value for thin film based PS-OFETs with remarkably low operating voltage of -7 V, on low-cost glass substrates avoiding ITO or/and Si/SiO_2.

In the next step again the operating voltage of OFET was successfully reduced by a novel combination of hybrid tri-layer dielectric system. Additionally this study further described the importance of controlled thickness of Titanium dioxide (TiO_2) nanoparticle (NPs) thin film in hybrid tri-layer dielectric system, for the performance of ultra-low

operating voltage, PDI-C8 and NDI-CY2 molecules based n-type OFETs. The TiO_2 NPs dielectric was synthesized by inexpensive sol-gel method and then thoroughly examined by different characterization techniques. To check the influence of thickness of this TiO_2 NPs dielectric material in nanoscale range, the thickness of TiO_2 was varied with different r.p.m. viz., 2000, 3000, 4000 and 5000 respectively. It has been observed that at 4000 r.p.m. (~100 nm of TiO_2) the devices with top contact Ag/Al electrodes exhibit excellent n-channel behavior compared to other r.p.m., with highest electron mobility values with an operating voltage of only 2V, which is due to the better capacitor coupling among the tri-layer dielectric materials at this optimum thickness of TiO_2 which further helps to accumulate maximum number of charge at the channel at very low gate bias. The bias stress instability effects of the devices at all r.p.m. were also investigated by applying constant voltage for half an hour under vacuum condition, where only ~10% decrements of source-drain current, I_{DS} was observed at 4000 r.p.m. It has also been demonstrated that this optimum low-cost hybrid tri-layer dielectric system showed similar suitable gate dielectric property for flexible and transparent organic devices to operate under same ultra-low voltage which is expected to have diverse applications in future for portable organic electronics application.

Finally, in the next steps the application of hybrid tri-layer dielectric contained ultra-low operating voltage OFETs were demonstrated in the thesis. The last chapter reports the fabrication and rapid detection method of gram positive and gram negative bacteria by using ultra-low operating voltage, highly sensitive, n-type Organic Field Effect Transistor. PDI-C8 was chosen as the active layer material for the detection of gram positive and gram negative bacteria with the sensing area of ~S= 3.12×10^{-4} cm^2. Due to the electrostatic interaction between the differentiable surface charge density of the bacteria and the majority carrier flowing through the channel, the device is successfully able to distinguish the gram positive and gram negative bacteria. The minimum detection limits for the type of bacteria were observed to be ~10^3 cfu/mL. This chapter relates to the fabrication of ultra-low operating voltage organic thin film transistors comprising of hybrid organic tri-layer dielectrics system which are compatible with any desire substrate on simple glass slide or OHP plastic substrate which can be used for the detection of gram positive and gram negative with n-type organic semiconductor as the active layer under room temperature.

Thus, by step wise standardization this thesis successfully explained some facile methods with sensor applications by which the operating voltage of OFET was reduced from 50V to 2V. The methods which are described herein can be further used in future for

highly efficient application of other chemical, optical and biosensor applications. A schematic representation of the overall thesis overview is shown in Figure. 8.1 below-

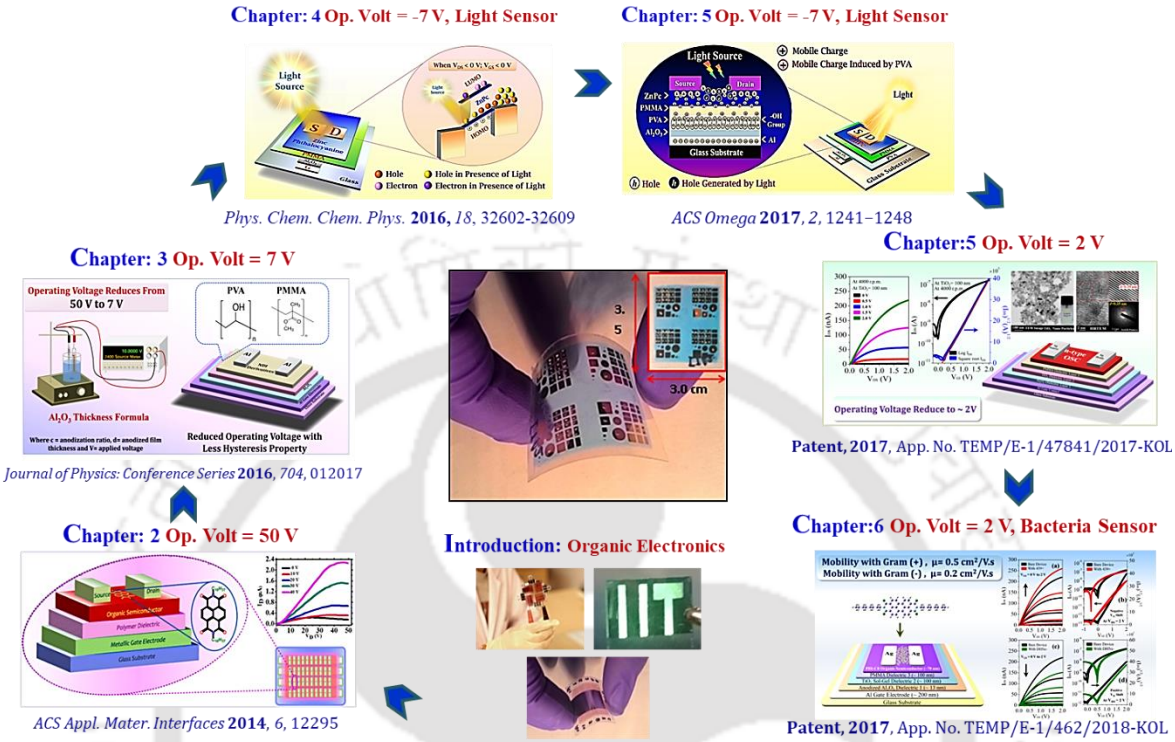

Figure 8.1 Schematic of the Thesis overview.

Publications

Journals:

[1] **Dey, A.;** Singh, A.; Dutta, D.; Ghosh, S. S.; Iyer, P. K. Rapid and Facile Label-Free Bacteria Detection using Hybrid Tri-Layer Dielectrics Contained Ultra-low Operated n-Type Organic Field Effect Transistor. **Communicated**.

[2] **Dey, A.;** Singh, A.; Iyer, P. K. Cost Effective Tri-layers Dielectric System for Ultralow Operating Voltage, Electrically Stable n-channel Organic Field Effect Transistors. **Communicated**.

[3] **Dey, A.;** Singh, A.; Das, D.; Iyer, P. K. High-Performance ZnPc Thin Film-Based Photosensitive Organic Field-Effect Transistors: Influence of Multilayer Dielectric Systems and Thin Film Growth Structure. *ACS Omega* **2017,** *2,* 1241-1248.

[4] **Dey, A.;** Singh, A.; Das, D.; Iyer, P. K. Photosensitive Organic Field Effect Transistor: Influence of ZnPc Morphology and Bilayer Dielectrics to Achieve Low Operating Voltage and Low Bias Stress Effect. *Phys. Chem. Chem. Phys.* **2016,** *18,* 32602-32609.

[5] **Dey, A.;** Kalita, A.; Iyer, P. K. High-Performance n-Channel Organic Thin-Film Transistor Based on Naphthalene Diimide. *ACS Appl. Mater. Interfaces* **2014,** *6,* 12295-12301.

Proceedings:

[1] **Dey, A.;** Singh, A.; Kalita, A.; Das, D.; Iyer, P. K. High Performance, Low Operating Voltage n-Type Organic Field Effect Transistor Based on Inorganic-Organic Bilayer Dielectric System. Journal of Physics: Conference Series, **2016**, 704, 012017 (1-8).

Patents:

[1] **Dey, A.;** Singh, A.; Iyer, P. K. Method for the Fabrication of Solution Process, Ultra-low Operating Voltage, Stable Organic Field Effect Transistor, 2017, Ref. No. 201731046915, App. No. TEMP/E-1/47841/2017-KOL.

[2] **Dey, A.;** Singh, A.; Iyer, P. K. Method for the Fabrication of Low Cost, Reduced Bias Stress Multi-layers Dielectric System Ultralow Operated n-type Organic Field Effect Transistors, 2017, Ref. No. 201731046914, App. No. TEMP/E-1/47853/2017-KOL.

[3] **Dey, A.;** Singh, A.; Dutta, D.; Ghosh, S. S.; Iyer, P. K. Method for the Detection of Gram Positive and Gram Negative Bacteria by Ultra-low Operating Voltage n-type Organic Field Effect Transistor, 2017, Ref. No. 201831000478, App. No. TEMP/E-1/462/2018-KOL.

Book Chapter:

[4] **Dey, A.;** Singh, A.; Das, D.; Iyer, P. K. Organic Semiconductors: A New Future of Nano Devices and Applications in Thin Film Structure in Energy Applications. Springer, **2015**, 97-128.

Journals (not included in the Thesis):

[1] Singh, A.; **Dey, A.;** Iyer, P. K. Effect of Molar Concentration Ratio, Annealing Temperature and Single Cathode Buffer Layer on rrP3HT: $PC_{71}BM$ Based Bulk Heterojunction Solar Cell, *Organic Electronics,* **2017,** *51,* 428-434.

[2] Gupta, A.; Dhakate, S.; Pal, P.; **Dey, A.;** Iyer, P. K.; Singh, D. K. Effect of Graphitization Temperature on Structure and Electrical Conductivity of Poly-Acrylonitrile Based Carbon Fibers. *Diamond Relat. Mater.* **2017,** *78,* 31–38

[3] Singh, A.; **Dey, A.;** Das, D.; Iyer, P. K. Combined Influence of Plasmonic Metal Nanoparticle and Dual Cathode Buffer Layer for Highly Efficient rrP3HT: PCBM Based Bulk Heterojunction Solar Cell. *J. Mater. Chem. C* **2017,** *5,* 6578-6587.

[4] Das, D.; Gopikrishna, P.; Singh, A.; **Dey, A.;** Iyer, P. K. Solution Processed WPLEDs with Good Color Stability and High Color Rendering Index via a Phosphor-Sensitized System. *Chemistry Select* **2017,** *1,* 1-8.

[5] Das, D.; Gopikrishna, P.; Narasimhan, R.; Singh, A.; **Dey, A.;** Iyer, P. K. White Polymer Light Emitting Diodes Based on PVK: The Effect of the Electron Injection Barrier on Transport Properties, Electroluminescence and Controlling the Electroplex Formation. *Phys. Chem. Chem. Phys.* **2016,** *18,* 33077-33084.

[6] Singh, A.; **Dey, A.;** Das, D.; Iyer, P. K. Effect of Dual Cathode Buffer Layer on the Charge Carrier Dynamics of rrP3HT: PCBM Based Bulk Heterojunction Solar Cell. *ACS Appl. Mater. Interfaces* **2016,** *8,* 10904-10910.

[7] Kalita, A.; **Dey, A.;** Iyer, P. K. Influence of polymer dielectric layer on the morphology and performance of n-channel OFETs. *Phys. Chem. Chem. Phys.* **2016,** *18,* 12163-12168.

[8] Das, D.; Gopikrishna, P.; Singh, A.; **Dey, A.;** Iyer, P. K. Efficient Blue and White Polymer Light Emitting Diodes Based on a Well Charge Balanced, Core Modified Polyfluorene Derivative. *Phys. Chem. Chem. Phys.* **2016,** *18,* 7389-7394.

[9] Singh, A.; **Dey, A.;** Iyer, P. K. Collective Effect of Hybrid Metals Nanoparticles and Dual Cathode Interfacial Layers for High Performance Organic Bulk Heterojunction Solar Cell. **Communicated**.

[10]Singh, A.; **Dey, A.;** Iyer, P. K. Influence of Different Shaped Plasmonic AuNPs on Power Conversion Efficiency of Double Cathode Interfacial Layer Contained rrP3HT: PCBM based Organic Bulk Heterojunction Solar Cell. **Communicated.**

Proceedings (not included in the Thesis):

[1] **Dey, A.; Singh, A.;** Iyer, P. K. Ultra-Low Operating Voltage, Poly (3-hexylthiophene-2,5-diyl) based Highly Light-sensitive Organic Field Effect Transistor, *IEEE Conference Proceeding,* DOI: 10.1109/ICEmElec.2016.8074605.

[2] Singh, A.; **Dey, A.;** Das, D.; Iyer, P. K. Effect of Substrate Temperature on Twin Donor Layer Organic Solar Cell, Conference Proceeding, Under Revision, Material Today Proceeding.

[3] Singh, A.; **Dey, A.;** Das, D.; Iyer, P. K. Improvement of Charge Carrier Dynamics in P3HT:$PC_{61}BM$ Based Solar Cell in Presence of Organic Cathode Interfacial Layers, *IEEE Conference Proceeding,* DOI: 10.1109/ICEmElec.2016.8074606.

[4] Das, D.; Gopikrishna, P.; Singh, A.; **Dey, A.;** Iyer, P. K. Influence of Emissive Layer Thickness on Electrical Characteristics of Polyfluorene Copolymer Based Polymer Light Emitting Diodes, Journal of Physics: Conference Series, **2016**, *704*, 012016 (1-6).

[5] Subbarao, N.V.V.; Gedda. M.; Vasimalla, S.; **Dey, A.;** Iyer, P. K.; Goswami, D. K. Growth and characterization of N,N'-dioctadecyl-1,7-dibromo-3, 4, 9, 10-perylenetetracarboxylic-diimide micron/nano wires for organic field effect transistors, AIP Conference Proceedings **2014**, *1576*, 42–45.

Vitae

Anamika Dey was born in Guwahati, India. She obtained her Bachelor of Science from Pandu College, Guwahati and completed Master of Science in Physics from Gauhati University, India. Under the supervision of Prof. Parameswar Krishnan Iyer, she started her research career at the Centre for Nanotechnology, IIT Guwahati – with the development of ultra-low operating voltage organic field effect transistor for various sensor applications. Her current research interests are the physics behind π-conjugated organic semiconducting materials based thin film devices and finding their applications as portable organic chemical and bio-sensors. She is also interested in functional organic electronic devices such as plasmonically enhanced organic bulk heterojunctions and perovskite solar cells, light emitting diodes and organic memory devices.